THESIS

COMPREHENSIVE VISCOELASTIC CHARACTERIZATION OF HUMAN LOWER CERVICAL SPINE LIGAMENTS

Submitted by

Kevin L. Troyer

Department of Mechanical Engineering

In partial fulfillment of the requirements

For the Degree of Master of Science

Colorado State University

Fort Collins, Colorado

Spring 2010

COLORADO STATE UNIVERSITY

March 30, 2010

WE HEREBY RECOMMEND THAT THE THESIS PREPARED UNDER OUR SUPERVISION BY KEVIN L. TROYER ENTITLED COMPREHENSIVE VISCOELASTIC CHARACTERIZATION OF HUMAN LOWER CERVICAL SPINE LIGAMENTS BE ACCEPTED AS FULFILLING IN PART REQUIREMENTS FOR THE DEGREE OF MASTER OF SCIENCE.

Committee on Graduate work

_____
Paul Heyliger

_____
Hiroshi Sakurai

_____
Advisor: Christian Puttlitz

_____
Department Head: Allan Kirkpatrick

ABSTRACT OF THESIS

COMPREHENSIVE VISCOELASTIC CHARACTERIZATION OF HUMAN LOWER CERVICAL SPINE LIGAMENTS

Accurate definition of cervical spine ligament mechanical properties is requisite to understand and model global cervical spine biomechanics. These ligaments have been shown to exhibit complex nonlinear elastic behavior. In addition, ligamentous mechanical behavior is highly time-dependent (viscoelastic). Previous investigators have reported the viscoelastic stress relaxation behavior of the anterior longitudinal ligament (ALL), posterior longitudinal ligament (PLL), and ligamentum flavum (LF) of the lower cervical spine using quasi-linear viscoelastic (QLV) theory. However, QLV theory assumes that the viscoelastic behavior is independent of the applied strain magnitude. Cervical spine ligaments are subjected to multiple strain magnitudes and loading rates during physiologic loading regimes. Thus, in order to characterize the comprehensive viscoelastic behavior of cervical spine ligaments within their physiological range, and to test the validity of the use of QLV theory to model this behavior, the mechanical response of human lower cervical spine ALL, PLL, and LF was recorded from stress relaxation experiments at multiple strain magnitudes and from cyclic experiments at multiple strain amplitudes and frequencies.

The ALL, PLL, and LF were dissected from the C5-C6 level of human cadaveric cervical spines. Each ligament was isolated into a bone-ligament-bone (B-L-B) preparation by removing all surrounding non-osteoligamentous tissue. Each B-L-B preparation was placed in an environmental chamber, submerged in warmed saline (37 °C), and mounted to a servo-hydraulic materials testing machine. Ligaments were subjected to a uniaxial cyclic testing protocol at multiple strain amplitudes and frequencies, as well as a stress relaxation protocol at multiple

strain magnitudes. Dynamic material properties (phase shift, storage modulus, and loss modulus) were determined from the resulting load displacement data via transformation into the stress-strain space. Stress relaxation data were fitted to QLV theory and a power law formulation in order to characterize the appropriate analytic function that best described the ligament relaxation behavior.

Experimental results indicated that the dynamic material properties of the ALL, PLL, and LF were dependent upon both strain amplitude and frequency. In general, the dynamic material properties of the ALL and the PLL were not statistically different, but both were statistically different form the LF. The stress relaxation data was strongly dependent on the applied strain magnitude. Also, the relaxation rate of the ALL and PLL exhibited a converging trend as strain magnitude increased, while the relaxation rate of the LF diverged with increasing strain magnitude. The different strain-dependent relaxation rate behavior of the longitudinal ligaments and the LF is possibly a result of the compositional and microstructural differences between the two ligament types. Results from both the cyclic and stress relaxation experiments indicated that QLV theory cannot adequately describe the comprehensive viscoelastic behavior of these ligaments within the physiologic loading range. Therefore, a more rigorous, fully nonlinear, viscoelastic formulation is required to model the comprehensive viscoelastic behavior of the ALL, PLL, and LF in the human lower cervical spine.

Kevin Levi Troyer
Department of Mechanical Engineering
Colorado State University
Fort Collins, CO 80523
Spring 2010

ACKNOWLEDGEMENTS

This thesis could not have been prepared without the help of many people. My advisor, Dr. Christian Puttlitz, has provided substantial support, guidance, and encouragement throughout my time at the OBRL. He has been an outstanding mentor, and I greatly appreciate the time that he has committed to the preparation of this manuscript.

My committee members, Dr. Hiroshi Sakurai and Dr. Paul Heyliger, have both contributed greatly to my professional development. Much of my fundamental engineering background is attributed to their classroom lectures. I hold their opinions in high regard and I appreciate the time that they have devoted to me as their student as well as the time they have committed to this thesis.

Jim zumBrunnen from CSU's Center for Applied Statistical Expertise was an invaluable resource for the development and interpretation of the SAS code and output.

All of the staff and students at the OBRL biomechanics lab have, in one way or another, contributed to the preparation of this thesis. Specifically, Dr. Brandon Santoni taught me how to use the experimental equipment and the corresponding software. Also, Dr. Kirk McGilvray helped me with some of the experimental methods and with the mathematical modeling used in this thesis. I consider everyone at the lab a friend and I feel lucky to be part of such a bright and hard-working group. Thank you for all of your help everyone!

This thesis could not have been prepared without the never-ending love and support of my family and friends. My parents and brother have made countless sacrifices to send me to college so that I could fulfill my dreams and I will be forever grateful for the opportunities that they have provided for me. My best friend Brian has been there for me since we were kids, and I thank him for his continued support and encouragement while I have been away at college to work on this thesis.

DEDICATION

This thesis is dedicated to my older brother, Jason, whose severe developmental disability prevented him from pursuing higher education and possibly writing a thesis of his own. Jason has overcome tremendous challenges in his own life that easily overshadow those of obtaining a mere academic degree. It is an absolute pleasure to have Jason in my life, and I am grateful to have an intelligent, courageous, and inspirational older brother that I will always look up to.

TABLE OF CONTENTS

1. INTRODUCTION/BACKGROUND

1.1. Spine Anatomy and Function

The human spine is an interesting and complex anatomical structure. It provides flexible and mobile support for the upper body as it transmits loads from the head, muscles, and external sources to the lower limbs, and protects the fragile spinal cord [1]. These tasks are accomplished through a combination of hard and soft tissue components that form the spinal column. Boney segments (hard tissue) termed *vertebra* provide structural support and protect the spinal cord. Soft tissue constituents, such as the intervertebral discs, ligaments, and cartilage, allow relative movement between the vertebra through activation of musculature, permitting the spine to rotate and bend.

The first twenty-four vertebrae extending caudally from the occiput of the cranium are grouped into cervical, thoracic, and lumbar regions, respectively (Figure 1.1). All vertebrae in these segments, except for the two most cranial vertebrae in the cervical spine, are separated by intervertebral discs. The remaining vertebrae caudal to the lumbar region are fused and grouped into the sacral and coccygeal regions.

A sagittal view of a normal spine, seen in Figure 1.1, displays four anterior-posterior curves that serve to increase its flexibility and shock absorbing characteristics [1]. Convex curvature towards the anterior, called *lordosis*, is present in the cervical and lumbar regions. The thoracic and sacral/coccygeal regions display *kyphosis*, or posterior convex curvature. This thesis is focused on the cervical region of the human spine, which serves to support the head and allows it to be oriented in three-dimensions.

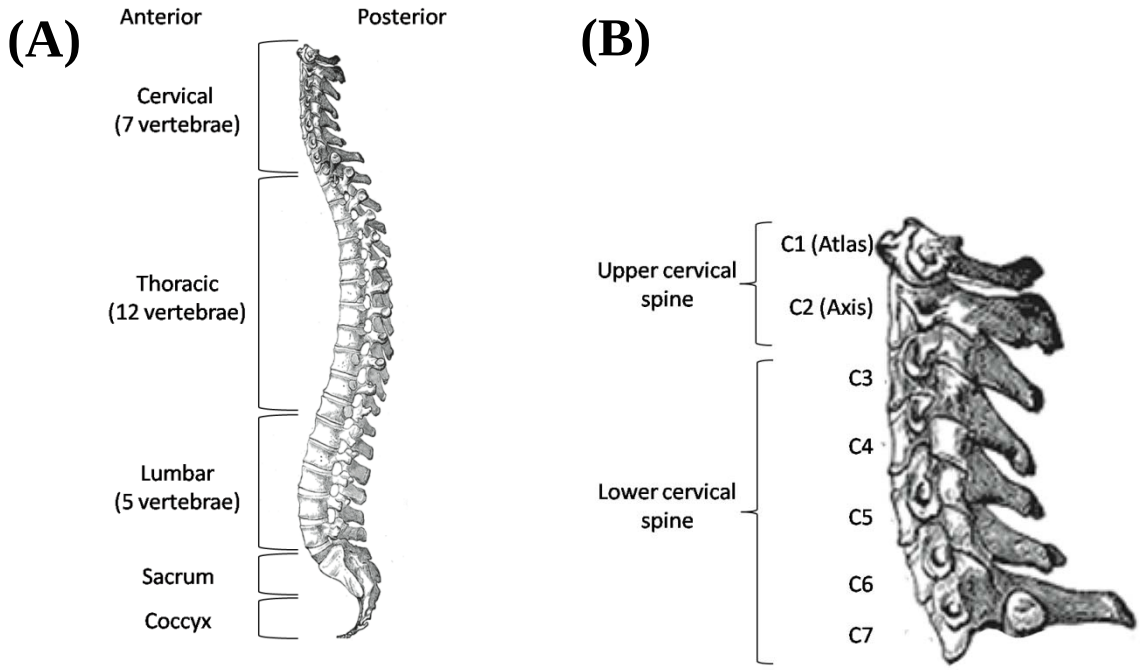

Figure 1.1: (A) Sagittal view of the full human spine depicting the different levels. (B) Sagittal view of the human cervical spine. Adapted from Gray's Anatomy [2].

1.1.1. Vertebrae of the cervical spine

The vertebrae of the cervical spine can be subdivided into upper (occiput – C2) and lower (C3 – C7) sections (Figure 1.1B), where the vertebral geometry of the upper cervical spine is greatly distinguished from the lower. The ring shaped *atlas* vertebra (C1) is the most cranial vertebra and supports the occiput bone of the skull. Caudal to the atlas is the *axis* (C2), which contains a distinct bony process extending cranially from its anterior body called the odontoid process, or *dens*, that the atlas pivots about. The majority of the range of axial rotation of the cervical spine occurs at the atlanto-axial joint [3]. The vertebral geometry in the lower cervical spine, shown in Figure 1.2, is more consistent than that of the upper cervical spine. Each subaxial cervical vertebra contains a cylindrically shaped anterior body and a posterior ring, called the *neural arch*, that is composed of a pair of pedicles and a pair of lamina that contain four articular processes (two superior and two inferior), two transverse processes, and one spinous process (Figure 1.2). The lamina, transverse processes, and spinous process are attachment points for ligaments and/or muscles. The pedicles connect the lamina to the body, forming the *vertebral foramen* that

encloses and protects the spinal cord. The four articular processes contain hyaline cartilage on the articulating surfaces of the joints, called the *zygapophysial* or *facet* joints, between adjacent vertebrae.

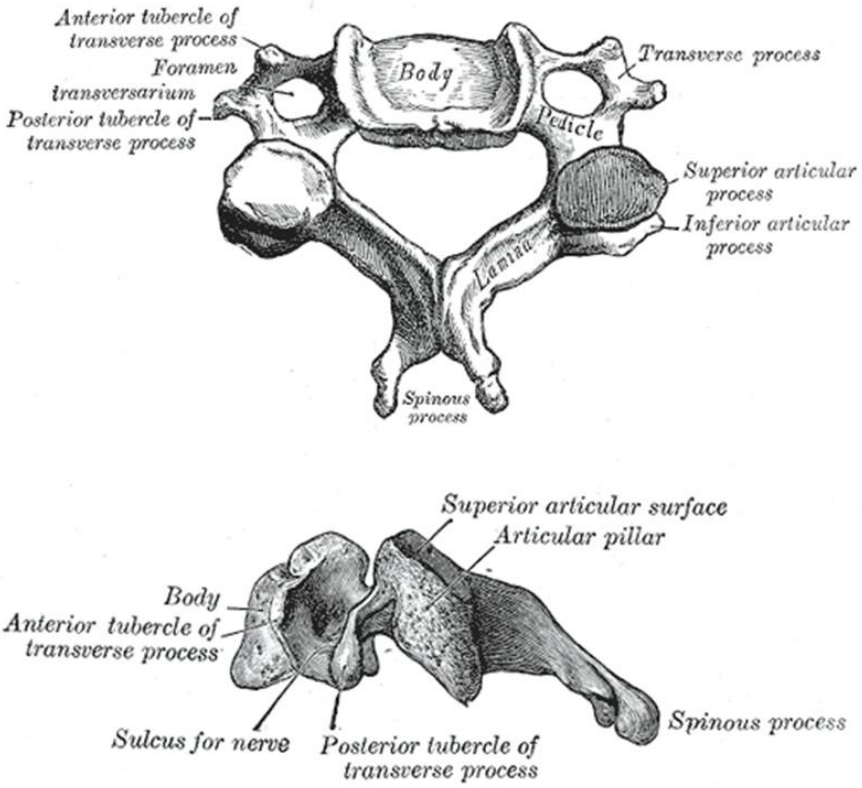

Figure 1.2: Top (upper) and lateral (lower) view depicting the anatomy of a regular lower cervical spine vertebra. Adapted from Gray's Anatomy [2].

The anatomy and geometry of vertebrae in the lower cervical spine is unique. For example, the opposing surfaces of the anterior body have a distinct saddle-shape. A bony lip on the front side of the inferior surface of the body, shown in the lateral view of Figure 1.2, slopes down and anteriorly while the body's superior surface has an opposing shape that accepts this lip. Distinct *uncinate processes* rise cranially from the lateral ends of the body's superior surface. Further, the surfaces of the articular processes are angled 45° from the transverse plane. These unique anatomical characteristics are conductive to flexation/extension being the primary motion (i.e., having the largest range of motion) of the lower cervical spine [4]. Additionally, all

vertebrae in the cervical spine contain an opening in the transverse process, called the *foramen transversarium*, to provide passage for the vertebral artery, the vertebral vein, and nerves.

Osseous tissue is the primary structural component that resists the typical compressive loads experienced by the vertebrae. These forces are shared between the anterior body and the posterior arch through the facets. The bulk of the anterior body is formed from cancellous, or trabecular, bone enclosed in a thin cortical shell (Figure 1.3). Within the cancellous bone is bone marrow and vasculature. The bones of the neural arch have thicker cortical shell and less trabeculae than the anterior body.

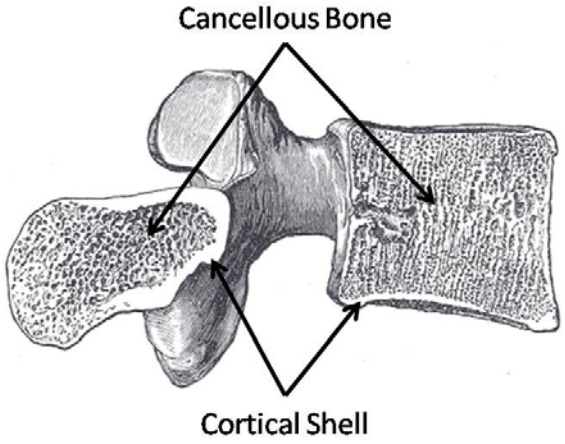

Figure 1.3: Sagittal cut view of a cross section of a lumbar vertebra. The vertebral body is mostly comprised of highly vascularized cancellous bone, containing bone marrow, enclosed by a thin shell of cortical bone. The cortical shell in the neural arch is thicker and contains less cancellous bone. Adapted from Gray's Anatomy [2].

1.1.2. Intervertebral disc

Human vertebrae from the C2-C3 level to the L5-sacrum level are separated by avascular intervertebral discs that lie between anterior bodies of adjacent vertebrae. They allow relative motion between adjacent vertebrae and transfer loads between levels. During motion, the disc is subjected to multiple loading conditions, sharing compressive loads with the facets and also experiencing tensile as well as torsional loads throughout physiological motion [1]. These loads are distributed evenly over the surface of the connected vertebral body [5].

Intervertebral discs are composed of an inner gelatinous nucleus pulposus, surrounded by the annulus fibrosis around its radial periphery. Thin cartilaginous endplates lie on the cranial and caudal surfaces of the disc that mate it to adjacent vertebral bodies (see Figure 1.4A).

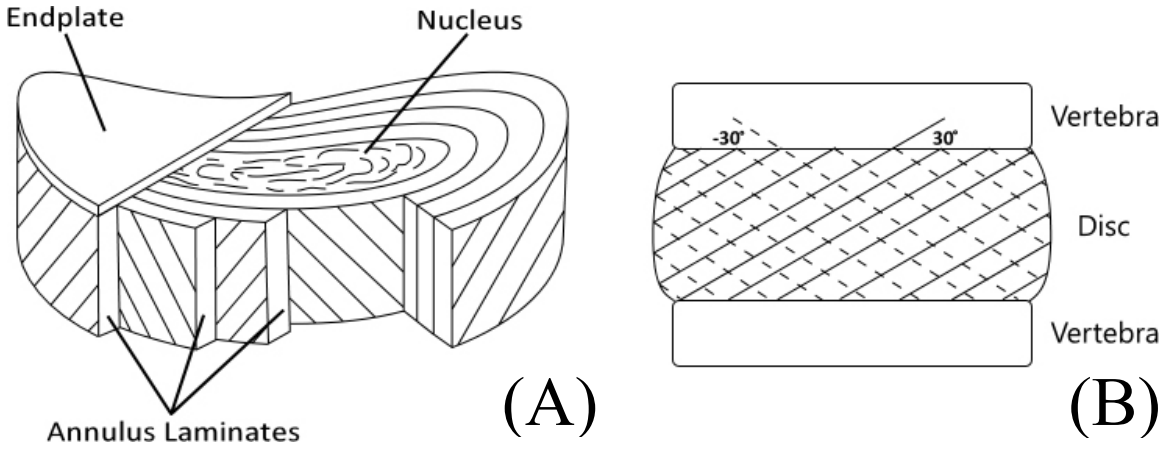

Figure 1.4: Schematic of the human intervertebral disc. (A). Layers of fibrous annulus tissue enclose an inner gelatinous nucleus. Endplates lie on the cranial (shown) and caudal (not shown) surfaces, connecting to the vertebral body. (B). Adjacent layers of annular lamellae contain aligned collagen fibers alternate between ±30° with respect to the disc plane.

The nucleus pulposus contains cells suspended in an extracellular matrix composed of proteoglycan macromolecules, water, type II collagen fibers, and elastin fibers [5]. It is highly hydrated, with water content ranging from 70-90% [1]. This high water content causes the nucleus to act hydrostatically when compressively loaded, distributing pressures evenly to the surrounding annulus and endplates [6].

The annulus fibrosis encloses the nucleus and consists of concentric layers (lamellae) of fibrous tissue containing highly aligned type I collagen fibers that span the disc space, providing resistance to tensile loads from bending and rotational movements (Figure 1.4). The fibers run diagonally, at ±30° to the transverse disc plane, and alternate with each layer so that there is 120° between fibers of adjacent lamina (Figure 1.4B) [1]. These fibers are encased in a ground substance containing water and mucopolysaccharide protein complexes [7]. Fibers along the outer periphery of the annulus are connected to the vertebral bodies to better resist tensile and torsion loads, while the fibers located more interiorly are attached to the endplates [1].

Cranial and caudal surfaces of the disc contain thin, avascular hyaline cartilage endplates that mate the disc to the vertebral body. The endplates absorb hydrostatic pressure from the disc during physiologic movements and prevent the nucleus from protruding into the vertebral body [8]. Further, the endplates supply the disc with nutrients from vasculature of the vertebral bone through diffusion [9].

1.1.3. Ligaments of the lower cervical spine

Ligaments are a dense fiberous connective tissue composed of cells, collagen and elastic fibers, proteoglycans, and water [10]. They provide passive stability for the spinal column, absorb energy during trauma, and allow the spine to move safely; preventing excessive motion that would harm the spinal cord [1]. The ligament is most effective when loaded along the axis of the fibers, resisting tension and buckling in compression. During normal spinal motion, multiple ligaments work in conjunction so that at least one ligament is actively resisting tension.

Six ligaments connect the vertebrae of the lower cervical spine (Figure 1.5). The anterior longitudinal ligament (ALL) is a continuous strip connected to the anterior aspect of the vertebral body and disc that extends the length of the lower cervical spine in the cranial-caudal direction. Similarly, the posterior longitudinal ligament (PLL) runs along, and is connected to, the posterior surface of the vertebral body and the disc. The ligamenta flava (LF) is located within the vertebral foramen and attaches the lamina of adjacent vertebra. Capsular ligaments (CL) surround each pair of articular processes, enclosing each facet joint. The interspinous ligament (ISL) connects the spinous process of adjacent vertebrae, and the supraspinous ligament (SSL) runs along the posterior tip of the spinous process, between adjacent vertebrae.

This thesis is focused on characterizing the mechanical behavior of the ALL, the PLL, and the LF, which are the primary ligaments of the lower cervical spine [11]. Additionally, the longitudinal ligaments (ALL and PLL) and the LF are interesting to study because they have different morphologies, and thus possess unique mechanical properties that are conducive to the motion/resistance required by the ligament. The ALL and PLL have similar structures, consisting

of mostly parallel collagen fibers, aligned along the axis of the spine, with the deep fibers interwoven with the outer layer of the annulus [12-14]. The dry weight of the PLL in the cervical spine was shown to contain 67.1% collagen fibers and 5.9% elastin fibers [15]. Conversely, the LF has been shown to contain a two-to-one elastin-to-collagen ratio [16].

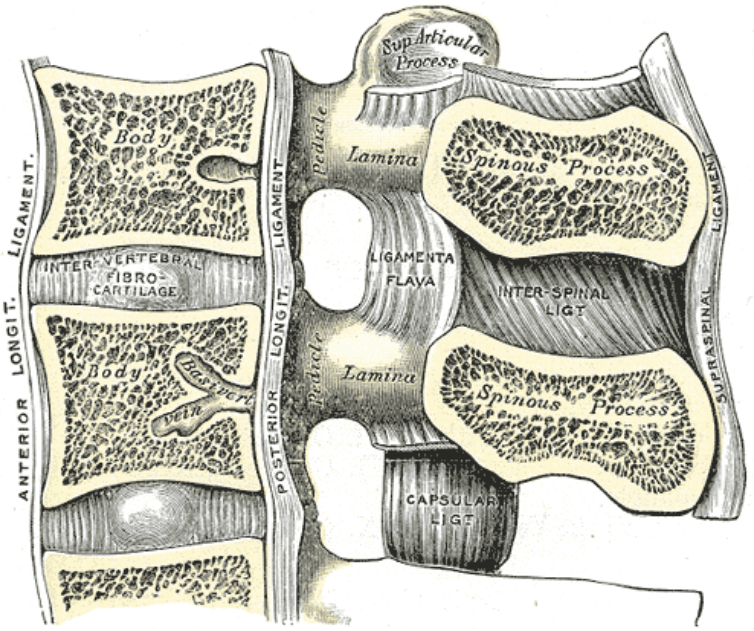

Figure 1.5: Sagittal cut view depicting the six ligaments of the spine. Adapted from Gray's Anatomy [2].

1.2. Viscoelastic Theory Background

Viscoelasticity describes the time-dependent and the history-dependent response of a material to an applied disturbance. All biological tissue displays viscoelastic behavior [17], especially soft tissue (e.g., ligaments). Viscoelastic phenomena commonly exhibited by biological tissues include: creep, stress relaxation, hysteresis, and strain-rate dependent stiffness (Figure 1.6). Creep describes the continued deformation of a body over time when it is subjected to a constant load. Stress relaxation describes the reduction in the induced stress within a body over time when it is subjected to a constant displacement. Hysteresis depicts the energy lost during cyclic loading, and appears as different loading and unloading curves on a stress-strain plot of the loading cycle. When a viscoelastic body is loaded at increasing rates of strain, the effective stiffness of the

material will increase. This thesis investigates the cyclic and stress relaxation phenomena of the ALL, PLL, and LF in the subaxial cervical spine.

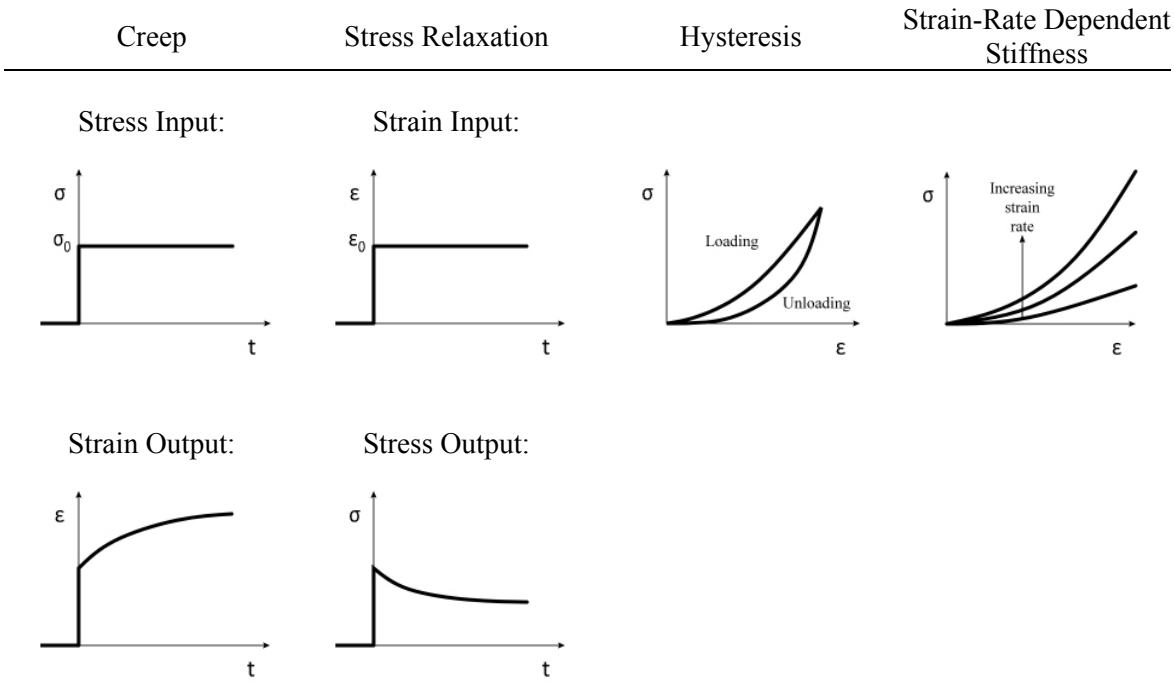

Figure 1.6: Viscoelastic phenomena commonly attributed to biological tissue. Creep: continued deformation with time following a step increase in strain. Stress relaxation: continued relaxation with time following a step increase in strain. Hysteresis: energy lost causing difference in loading and unloading curves. Strain-rate dependent stiffness: apparent material stiffness increases with increasing strain rate.

1.2.1. Linear viscoelasticity

Stress relaxation

Linearly viscoelastic materials must satisfy two conditions: the stress must be proportional to the strain at a given time and linear superposition must hold [18]. Hence, a linearly viscoelastic material must satisfy the following mathematical relationships:

$$\sigma[c\varepsilon(t)] = c\sigma[\varepsilon(t)] \tag{1}$$

$$\sigma[\varepsilon_1(t) + \varepsilon_2(t - t_1)] = \sigma[\varepsilon_1(t)] + \sigma[\varepsilon_2(t - t_1)] \tag{2}$$

where (for stress relaxation) ε is the strain input, c is a constant scalar, and σ is the stress output [18]. Graphical representations of equations (1) and (2) are shown in Figure 1.7. Equation (1) states that the stress relaxation curve resulting from any magnitude of input strain can be scaled

by c to match the relaxation curve resulting from an input strain that is scaled by c (Figure 1.7A). It follows from the relationship in equation (1) that the rate of relaxation (i.e., the slope of the relaxation curve) is independent of the magnitude of the input strain in a linear viscoelastic material. Furthermore, equation (2) states that the stress output resulting from the addition of two different strain inputs occurring at different times $\sigma[\varepsilon_1(t) + \varepsilon_2(t - t_1)]$ is equal to the sum of two separate stress outputs $\sigma[\varepsilon_1(t)]$ and $\sigma[\varepsilon_2(t - t_1)]$ that result from the same strain inputs (ε_1 and ε_2) acting separately (Figure 1.7B) [18]. This is the linear superposition that is imposed by equation (2).

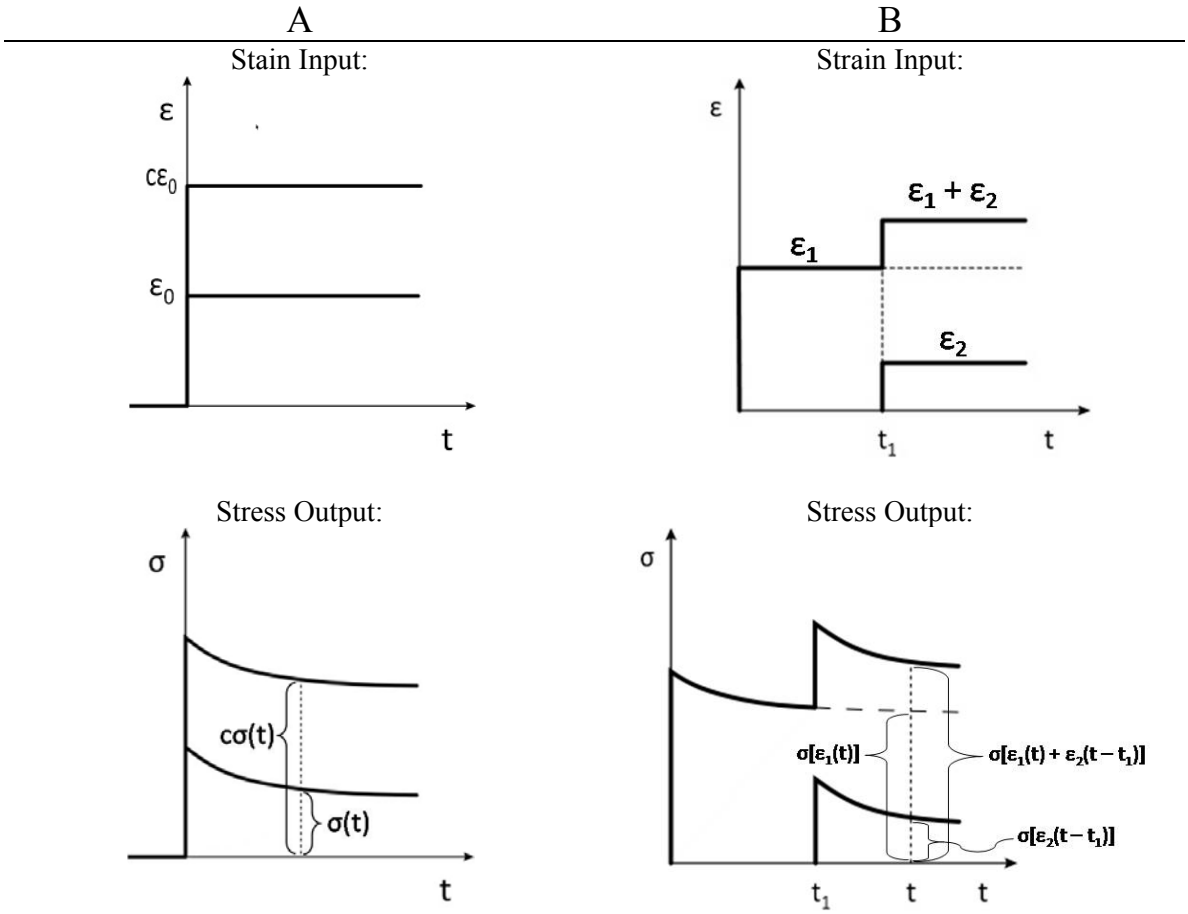

Figure 1.7: Stress relaxation behavior of a linear viscoelastic material.

The derivation of the constitutive relationship for a linear viscoelastic material utilizes the Boltzman superposition principal, which (in the case of stress relaxation) states that the current stress is a result of the complete strain history [17-19]. This thesis will follow the method of

derivation provided by [18]. In a stress relaxation test, a step increase in strain is applied to the body and the resulting stress is measured over time (see Figure 1.6 on page 8). For a single step input of strain:

$$\varepsilon(t) = \varepsilon_0 H(t) \tag{3}$$

where ε_0 is the input strain magnitude and $H(t)$ is the Heaviside step function defined as:

$$H(t) = \begin{cases} 0 & for \quad t < 0 \\ \frac{1}{2} & for \quad t = 0 \\ 1 & for \quad t > 0 \end{cases} \tag{4}$$

the resulting stress output is:

$$\sigma(t) = \varepsilon_0 E(t) \tag{5}$$

where $E(t) = \sigma(t)/\varepsilon_0$ is the relaxation function. A series of such step increases in strain can be used to describe any arbitrary strain input profile. For r step increases in strain equation (3) can be written as:

$$\varepsilon(t) = \sum_{i=1}^{r} \Delta\varepsilon_i \, H(t - \tau_i) \tag{6}$$

where $\Delta\varepsilon_i$ is the change in magnitude of the *i*th step in strain that occurs at time τ_i. From equation (5), the resulting stress output (using the Boltzmann superposition principal) is:

$$\sigma(t) = \sum_{i=1}^{r} \Delta\varepsilon_i \, E(t - \tau_i) H(t - \tau_i). \tag{7}$$

As the number of strain steps increases to infinity, equation (7) converges to the hereditary integral:

$$\sigma(t) = \int_0^t E(t - \tau) H(t - \tau) \, d\varepsilon(\tau). \tag{8}$$

In equation (8), the term $H(t) = 1$ since $\tau > 0$ is imposed and falls within the bounds of integration. Therefore, for a differentiable strain history, the final form of the constitutive relationship for a linear viscoelastic material is given by:

$$\sigma(t) = \int_0^t E(t-\tau)\,\frac{\partial \varepsilon(\tau)}{\partial \tau}\,d\tau. \tag{9}$$

It should be noted that the relaxation function $E(t-\tau)$ for a linearly viscoelastic material is solely dependent on time and does not vary with the magnitude of applied strain.

Cyclic loading

If a linear viscoelastic material is subjected to harmonic oscillations, the strain will "lag" the stress due to internal damping within the material (Figure 1.8); a consequence of the viscous component of the material [19].

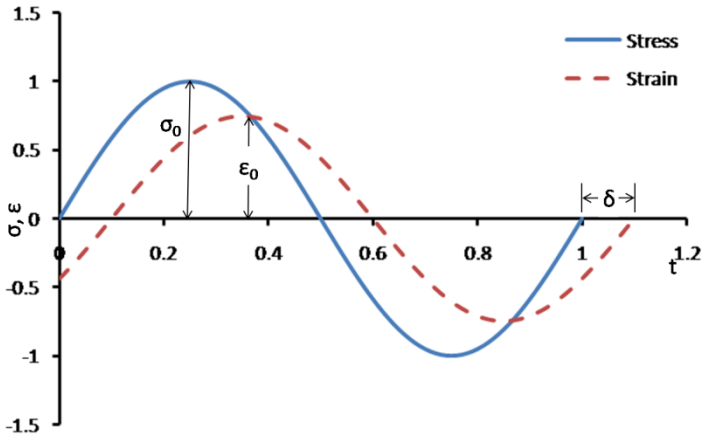

Figure 1.8: Plot of stress and strain vs time for a linear viscoelastic material subjected to cyclic loading. The strain lags the stress by δ.

A sinusoidal stress applied to a material at a frequency of ν (units of Hz) can be written as [19]:

$$\sigma(t) = \sigma_0 \sin(2\pi\nu t). \tag{10}$$

The resulting out-of-phase strain is:

$$\varepsilon(t) = \varepsilon_0 \sin(2\pi\nu t - \delta) \tag{11}$$

where δ is the phase lag between stress and strain (Figure 1.8). The tangent of the phase lag (i.e., $\tan\delta$) is called the loss tangent and is a measure of a material's internal damping [19].

Because of the phase lag between stress and strain, the dynamic stiffness (E^*) of a material can be expressed as a complex number [19]:

$$\frac{\sigma}{\varepsilon_0} = E^* = E' + E''i \tag{12}$$

with a magnitude of:

$$|E^*| = \sqrt{(E')^2 + (E'')^2}. \tag{13}$$

The storage modulus E' and the loss modulus E'' in (12) and (13) are defined as:

$$E' = |E^*|\cos(\delta) \tag{14}$$

$$E'' = |E^*|\sin(\delta). \tag{15}$$

The storage modulus represents the energy stored in the material and the loss modulus represents the energy dissipated per cycle [20].

1.2.2. Quasi-linear viscoelasticity

Quasi-linear viscoelasticity (QLV), developed by Fung [17], is a generalized form of linear viscoelastic theory in that it allows the stress developed within the material to be a function of time as well as the deformation (i.e., the stretch). Specifically, QLV modifies the relaxation function of linear viscoelastic theory to include the nonlinear stress-strain characteristics. Accordingly, the relaxation function that describes the stress history response of a material stretched from $\lambda = \frac{L}{L_0} = 1$ (where L_0 and L are the reference length and the current length, respectively) to λ is given by the separable equation:

$$K(\lambda, t) = G(t)T^{(e)}(\lambda) \tag{16}$$

where $G(t)$ is the reduced relaxation function, and $T^{(e)}(\lambda)$ is the instantaneous elastic response defined as the tensile stress resulting from an instantaneous application of stretch [17]. The reduced relaxation function is defined so that $G(0) = 1$. If the material is unstressed and unstrained prior to load (or strain) application, and the deformation begins at $t = 0$, the stress developed in a material under quasi-linear theory is given by [17]:

$$T(t) = \int_0^t G(t-\tau)\frac{\partial T^{(e)}[\lambda(\tau)]}{\partial \lambda}\frac{\partial \lambda(\tau)}{\partial \tau}d\tau. \tag{17}$$

The QLV equation (17) has been used to describe the time dependent behavior of human subaxial cervical spine ligaments [11]. Although the theory approximated the experimental data well, QLV theory contains an inherent shortcoming in that the reduced relaxation function $G(t)$ is independent of applied strain level. Therefore, the relaxation function cannot vary with different levels of strain, and thus QLV assumes the rate of relaxation is the same for all levels of strain. This presents a problem if the material displays different rates of relaxation (i.e., different relaxation curves) at different levels of strain during stress relaxation experiments. One of the objectives of this thesis is to determine the validity of applying the aforementioned QLV assumption to cervical spine ligaments when subjected to multiple magnitudes of strain.

1.2.3. Nonlinear viscoelasticity

A viscoelastic material that does not satisfy equations (1) and (2) is a nonlinear viscoelastic material. When a nonlinear viscoelastic material is subjected to a stress relaxation experiment, the rate of relaxation, and thus the relaxation modulus, is dependent on the magnitude of the applied strain [19].

Recently, nonlinear viscoelastic behavior has been reported for rat [21] and rabbit medial collateral ligaments [22], and for porcine digital flexor tendon [23]. These studies suggested that these tissues be described by a single integral form of nonlinear superposition

$$\sigma(t) = \int_0^t E\big(t-\tau, \varepsilon(\tau)\big)\frac{d\varepsilon}{d\tau}d\tau, \tag{18}$$

where the relaxation function $E(t, \varepsilon)$ is dependent on both time and the applied strain.

1.3. Mechanical Properties of Spinal Ligaments

1.3.1. Nonlinear elastic behavior

An early study by Nachemson and Evans revealed a nonlinear, sigmoidal, stress-strain relationship for human lumbar LF [16]. Similar behavior was later reported for the human ISL [24] and lumbar longitudinal ligaments [25]. The reported ligament behavior, shown in Figure

1.9, consisted of an initial nonlinear toe region followed by a linear ramp region, and subsequently ending with a failure region. From Figure 1.9, one can see that there is little resistance to motion at small deformations until a defined point where the resistance greatly increases until failure. A detailed study by Panjabi et al. related the shape of the ligament stress-strain curve to physiologic spinal movements [26]. They concluded that the nonlinear ligament behavior allows spinal mobility with minimum expenditure of muscle energy at small strains, while the high stiffness of the ligament at larger strains protects the spinal cord and nerves by offering an increased resistance to motion and energy absorbing capacity. Subaxial cervical spine ligaments have been shown to display the same nonlinear stress-strain behavior (Figure 1.9) as that reported for lumbar ligaments [27-29].

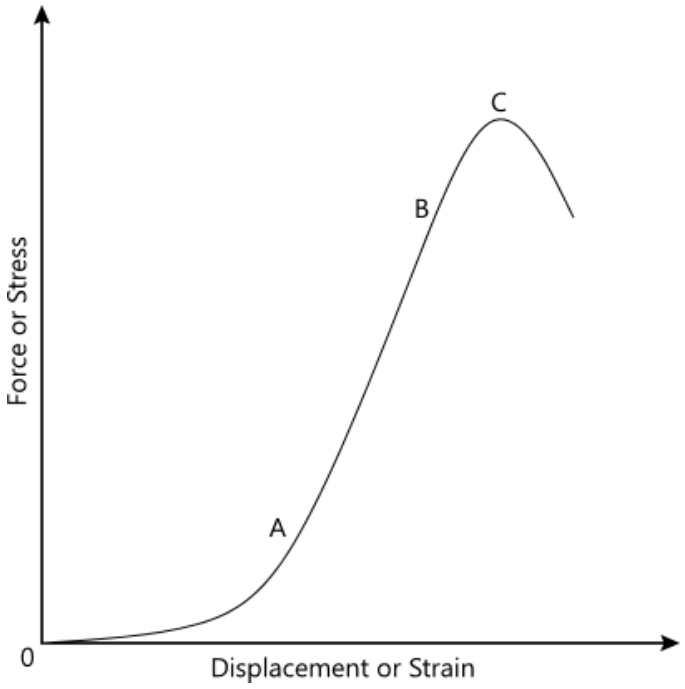

Figure 1.9: Representative stress-strain (or force-displacement) curve for spine ligaments. Spinal ligaments have an initial nonlinear toe region (0-A), followed by a linear ramp (A-B) that precedes ultimate failure (C).

Researchers have attributed this nonlinear stress-strain behavior to the microstructure of these ligaments. Ligaments contain varying levels of collagen fibers that are initially crimped, but become straightened as the ligament is deformed, thus providing more resistance to further

deformation [14, 30-32]. Using x-ray diffraction to view the collagen fiber orientation and recruitment of lumbar spine ligaments, Hukins et al. determined that the collagen fibers in the longitudinal ligaments (ALL and PLL) in the original, unloaded, state had a three-dimensional "wavy" structure [14]. As the longitudinal ligaments were stretched, the collagen fibers became straightened and more aligned to the ligament axis. Consequently, the longitudinal ligaments are compliant at small strains and become stiffer as the fibers straighten [14, 32]. Conversely, the LF has a high elastin-to-collagen ratio, with the collagen fibers showing little preferential orientation until the ligament is significantly stretched [14, 16, 32]. A higher proportion of the low stiffness elastin fibers makes the LF more compliant, allowing it to lengthen considerably more than the longitudinal ligaments under similar loads [28, 29, 33]. Large elastic deformation of the LF is required under flexion of the spine. Thus, the unique microstructure structure of these spinal ligaments (i.e., the ALL and PLL versus the LF) produce specific stress-strain curves that are conductive to the motion required by the spine [26].

1.3.2. Viscoelastic behavior

Several studies have observed viscoelastic behavior of spine ligaments. Nachemson and Evans performed cyclic and stress-relaxation experiments on human lumbar LF and reported that the ligament displayed nonlinear viscoelastic behavior; the time-dependent properties of human LF were dependent on the level of applied stress [16]. Waters and Morris reported stress-relaxation behavior of human ISL at multiple spine levels [24]. Hysteresis phenomena were observed for various spinal ligaments (ALL, PLL, LF, ISL+SSL, and intertraverse ligaments), at spine levels ranging from C3-C4 to L5-S1, by Chazal and colleagues [34]. Yoganandan et al. determined that the tensile strength, stiffness, and energy absorbing capacity of cervical spine ALL and LF were dependent on the rate of applied loading [29]. Interestingly, this study also reported that while the failure loads increased with increasing strain rate, the ligament elongation at failure was not strain rate dependent [29]. Hukins et al. reported that human lumbar longitudinal ligaments (ALL and PLL) displayed stress-relaxation and hysteresis behavior [14]. Yahia et al. observed hysteresis,

stress relaxation and stepwise load relaxation behavior of human lumbar ISL+SSL ligament complexes [35].

Few researchers, however, have attempted to develop a mathematical model to describe the viscoelastic behavior of spinal ligaments. An in-depth study by Little and Khalasa tested human lumbar CL under a uniaxial ramp-hold (stress relaxation) and a cyclic protocol in the directions parallel and perpendicular to the dominant collagen fiber orientation [20]. Under stress-relaxation, it was reported that rate of relaxation of the human lumbar CL was dependent on the applied strain parallel to the collagen fibers, and was independent of applied strain when extended in a direction perpendicular to the collagen fibers. An equation relating the strain level and rate of relaxation were reported. Also, these researchers reported that the dynamic moduli (E^*, E', and E'') of the human lumbar CL, in a direction parallel to the collagen fiber orientation, were dependent on the cyclic strain amplitude. Furthermore, a recent study by Lucas et al. [11] examined the force-relaxation behavior of multiple levels (C3-C4, C5-C6 and C7-T1) of human cervical spine ligaments (ALL, PLL, and LF) by conducting a ramp-hold protocol at magnitudes of 25% and 50% engineering strain. They fitted the 50% strain magnitude force-relaxation experimental data using a QLV model, and validated their results by using this model to predict both the 25% strain magnitude force-relaxation behavior and a cyclic load with an amplitude of 50%. Using the coefficients determined by their QLV mathematical model, Lucas et al. found statistically significant differences in the QLV fitting parameters that were based on ligament type, cervical spine level and gender.

The QLV theory used by Lucas et al. to model viscoelastic behavior of spine ligament was shown to accurately model the relaxation behavior at two levels of engineering strain (25% and 50%) [11]. However, the QLV model is limited in that its relaxation function is independent of the strain magnitude. Several publications have reported that the rate of relaxation, and hence the reduced relaxation function, of collagenous tissue is dependent on the magnitude of applied strain. As stated earlier, nonlinear viscoelastic behavior has been reported for rat medial collateral

ligaments (MCL) [21], rabbit MCL [22], and porcine digital flexor tendon [23]. More importantly, Nachemson and Evans [16] and Little and Khalasa [20] have reported nonlinear viscoelastic behavior of human spine ligaments.

1.4. Motivation for Current Study

Ligaments play an important role in spine biomechanics. Therefore, in order to understand and accurately model spine biomechanics, a precise understanding of the mechanical properties of ligaments is requisite. In-depth knowledge of spine ligament mechanics is also essential in the development of accurate computational models to simulate spinal behavior. Finite element (FE) analysis, for example, is a commonly used mathematical technique to model spinal behavior that requires the input of accurately defined material properties [28].

In vivo, spinal ligaments are subjected to various magnitudes of strains throughout their physiologic loading regimes. Therefore, it is important to understand the viscoelastic behavior of spine ligaments at multiple magnitudes of strain. To the author's knowledge, there is no published experimental data which examines the dependence of viscoelastic behavior, if any, on the magnitude of applied strain for cervical spine ligaments. Hence, there exists no experimental validation for or against the use of QLV to model subaxial spine ligaments. Furthermore, there is a lack of published data concerning the cyclic viscoelastic properties of human spinal ligaments in the current literature. Experimentally determining both the cyclic and stress-relaxation viscoelastic behavior of spinal ligaments are important in the development of accurate mathematical representations of this behavior, which can be used to predict global spine mechanics. The objective of this thesis is to determine the effect of multiple magnitudes of strain on the viscoelastic properties of subaxial cervical spine ligaments (ALL, PLL and LF) when subjected to stress relaxation and cyclic loading.

1.5. Specific Aims

In order to achieve the stated objective, the following specific aims of this thesis are proposed:

- Perform stress relaxation experiments at multiple magnitudes of strain to:
    - determine if the rate of relaxation is dependent on the magnitude of applied strain (indicating nonlinear viscoelastic behavior) for each ligament type (ALL, PLL LF).
    - determine if the initial stress induced by the relaxation test is dependent on the magnitude of applied strain for each ligament type.
    - determine if the percent of stress relaxation from the initially induced stress is dependent on the magnitude of applied strain for each ligament type.
    - compare the stress relaxation behavior of the different ligament types .
- Perform cyclic loading at multiple levels of strain and frequency to:
    - determine the effect of strain level on the cyclic mechanical properties (E^*, E', E'', and tanδ) based on ligament type.
    - determine the effect of frequency on the cyclic mechanical properties (E^*, E', E'', and tanδ) based on ligament type.
    - compare the cyclic mechanical properties of the different ligament types.
- Determine the validity and applicability of the QLV theory by:
    - fitting the experimental stress relaxation data to QLV theory and performing a statistical analysis of the fitted parameters to determine any strain magnitude dependence of the reduced relaxation function.

2. MATERIALS AND METHODS

2.1. Experimental Design/Overview

The methods in this thesis were designed to characterize the stress relaxation and cyclic viscoelastic properties of human subaxial cervical spine ligaments at multiple magnitudes of strain and cyclic frequencies. Three ligaments (ALL, PLL, LF) were isolated from the surrounding tissue at the C5-C6 level of cadaveric cervical spines and dissected to form bone-ligament-bone preparations. Each preparation was potted in polymethylmethacrylate (PMMA) that allowed them to be mounted to a servo-hydraulic testing machine. Nondestructive dynamic mechanical analysis (DMA) was performed at two strain amplitudes and four frequencies to determine the effect of strain magnitude and frequency on the cyclic viscoelastic properties of these ligaments. Stress-relaxation experiments were subsequently conducted at multiple magnitudes of physiologic strain to investigate the effect of strain level on the stress relaxation behavior of these ligaments. Quasi-linear viscoelastic theory was fitted to the experimental stress relaxation data to determine the validity and applicability of this theory to model the relaxation behavior of these ligaments. All experiments were conducted in an environmental chamber that was filled with physiologic saline heated to body temperature (37 °C).

2.2. Specimen Preparation

2.2.1. Specimen dissection

Eight C5-C6 vertebra-disc-vertebra functional spinal units (FSUs) were isolated from human cadaver cervical spines (mean age 59 ± 9.2 years; 2 females/6 males) by cutting through the adjacent discs and ligaments at the C4-C5 level above and the C6-C7 level below. Specimen

donor information was used to eliminate any tissue with pre-existing bone or ligament pathology. Four of these FSUs were taken from cervical spines that were used in a previous non-destructive experiment [36] which loaded the full lower cervical spine (C3-C7) in its physiologic range. The remaining four FSUs were taken from cervical spines that were used solely for the experiments in this thesis.

After isolating the C5-C6 level, all surrounding non-osteoligamentous tissue was carefully removed from the FSU. The posterior arch of the FSU was then separated from the anterior vertebral body by carefully sawing through the pedicles of the adjacent vertebrae in the cranial-caudal direction (Figure 2.1B). On the separated posterior arch, the LF was isolated into bone-ligament-bone (B-L-B) preparations by carefully transecting the SSL and the ISL, and by cutting the CLs to disarticulate the facet joints. The LF was easily distinguished from the surrounding tissue because of its relatively large size and yellow color [33]. The ALL and PLL were separated into B-L-B preparations by sawing through the mid-coronal plane of the anterior vertebral bodies of the FSU (Figure 2.1C). Then, approaching from this newly cut surface, the annulus fibrosis and nucleus pulposus, along with the endplates, were carefully removed from the inferior surface of the cranial vertebral body, the superior surface of the caudal vertebral body, and the ligaments using a bone curette and a scalpel. Hydration was maintained throughout specimen dissection via periodic saline spray. When ligament isolation was complete, the B-L-B preparations were wrapped in saline soaked gauze while waiting to be potted (see Section 2.2.2).

For some specimens, the lateral boundaries of the ALL and PLL were difficult to distinguish from the adjacent tissue, as reported previously [12]. To isolate the ALL, the ligament was located on the vertebral body since it was easier to discern the ligament from the osseous tissue than from the annulus fibrosis tissue. These boundaries were followed onto the annulus. The annulus tissue was then carefully removed from the lateral ligament boundaries using a scalpel and a bone curette.

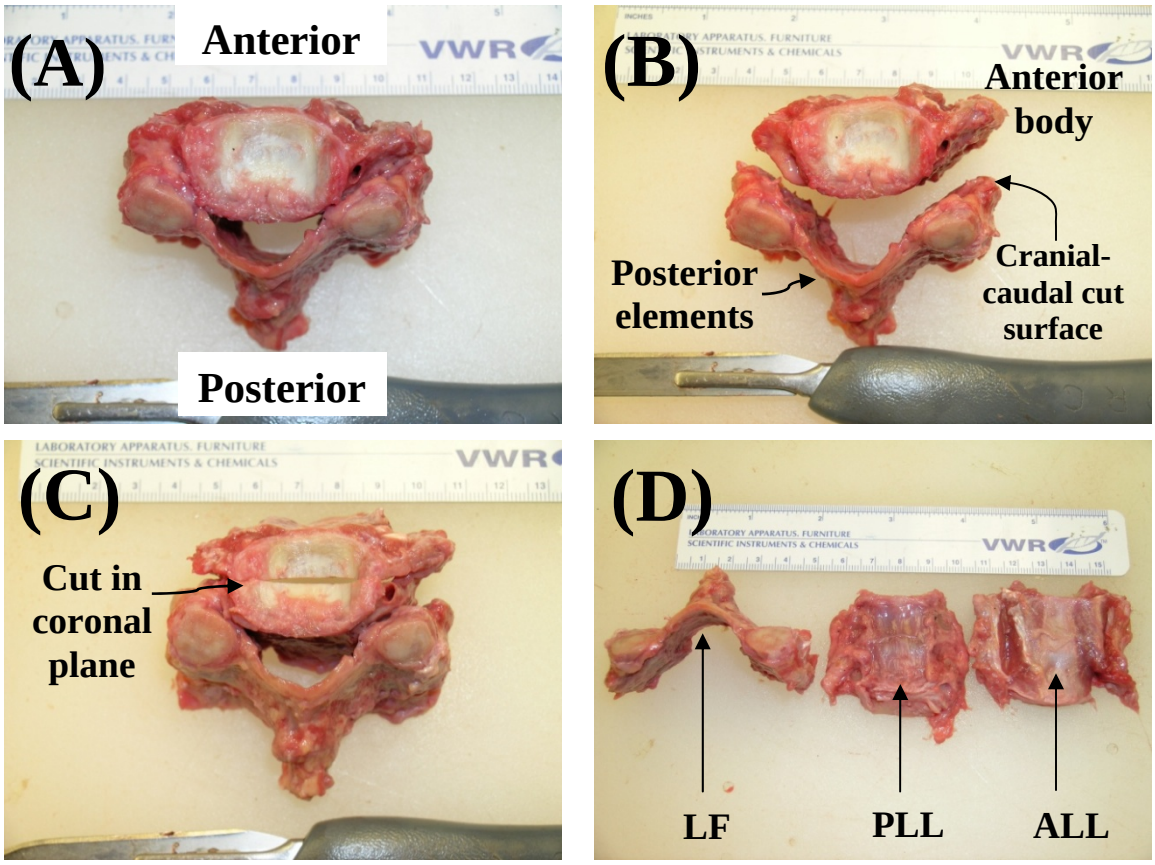

Figure 2.1: Photographs of the dissection process. (A) Cranial-to-caudal view of an intact C5-C6 FSU. (B) Separation of the posterior elements from the anterior body to isolate the LF. (C) The anterior body was cut in its coronal plane to separate the ALL and the PLL. (D) The separated segments containing the LF, PLL, and ALL.

Furthermore, fibers from the ALL and PLL are intertwined with the annulus fibrosis [13], with the PLL fibers extending more broadly around the circumference of the intervertebral disc [37] than the ALL. This made identification of the boundary between the annulus and the longitudinal ligaments, especially the PLL, difficult for some specimens. Consequently, attempts to separate the longitudinal ligaments from the annulus fibrosis were ceased once the annulus tissue was no longer readily removed with the bone curette to avoid damaging the ligament.

The PLL was more difficult to distinguish than the ALL because of the dura matter (a membrane that surrounds the inside surface of the neural arch). In some specimens, the dura matter was strongly attached to the PLL while in others it was easily removed. For the specimens in which the spinal dura was strongly attached to the PLL, tweezers were used to gently pull the dura matter away from the PLL while a scalpel, with the cutting edge facing towards the dura

matter, was cautiously used to separate the dura matter away from the PLL. The difficulties of distinguishing the PLL from the dura matter have been previously reported [37, 38].

Some ligaments could not be used in this experiment because they were either damaged during dissection for this thesis or during the preparation of previous experiments [36]. As a result, the final sample size was $n = 8$ for the ALL, $n = 8$ for the PLL, and $n = 6$ for the LF.

2.2.2. Specimen potting

Following isolation of the B-L-B preparations, the cranial and caudal vertebrae were potted in polymethylmethacrylate (PMMA) bone cement to be attached to custom built fixtures that mounted the specimen to the testing machine. Ligaments were wrapped in saline soaked gauze to maintain hydration during the potting procedure. A specific potting procedure was followed to ensure consistent physiologic alignment of the vertebral segments for all B-L-B preparation.

Wood screws were affixed to the superior surface of the cranial vertebra and to the inferior surface of the caudal vertebra in the case of the ALL and PLL preparations, and to the superior and inferior surfaces of the articulating processes for the LF preparations (Figure 2.2). Theses screws provided a more secure attachment to the PMMA than bone alone.

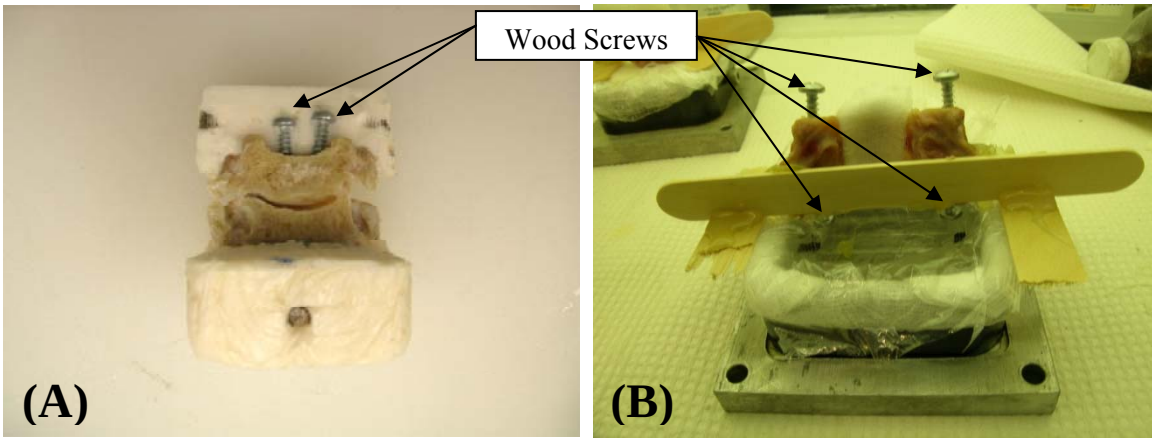

Figure 2.2: (A) Cut away of the PMMA showing cranial wood screw placement for the longitudinal ligaments. Caudal placement (not shown) was similar. (B) Wood screw placement for the LFs.

Wooden tongue depressors were used to provide removable support for the specimens while being potted and also ensured consistent ligament alignment. For the longitudinal ligaments, one wooden tongue depressor was hot glued across the two vertebrae on the surface of

the coronal cut (see Figure 2.1C) of the B-L-B preparation (Figure 2.3). Care was taken so that the hot glue did not come into contact with the ligament. Two more tongue depressors were glued perpendicular to the previously affixed tongue depressor. Perpendicular alignment was achieved by using a small square during gluing.

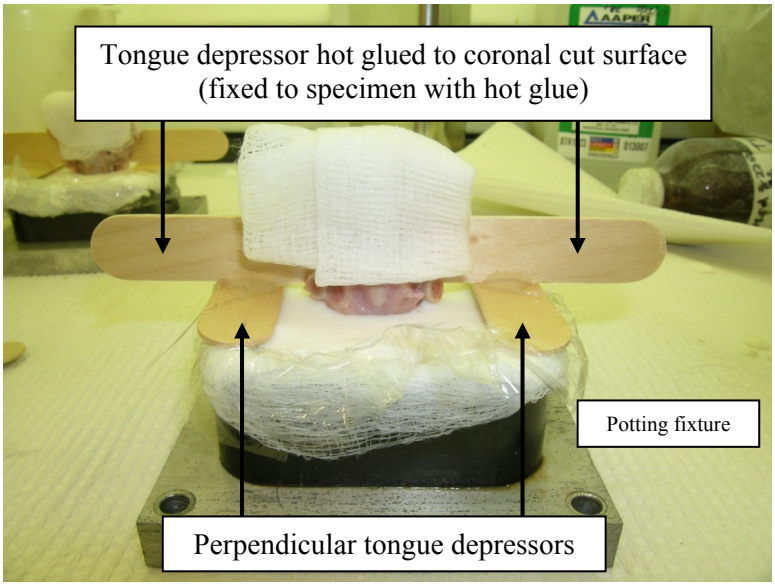

Figure 2.3: Tongue depressor structure for the longitudinal ligaments used to aid in the potting process.

A similar tongue depressor construct, shown in Figure 2.4, was used to hold and align the LF B-L-B preparations during potting. In this case, a tongue depressor was hot glued across the adjacent posterior vertebral elements on the surface created by the cranial-caudal cut shown in Figure 2.1B. The LF specimens had to be oriented so that the PMMA did not interfere with the B-L-B preparation movement. Hence, the caudal vertebral element was placed on the potting fixture so that it was supported by the affixed tongue depressor and the spinous process while two more tongue depressors were hot glued underneath the affixed tongue depressor (Figure 2.4B).

Once the glue was fully cured, PMMA was mixed and poured into the custom fixtures to set the caudal vertebral bone elements.

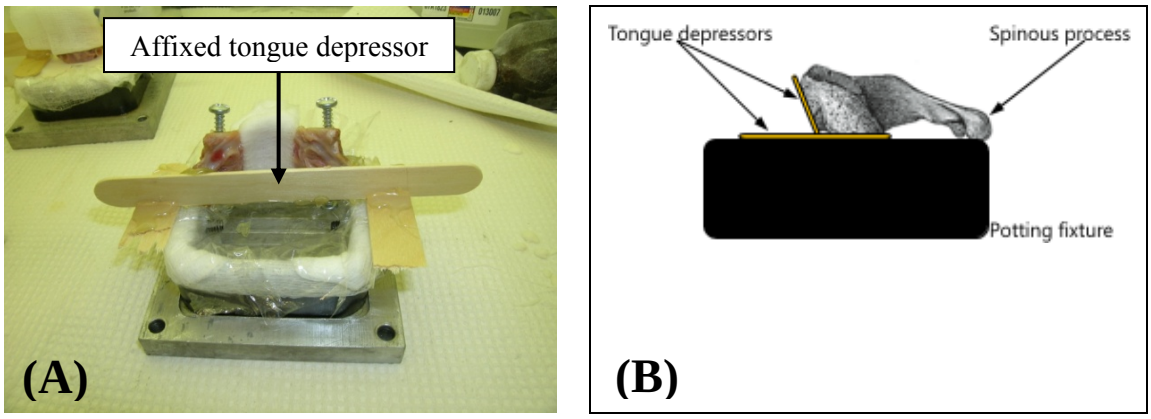

Figure 2.4: (A) Tongue depressor construct for the LFs used to aid in the potting procedure. (B) Side view of vertebral orientation for potting (cranial vertebra not shown in drawing).

After the PMMA was set for the caudal vertebral elements, the potting fixture was inverted and the cranial vertebral elements of the B-L-B preparations were potted using the construct shown in Figure 2.5. Tongue depressors remained attached to maintain alignment of the vertebral elements. The nuts on the vertical threaded rods of the fixture in Figure 2.5 were used to adjust the upper potting fixture so that it was parallel to the lower fixture (verified by the use of a level on the upper potting fixture).

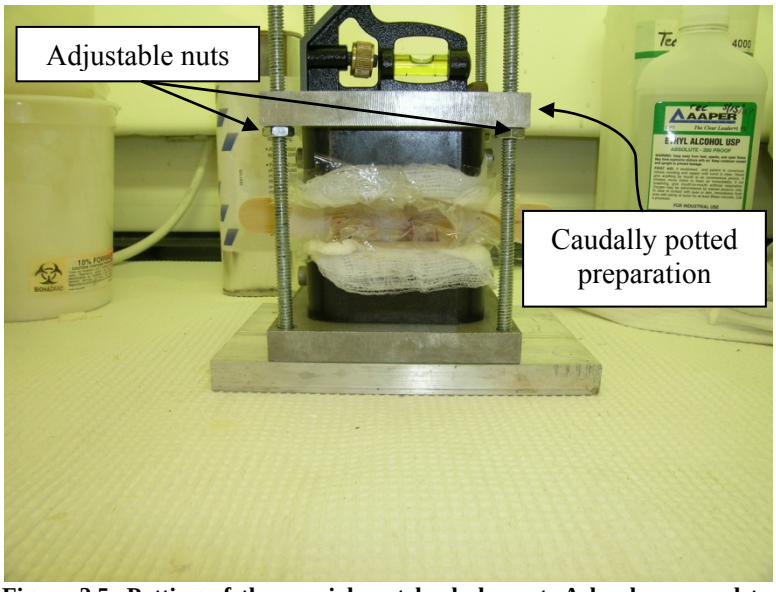

Figure 2.5: Potting of the cranial vertebral element. A level was used to ensure that the upper and lower plates were parallel.

After the PMMA was set for the cranial vertebral elements, the potted specimens were removed from their potting fixtures, wrapped in fresh saline soaked gauze, placed in a sealed bag, and frozen at -20 °C until the day of testing.

2.3. Experimental Methods

2.3.1. Experimental setup and preparation

All experiments were conducted in an environmental chamber that was filled with physiologic saline warmed to human body temperature (37 °C). Both temperature [39] and hydration [40] have been shown to affect the viscoelastic properties of ligaments. Temperature was monitored during testing via a thermocouple placed near the ligament (Figure 2.6). A digital readout displayed the temperature in real time.

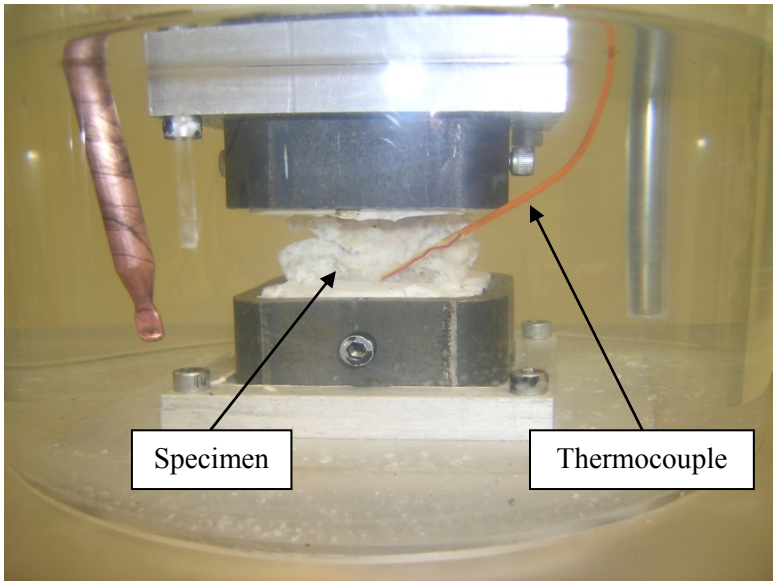

Figure 2.6: To monitor saline temperature, a thermocouple was place in close proximity of the ligament.

Figure 2.7 shows a picture of the experimental setup. The environmental chamber was attached to a translation (x-y) table that was rigidly fixed to the base of a servo-hydraulic testing machine (858 Mini Bionix II, MTS, Eden Prairie, MN). The translation table was used to ensure ligament alignment. A uni-axial load cell (500 N capacity, model 661.11B-02, MTS, Eden

Prairie, MN) was placed in the load-train between the MTS actuator and a custom upper fixture that attached to the cranially potted vertebral element.

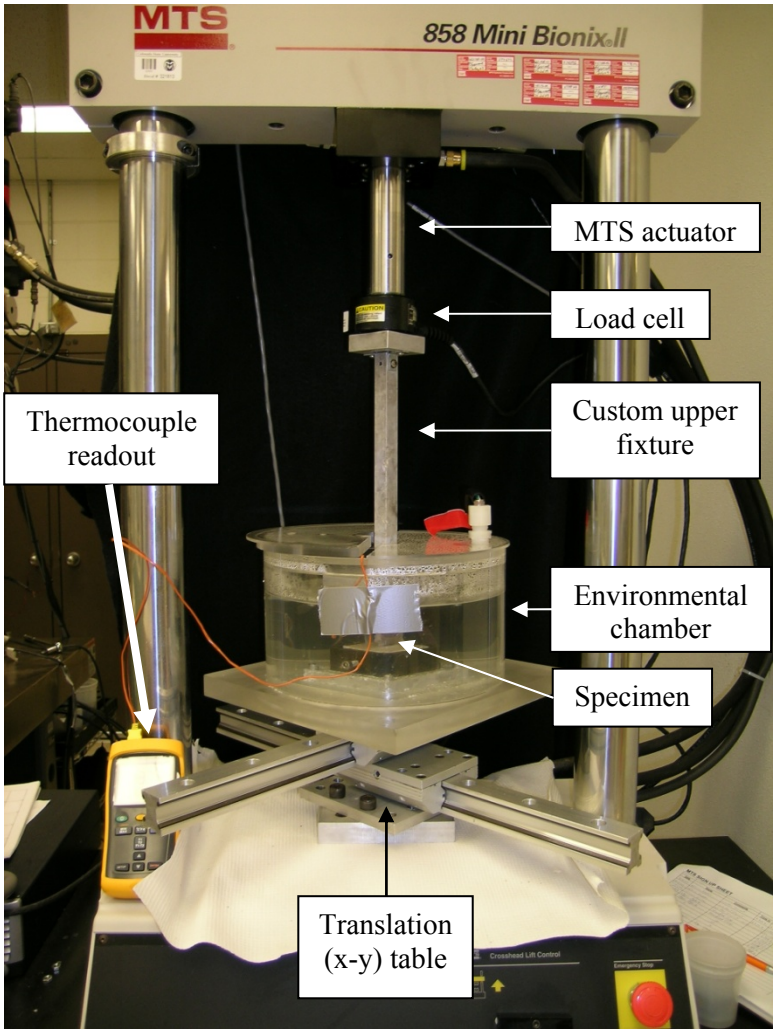

Figure 2.7: Picture of the experimental setup. An environmental chamber was attached to a translation table that was rigidly fixed to the base of the MTS.

Prior to mechanical testing, frozen specimens were allowed to gradually thaw to room temperature for at least 12 hours. After the specimen was thawed, the caudally potted vertebral element was attached to the environmental chamber. Then the upper fixture was lowered close to, but not contacting, the cranially potted vertebral element and the load cell force readout was zeroed. This process removed the weight of the custom upper fixture and accounted for the buoyancy force placed on this fixture due to the saline bath. The cranially potted vertebral element was subsequently attached to the upper fixture, and the MTS actuator was moved to the

zero force configuration for 1 hr to assure specimen equilibration. After equilibration, the cranial and caudal vertebral elements were compressed to 25 N and MTS crosshead displacement readout was zeroed. The specimen was subsequently ramped at a slow displacement rate of 0.05 mm/s to 5 N of pretension [41] and allowed to relax for 600 s. The resulting displacement was recorded and used as the reference configuration for engineering stain calculations.

2.3.2. Dynamic mechanical analysis (DMA) methods

After the specimen was fully relaxed, it was subjected to the following sinusoidal displacement regimen with a peak-to-peak amplitude of 10% engineering strain: 2 cycles at 0.001 Hz; 5 cycles at 0.01 Hz; 10 cycles at 0.1 Hz; 10 cycles at 1 Hz. Data were sampled at 2 Hz for the 0.001 Hz and 0.01 Hz frequencies, 32 Hz for the 0.1 Hz frequency and 128 Hz for the 1 Hz frequency. Another sinusoidal displacement regimen was subsequently repeated with a peak-to-peak amplitude of 15% engineering strain at the aforementioned four frequencies. The cyclic material properties determined from these procedures were the complex stiffness, the loss stiffness, the storage stiffness, and the tan δ. These properties were calculated using the software provided by the manufacturer of the testing system (Model 793.31 Dynamic Characterization, MTS, Eden Prairie, MN).

Multiple strain amplitudes and frequencies were chosen to investigate any respective strain amplitude and/or frequency dependence of the measured parameters.

2.3.3. Stress relaxation methods

Following the DMA protocol, the initial length was redefined by compressing the cranial and caudal vertebral elements to 25 N, zeroing the MTS crosshead displacement, extending the ligament a rate of 0.05 mm/s to 5 N of pretension, and allowing it to relax for 600 s. The resulting length was again recorded and used as the reference configuration. Each ligament was preconditioned by applying a sinusoidal displacement with a peak-to-peak amplitude of 10% engineering strain applied at 1 Hz for 120 cycles. The ligament was then returned to its reference

configuration for 600 s. Relaxation experiments were subsequently preformed by subjecting each ligament to a randomized application of 4%, 6%, 8%, 10%, 12%, 14%, 16%, 18%, 20% and 25% engineering strain applied at 5 mm/s. Each strain level was held for 100 s and then returned to the reference configuration for 600 s before the application of the next strain magnitude. Force, displacement, and time data were recorded at 60 Hz.

These stress relaxation experiments were performed to define the relaxation behavior of human lower cervical spine ligaments when subjected to multiple magnitudes of strain and to investigate the dependence of this behavior, if any, on the applied strain magnitude.

The range of strain magnitudes used in both the DMA procedure and the stress relaxation experiments were well below the previously reported failure strains for these ligaments [42], and includes physiologic strains that can be expected during activities of daily living, as predicted from computational modeling [43].

2.4. Measurement of Ligament Area

Recorded structural data from the DMA (e.g. storage stiffness) and relaxation procedures were converted to engineering stress by normalizing the data to the undeformed cross-sectional area, measured using the following *post hoc* digital image capture method.

Each ligament was carefully transected at its mid-substance and again at its insertion to the vertebral bone. The cut ligament was then placed on painted plastic rectangular cards that gave a high contrast between the ligament and the card color. Ligament hydration was maintained throughout the imaging procedure via periodic saline spray. Hydration kept the ligament adhered to the plastic card. Smaller ligaments (all ALLs and most PLLs) were placed under a dissection microscope, next to a ruler with 0.5 mm resolution, and a digital image was taken of the cross-section (Figure 2.8). Ligaments with dimensions that were too large to be viewed under the dissection microscope (all LFs and some PLLs) were imaged using a digital camera that was attached to a tripod and positioned, using a level, perpendicular to the cross-section (Figure 2.8).

The same plastic cards and ruler were used to image the larger ligaments. The ligament area was calculated using ImageJ software (ver. 1.41, National Institutes of Health, Bethesda, MD). Image resolution was >80 pixels/mm for the ligaments imaged under the dissection microscope and >50 pixels/mm for ligaments imaged using the digital camera attached to the tripod.

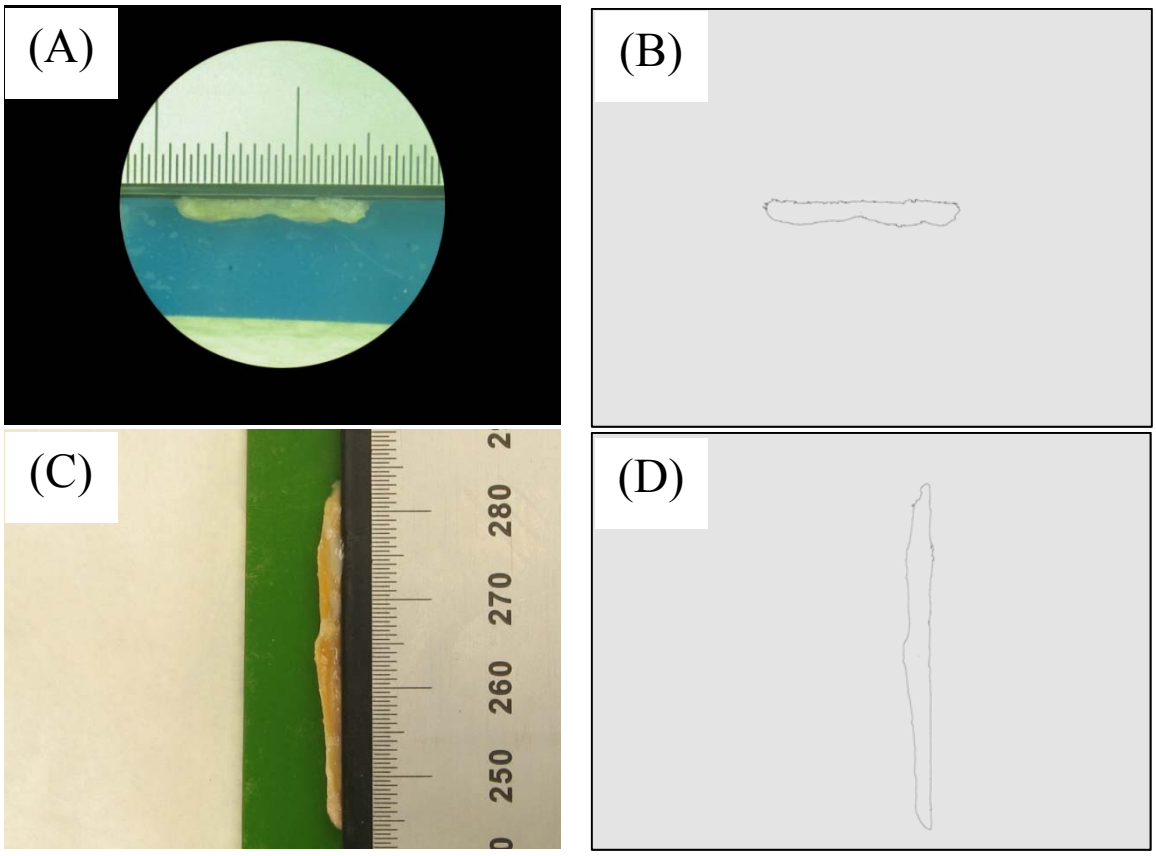

Figure 2.8: Representative digital images used to measure the cross-sectional area of the ligament. Top: (A) Ligament imaged under a dissection microscope and (B) its cross-sectional area approximated by ImageJ software. Bottom: (C) Ligament imaged without a dissection microscope and (D) its cross-sectional area approximated by ImageJ software.

2.5. QLV Fitting Procedure

The stress relaxation data for each ligament, at each strain magnitude, were fitted using QLV theory to investigate the validity and applicability of this theory to accurately model the experimental behavior of the ligaments. Data were fitted to the QLV equation (17), that was re-written in terms of engineering strain, ε, as [44]:

$$\sigma(t) = \int_{-\infty}^{t} G(t-\xi)\frac{\partial \sigma^e(\varepsilon)}{\partial \varepsilon}\frac{\partial \varepsilon}{\partial \xi}\partial \xi \tag{19}$$

where $\sigma(t)$ is the engineering stress at time t, $G(t)$ is the reduced relaxation function, $\sigma^e(\varepsilon)$ is the instantaneous elastic stress, and ξ is a dummy variable of integration. Quasi-linear viscoelastic theory assumes that $G(t)$ is independent of the applied magnitude of strain. Hence, for QLV theory to be a suitable model for the viscoelastic behavior of cervical spine ligaments, the $G(t)$ determined from physical experiments must be independent of the strain magnitude.

The reduced relaxation function $G(t)$ was approximated by the Prony series [11]:

$$G(t) = G_\infty + \sum_{n=1}^{4} G_n e^{-t/\tau_n} \tag{20}$$

where G_∞ is the long-term relaxation parameter (i.e., $G_\infty = \lim_{t\to\infty} G(t)$), and G_n is the relaxation parameter associated with the time constant τ_n. The time constants τ_1, τ_2, τ_3, τ_4, were fixed at decade values [11] of 0.1 s, 1 s, 10 s, and 100 s for all fitting procedures. Equation (20) was subjected to the constraint [11]:

$$G_1 + G_2 + G_3 + G_4 + G_\infty = 1 \tag{21}$$

The instantaneous elastic stress was approximated as:

$$\sigma^e(\varepsilon) = A(e^{B\varepsilon} - 1) \tag{22}$$

where parameters A and B are material constants [44, 45].

Since the stress relaxation experiments consisted of a finite ramping time (versus an instantaneous Heaviside step function), it is possible (and expected) for relaxation to occur during the ramping phase. To account for this, equation (19) was separated into ramping and relaxation regions (Figure 2.9) and the parameters were simultaneously fitted to both regions using a previously reported procedure [44]. During the ramping region, from $0 < t \leq t_0$, the ligament was subjected to a constant strain rate γ. The time t_0 was determined by finding the time associated with the maximum stress magnitude of the stress versus time curve. After inputting the relations $\varepsilon = \gamma t$ and $\frac{\partial \varepsilon}{\partial \xi} = \gamma$ (for $0 < t \leq t_0$), finding $\frac{\partial \sigma^e(\varepsilon)}{\partial \varepsilon}$, and moving the constants out of the integrand, the ramping region of equation (19) was written as:

$$\sigma(t: 0 < t \leq t_0, \theta)$$

$$= AB\gamma \int_0^t \left(G_\infty + G_1 e^{(\xi - t)/\tau_1} + G_2 e^{(\xi - t)/\tau_2} + G_3 e^{(\xi - t)/\tau_3} \right. \tag{23}$$

$$\left. + G_4 e^{(\xi - t)/\tau_4}\right) e^{B\gamma\xi} \partial\xi$$

where $\theta = \{A, B, G_\infty, G_1, G_2, G_3, G_4\}$.

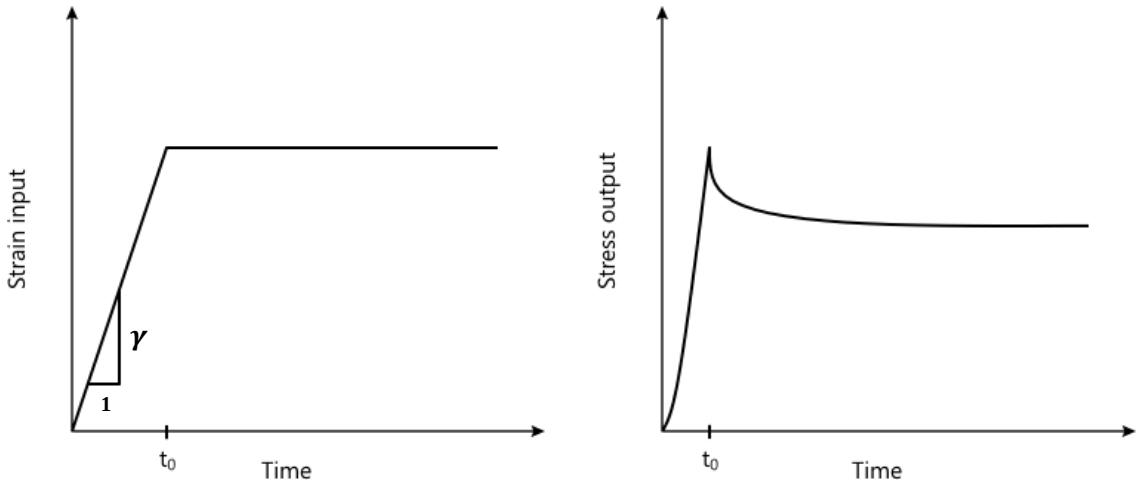

Figure 2.9: Representative strain input (left) and stress output (right) curves for the stress relaxation experiments. The stress output curve was split into a ramping region ($0 < t \leq t_0$) and a relaxation region ($t > t_0$) for the fitting procedure to account for relaxation that may have occurred during the finite ramp time. The strain rate is denoted as γ.

Equation (23) was symbolically integrated using MathCAD software (version 14.0, PTC, Needham, MA) to give:

$$\sigma(t: 0 < t \leq t_0, \theta)$$

$$= AB\gamma \left[\frac{G_\infty (e^{Bt\gamma} - 1)}{B\gamma} + \frac{G_1 \tau_1 \left(e^{Bt\gamma} - e^{-t/\tau_1}\right)}{B\tau_1\gamma + 1} + \frac{G_2 \tau_2 \left(e^{Bt\gamma} - e^{-t/\tau_2}\right)}{B\tau_2\gamma + 1} \right. \tag{24}$$

$$\left. + \frac{G_3 \tau_3 \left(e^{Bt\gamma} - e^{-t/\tau_3}\right)}{B\tau_3\gamma + 1} + \frac{G_4 \tau_4 \left(e^{Bt\gamma} - e^{-t/\tau_4}\right)}{B\tau_4\gamma + 1} \right]$$

The stress in the relaxation region of the curve is equal to the stress from the previous ramping region plus the stress history during the relaxation region. Thus, equation (24) can be recast as:

$$\sigma(t: t > t_0, \theta) = AB\gamma \int_0^{t_0} G(t - \xi) e^{B\gamma\xi} \partial\xi + AB\gamma \int_{t_0}^{t} G(t - \xi) e^{B\gamma\xi} \partial\xi \tag{25}$$

Since the strain is held constant during the relaxation region of the curve, the strain rate (γ) is equal to zero for the second term of equation (25); thus, eliminating the contribution of this term. Hence, the first term was symbolically integrated using MathCAD software to give:

$$\sigma(t: t > t_0, \theta) = AB\gamma \left[\frac{G_\infty (e^{Bt_0\gamma} - 1)}{B\gamma} + \frac{G_1\tau_1 e^{-t/\tau_1}\left(e^{t_0/\tau_1 + Bt_0\gamma} - 1\right)}{B\tau_1\gamma + 1} \right.$$
$$+ \frac{G_2\tau_2 e^{-t/\tau_2}\left(e^{t_0/\tau_2 + Bt_0\gamma} - 1\right)}{B\tau_2\gamma + 1} + \frac{G_3\tau_3 e^{-t/\tau_3}\left(e^{t_0/\tau_3 + Bt_0\gamma} - 1\right)}{B\tau_3\gamma + 1} \quad (26)$$
$$\left. + \frac{G_4\tau_4 e^{-t/\tau_4}\left(e^{t_0/\tau_4 + Bt_0\gamma} - 1\right)}{B\tau_4\gamma + 1} \right]$$

As described in [44], the experimental data for the ramping region was defined as (t_i, R_i) for $0 < t_i \leq t_0$ and the experimental data for the relaxation region was defined as (t_i, S_i) for $t_i > t_0$. The sum of squares difference between the experimental data and equation (24) was expressed as [44]:

$$f(\theta) = \sum_i [R_i - \sigma(t_i: 0 < t_i \leq t_0, \theta)]^2 \quad (27)$$

Since the data in the relaxation region was dominated by slow rate behavior, an exponentially weighted sum of squares difference was used to capture the initial, fast rate behavior of the relaxation region [46]. Thus, the weighted sum of squares difference for the relaxation region was expressed as:

$$g(\theta) = \sum_i \{w(t_i) \cdot [S_i - \sigma(t_i: t_i > t_0, \theta)]\}^2 \quad (28)$$

Where $w(t_i)$ is the weighting function defined as:

$$w(t) = e^{-t/\tau_1} + e^{-t/\tau_2} + e^{-t/\tau_3} + e^{-t/\tau_4} \quad (29)$$

All fits were performed using MATLAB software (ver. 7.8.0.347, The MathWorks, Inc., Natick MA). Parameter *A* was initially determined by fitting equation (22) to the ramping region of the experimental data using a nonlinear least-squares optimization (*lsqnonlin* MATLAB function), then fixing its value while the remaining parameters were fit using a constrained (see equation

(21)) nonlinear optimization (*fmincon* MATLAB function) that minimized the objective function $f(\theta) + g(\theta)$ [44].

The sensitivity of the fitted parameter values to the initial guesses required by the fitting algorithm was investigated by fixing each initial guess at a value of 0.001, 0.01, 0.1, 1, 10, or 100 and determining any statistical differences in the fitted parameter values. Thus, a total of six sets of fitted parameter values (one for each initial guess) for each ligament were generated for this statistical comparison. If no statistical differences were detected, the fitted parameters associated with the initial guesses that gave the minimum value for the objective function were assumed to be the global minimum [44] and, hence, these values were those reported in the Results section.

2.6. Examination of the Shape of the Relaxation Region

As stated earlier, QLV theory assumes that the shape of the stress relaxation curve is independent of strain level. Previous work has reported the stress relaxation behavior of rat [21] and rabbit [22] medial collateral ligaments by directly examining the shape of the relaxation curve, without fitting the data to QLV theory. These researchers used the power law:

$$\sigma(t) = \sigma_0 t^n \tag{30}$$

where σ_0 is the initial stress and n is the "rate" of relaxation, to describe the relaxation region of their data. Taking the logarithm of equation (30) yields a straight line with a slope n and an intercept of $\log(\sigma_0)$, i.e.:

$$\log[\sigma(t)] = \log(\sigma_0) + n\log(\mathrm{t}) \tag{31}$$

Equation (31) simplifies the interpretation equation (30) since different relaxation curve shapes are indicated by straight lines with different slopes. For QLV theory to be a suitable model for the viscoelastic behavior of cervical spine ligaments, the relaxation curves plotted on a log-log scale should have the same slope at each strain level. In order to further investigate the validity of QLV to model the viscoelastic behavior of cervical spine ligaments (in addition to the procedures in Section 2.5), experimental data in the relaxation region were fitted to equation (31) using

MATLAB (*polyfit* function) and the resulting fitted parameters (σ_0 and n) were compared across ligament types and strain levels.

2.7. Statistics

2.7.1. Ligament area statistics

The ligament cross-sectional areas of each ligament type (ALL, PLL, LF) were compared using the SAS PROC GLM (SAS Institute, Inc., Cary, NC) procedure. Statistical significance was set at $p<0.05$.

2.7.2. DMA statistics

A logarithmic transformation was used to normalize the residuals and equalize the error variance of the cyclic properties (loss modulus, storage modulus, and $\tan(\delta)$) determined from the DMA procedure. The SAS PROC MIXED procedure was performed on these transformed data to determine any strain and/or frequency dependence of these material properties for each ligament. This procedure was also used to compare the cyclic properties across ligament types. The loss modulus, storage modulus, and $\tan(\delta)$ were treated as categorical variables. Statistical significance was defined as $p<0.05$.

2.7.3. QLV fitted parameter statistics

A square root transformation was used to normalize the residuals of the A, G_∞, G_1, G_2, G_3, G_4 fitted parameters, while a logarithmic transformation was required to normalize the residuals parameter B because it exhibited a greater amount of variability than the other parameters. The SAS PROC MIXED procedure was performed on these transformed parameters to determine if the data exhibited a significant strain magnitude dependence, and to compare the parameters between the ligament types. To determine the effect of both ligament type and strain magnitude for each parameter, the strain magnitudes were treated as continuous variables and the PROC MIXED procedure regressed the parameter value on strain magnitude for each ligament type. Consequently, these data were analyzed to determine if the regression coefficients were

statistically different from zero and compared the regression coefficients across ligament types. A statistically significant slope regression coefficient indicated that the parameter value changed, and is therefore dependent on, strain magnitude. When comparing ligament types, the regression coefficient slopes were initially compared. If the slope comparison was not found to be significant, then a new regression was performed with the slope term removed from the model and the intercept regression coefficients were compared.

The SAS PROC MIXED procedure was also used to test the sensitivity of the fit to the initial guesses by comparing the parameter values computed from each initial guess. Statistical significance was defined as $p<0.05$.

2.7.4. Power law fitted parameter statistics

A logarithmic transformation was used to normalize the slope and the initial stress parameters found by fitting the data to equation (30). The SAS PROC MIXED procedure was performed on these transformed parameters to determine any strain dependence within each ligament type, and also to compare parameters between the three types of ligament. The strain dependence and ligament type comparisons were made by performing the same regression analysis as the QLV fitted parameters described above (Section 2.7.3), except in this case it was of interest to determine if a polynomial equation would provide a significantly enhanced description of the fitted parameters over the tested strain magnitudes. Therefore, a quadratic term was added to the linear regression model, and tested by SAS to determine if it was statistically different from zero. If the quadratic term was significant, it was retained in the model. If it was not found to be significant, the quadratic term was removed, and a new analysis was performed using a linear regression model. The polynomial regression model which had the highest statistically significant order was reported. Statistical significance was defined as $p<0.05$.

3. RESULTS

3.1. Ligament Geometry

The ligament initial lengths recorded under a reference tension of 5 N at the beginning of the DMA and relaxation procedures are given in Table 1.

Table 1: Initial ligament length (mean ± 1 SD) for the DMA and relaxation procedures.

	ALL (mm)	PLL (mm)	LF (mm)
DMA	3.06 ± 1.29	1.19 ± 0.69	3.31 ± 0.45
Relaxation	3.17 ± 1.34	1.31 ± 0.67	3.44 ± 0.49

The cross-sectional areas of the ligaments calculated from the digital images are given in Table 2. Figure 3.1 shows a box-and-whisker plot of the measured cross-sectional areas of the ligaments. The cross-sectional areas of the ALL and PLL were not statistically different ($p=0.7504$), while the LF had a larger cross-sectional area than both the ALL ($p<0.0001$) and the PLL ($p<0.0001$).

Table 2: Ligament cross-sectional area (mean ± 1 SD).

	ALL	PLL	LF
Area (mm^2)	30.23 ± 6.33	31.92 ± 9.67	86.15 ± 15.26

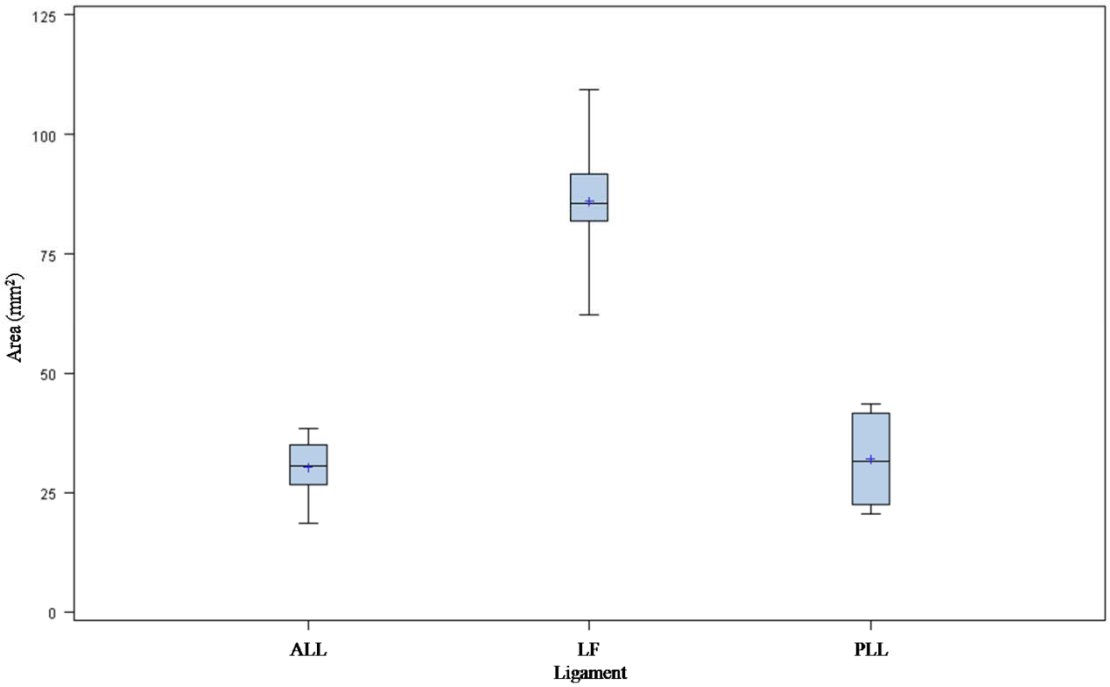

Figure 3.1: Box-and-whisker plot of the ligament cross-sectional areas, calculated from digital images of the ligament cross-sections.

3.2. DMA Results

DMA was performed on the ALL, PLL, and LF at two engineering strain amplitudes (10% and 15%) and four frequencies (0.001 Hz, 0.01 Hz, 0.1 Hz, 1 Hz) to determine the effect of strain level, frequency, and ligament type on the cyclic viscoelastic properties. The loss angle (δ), storage stiffness, and loss stiffness were determined for each experimental variant. The tangent of the loss angle, $\tan(\delta)$, was calculated to provide a measure of the internal damping of the ligament [19]. The storage stiffness and loss stiffness were normalized by the undeformed (reference configuration) cross-sectional area of the ligament to determine the intrinsic storage modulus (E') and loss modulus (E''), respectively, in order to quantify corresponding measures of the elastic (energy stored) and the viscous behavior (energy dissipated) of the ligament [20].

Tan delta

Statistical analysis indicated a significant effect of strain amplitude ($p<0.0001$), frequency ($p<0.0001$), and ligament type ($p=0.0037$) with respect to the $\tan(\delta)$ parameter.

The effect of strain amplitude is shown in Figure 3.2 for the ALL, Figure 3.3 for the PLL, and Figure 3.4 for the LF. For all ligaments, $\tan(\delta)$ at the 15% strain amplitude was significantly reduced compared to the 10% strain amplitude at 0.001 Hz frequency (p-values are indicated on respective figures). No statistically significant differences were observed for any of the other frequencies for each ligament type ($p>0.05$).

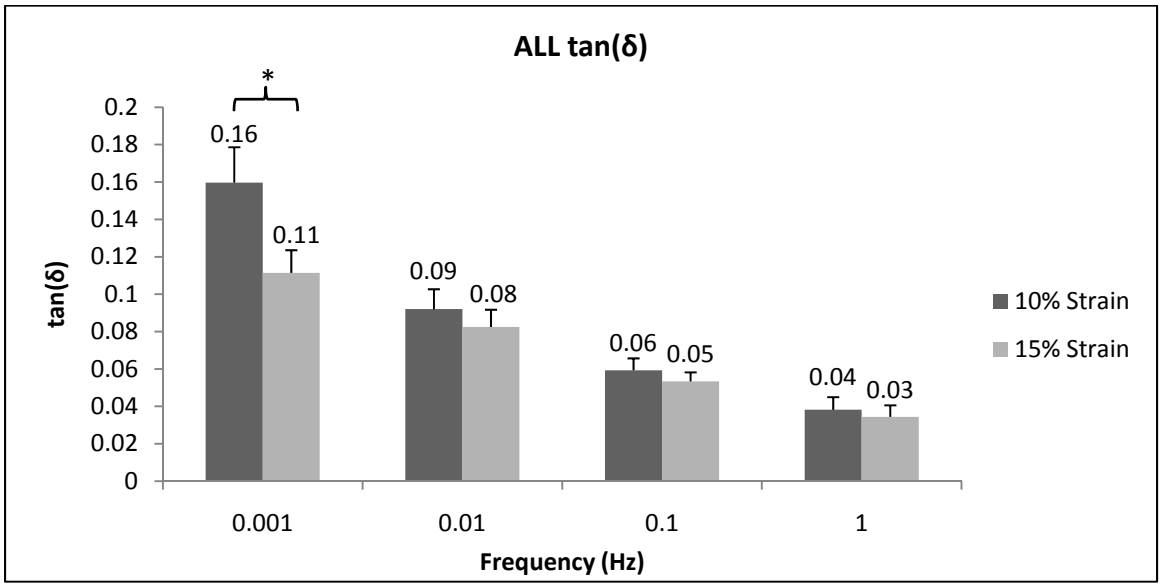

Figure 3.2: Effect of strain amplitude on the ALL $tan(\delta)$. *indicates p=0.0010. No statistical differences were observed, except for *. Error bars represent the standard error.

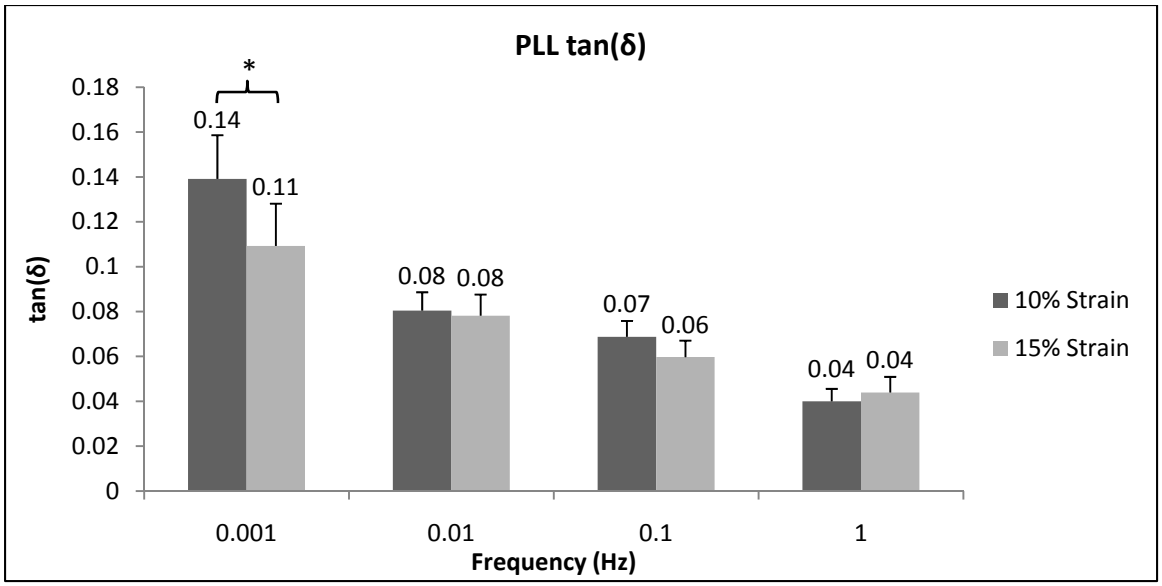

Figure 3.3: Effect of strain amplitude on the PLL $tan(\delta)$. *indicates p=0.0104. No statistical differences were observed, except for *. Error bars represent the standard error.

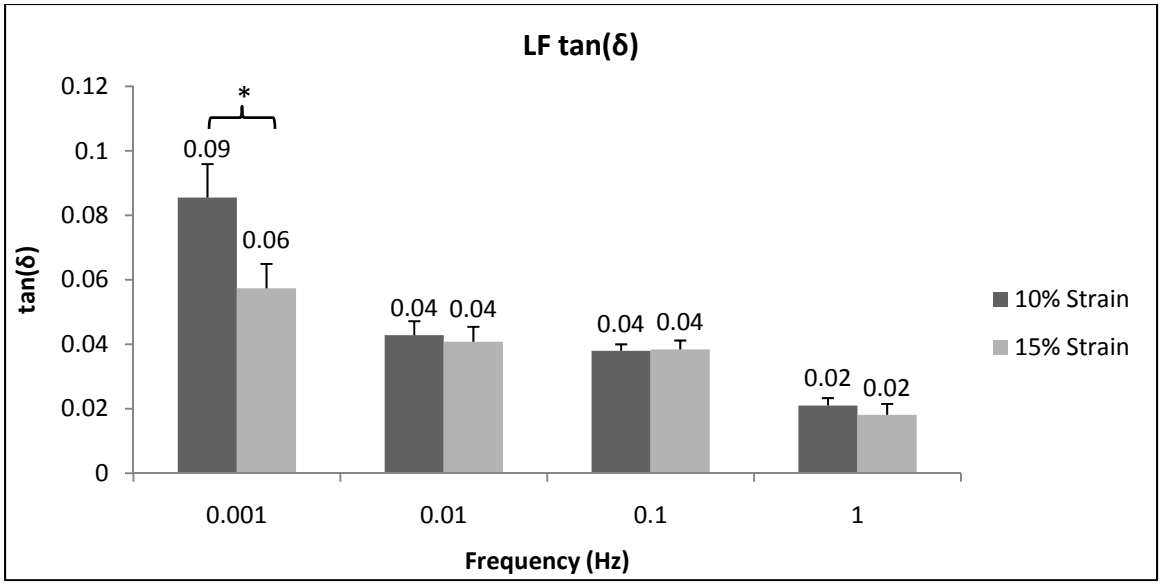

Figure 3.4: Effect of strain amplitude on the LF $tan(\delta)$. *indicates p=0.0011. No statistical differences were observed, except for *. Error bars represent the standard error.

The data were also analyzed in order to observe the effect of frequency on tan (δ) for each ligament type, independent of strain amplitude. For the ALL, the tan (δ) was observed to decrease as frequency was increased for both strain amplitude levels (Figure 3.5), with each frequency being statistically different than the others ($p<0.01$ for all comparisons).

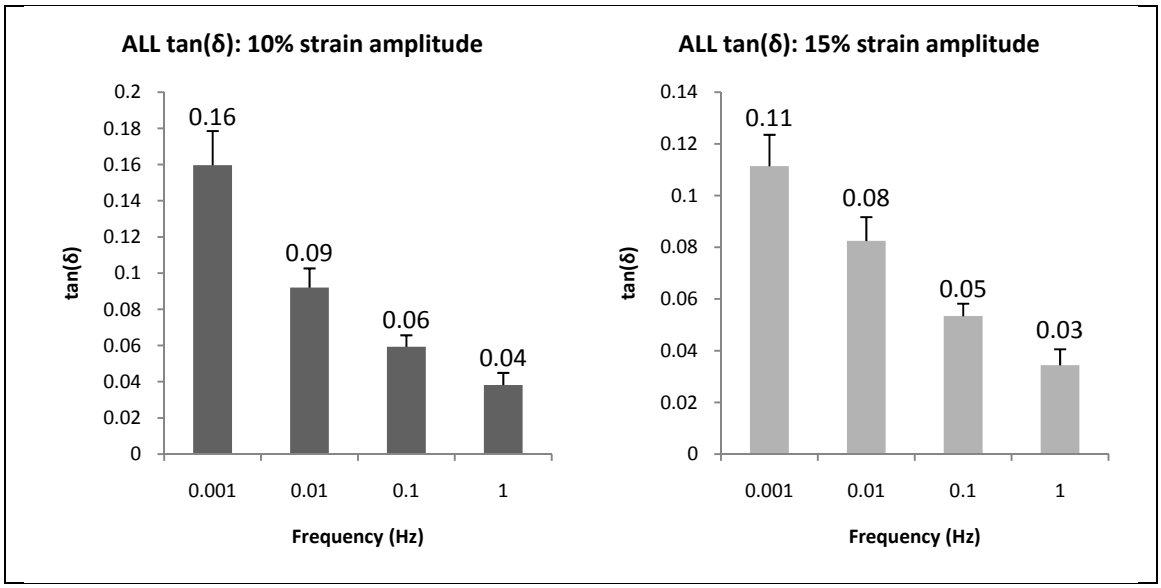

Figure 3.5: For both strain amplitudes, the ALL $tan(\delta)$ decreased as frequency was increased. For a given strain amplitude, $tan(\delta)$ at each frequency was found to be statistically different (p<0.0001). Error bars represent the standard error.

The tan (δ) for the PLL exhibited slightly different frequency-dependent behavior than the ALL tan (δ). The PLL tan (δ) decreased with increasing frequency, similar to the ALL, except that there was no statistical difference (p=0.1348) in the tan (δ) between the 0.01 Hz and 0.1 Hz frequencies for the 10% strain magnitude (Figure 3.6). All other comparisons for the PLL were statistically significant (p<0.0001 for all significant comparisons) at the 10% strain amplitude. For the 15% strain amplitude, the PLL tan (δ) at all frequencies were statistically different (p<0.05 for all comparisons).

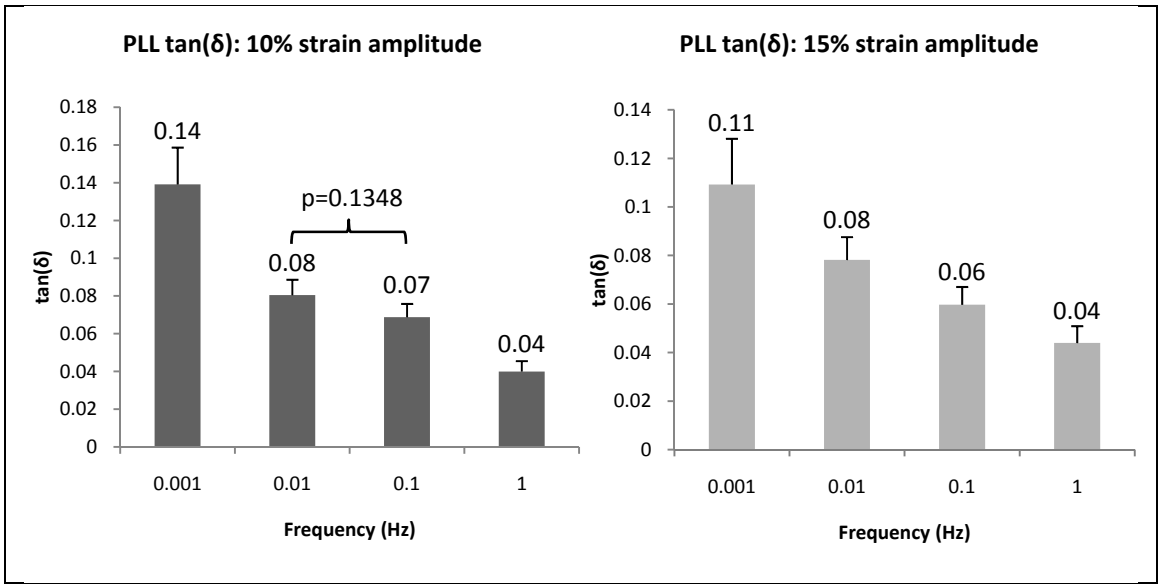

Figure 3.6: For both strain amplitudes, the PLL $tan(\delta)$ decreased as frequency increased. Within each strain amplitude, the $tan(\delta)$ at each frequency was statistically different (p<0.0001 and p<0.05 for 10% and 15% strain amplitude comparisons, respectively), except the comparison between the 0.01 Hz and 0.1 Hz frequencies at the 10% strain amplitude. Error bars represent the standard error.

The tan (δ) calculated for the LF also decreased with increasing strain, except that no statistical difference existed between the tan (δ) at the 0.01 Hz and 0.1 Hz frequencies at both strain amplitudes (p-values indicated on Figure 3.7). All other LF tan (δ) comparisons were statistically significant (p<0.0001 and p<0.05 for 10% and 15% strain amplitude comparisons, respectively).

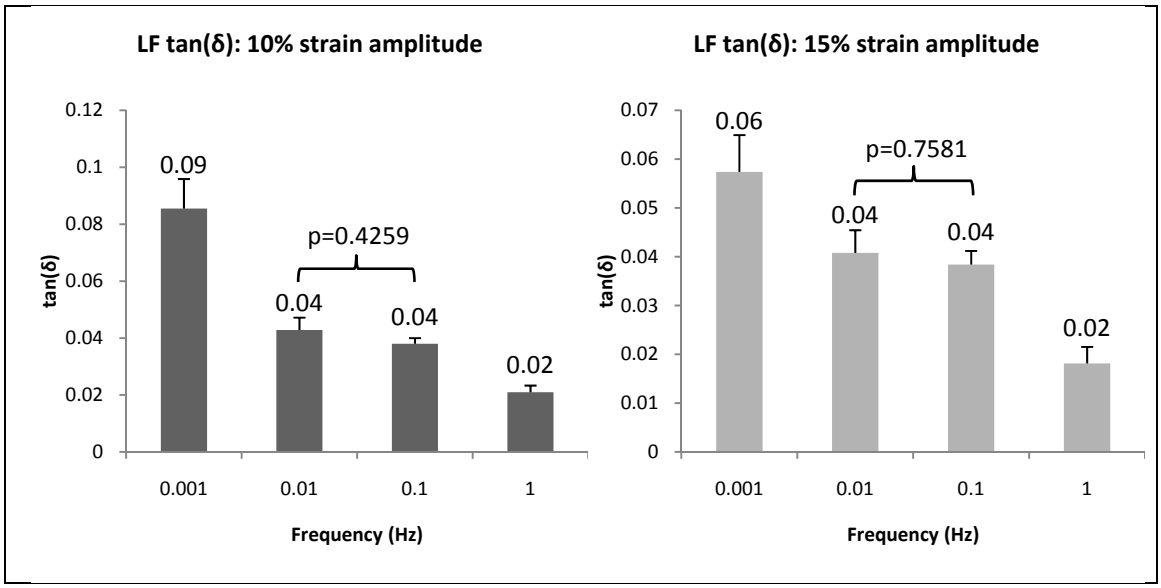

Figure 3.7: For both strain amplitudes, the LF $tan(\delta)$ decreased as frequency increased, the 0.01 Hz and 0.1 Hz frequencies. All other comparisons were significant (p<0.0001 and p<0.05 for 10% and 15% strain amplitude comparisons, respectively). Error bars represent the standard error.

Figure 3.8 compares the ligament types at the 10% strain amplitude. There was no significant difference between the ALL and the PLL tan (δ) at any of the tested frequencies. Also, the LF tan (δ) was smaller than that of both the ALL ($p<0.05$) and the PLL ($p<0.05$) at all frequencies.

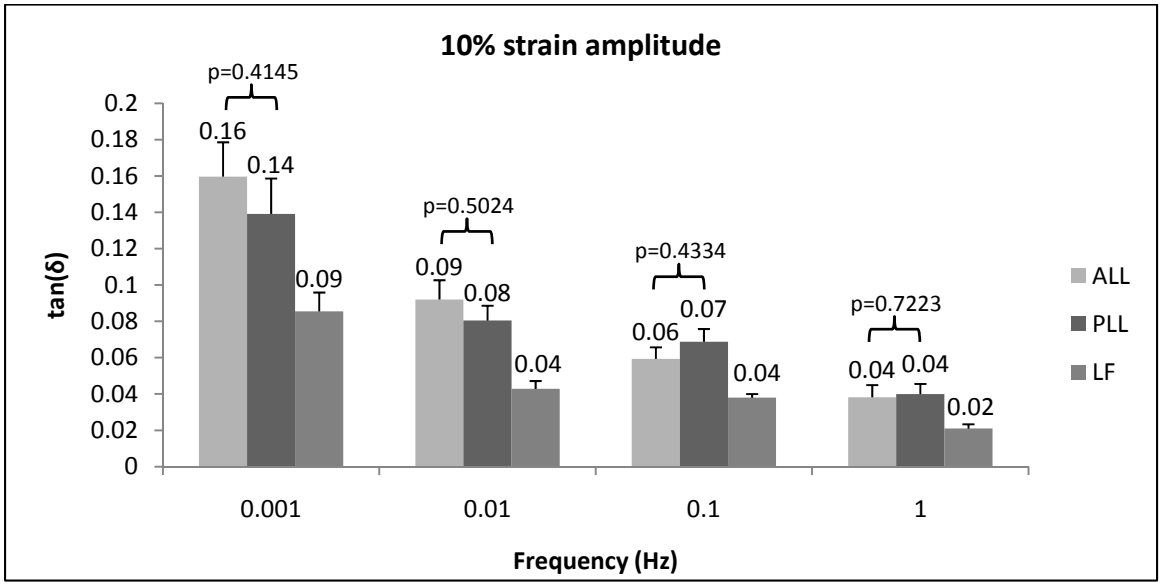

Figure 3.8: Comparing the $tan(\delta)$ across ligament types at the 10% strain amplitude. All other comparisons were significantly different ($p<0.05$). Error bars represent the standard error.

The effect of ligament type at 15% strain amplitude was similar to the 10% amplitude (Figure 3.9). No statistical difference existed between the ALL and the PLL at any frequency. Interestingly, at 0.1 Hz no statistical difference was observed between any of the ligament types. At all frequencies except for 0.1 Hz, the LF tan (δ) was smaller than that of the ALL ($p<0.01$) and the PLL ($p<0.01$).

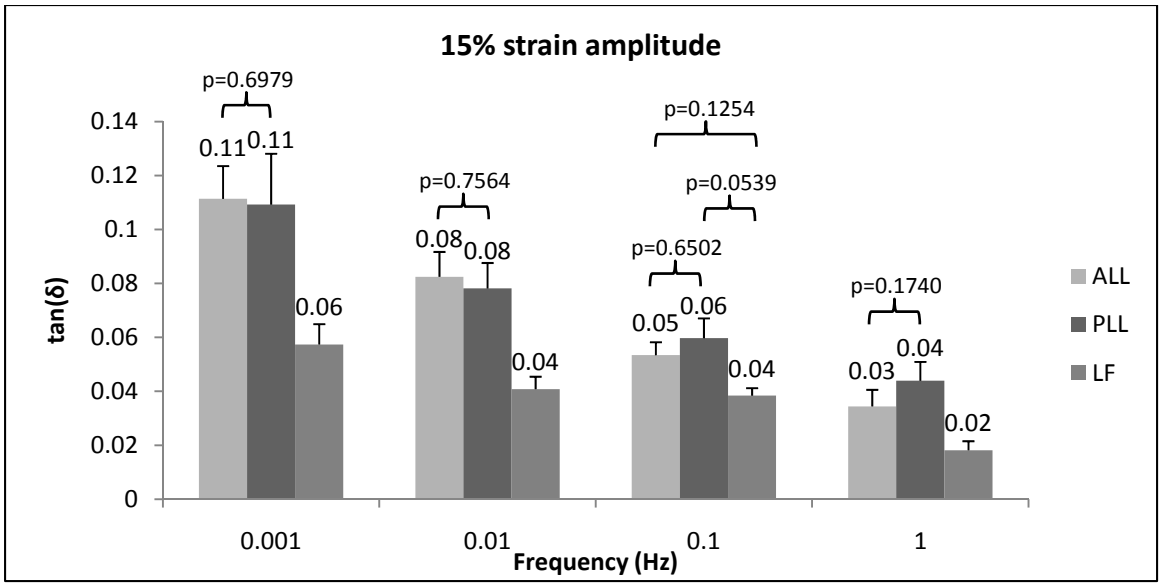

Figure 3.9: Comparing the $tan(\delta)$ across ligament types at the 15% strain amplitude. All other comparisons were significantly different (p<0.05). Error bars represent the standard error.

Storage modulus

Statistical analysis of the storage modulus (E') indicated a significant effect of strain amplitude (p<0.0001), frequency (p<0.0001), and ligament type (p=0.0034) on this parameter.

The effect of strain amplitude on the E' is shown in Figure 3.10 for the ALL, Figure 3.11 for the PLL, and Figure 3.12 for the LF. For the ALL, the E' calculated at the 10% strain amplitude was significantly reduced as compared to the E' calculated at the 15% strain amplitude at each frequency (p<0.05 for each comparison). For the PLL, the E' calculated at the 10% strain amplitude was significantly smaller than the E' determined at the 15% strain amplitude for the slower (0.001 Hz and 0.01 Hz) frequencies (p=0.0220 and p=0.0454, respectively). No significant differences existed between the strain amplitudes at the faster (0.1 Hz or 1 Hz) frequencies (p=0.0996 and p=0.0957, respectively). For the LF, no statistical difference in E' existed between the 10% and 15% strain amplitudes for all frequencies.

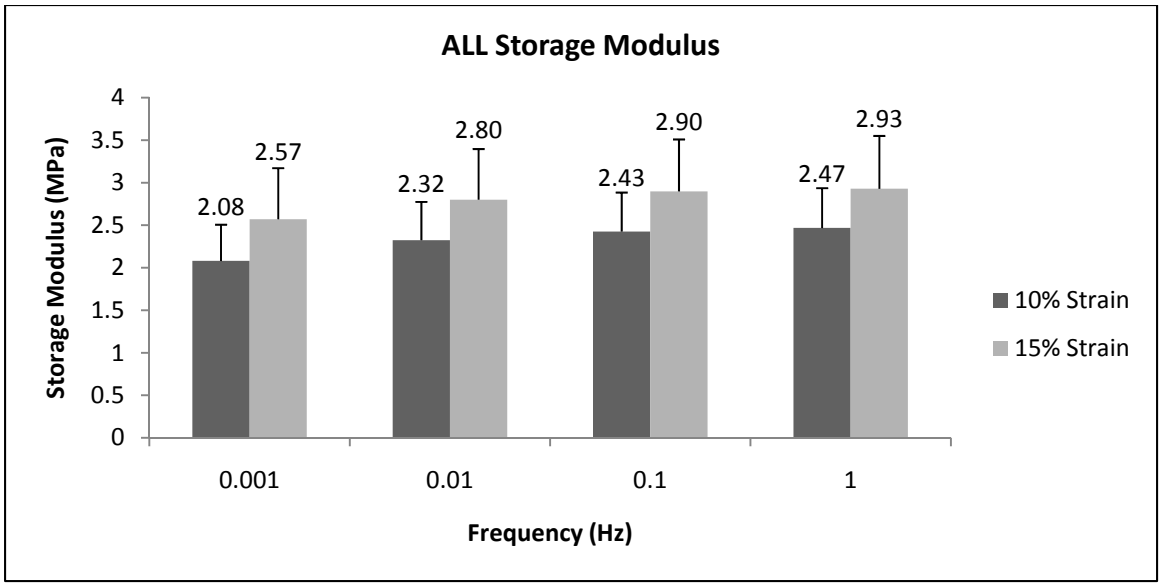

Figure 3.10: ALL storage modulus. There was a statistical difference ($p<0.05$) between the two strain amplitudes at each frequency. Error bars represent the standard error.

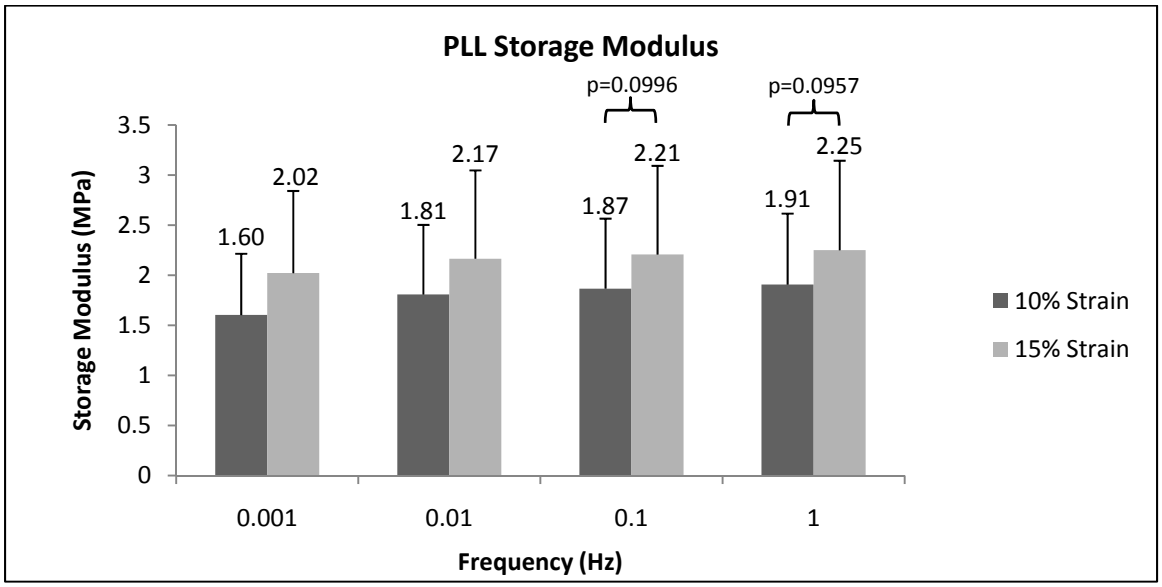

Figure 3.11: PLL Storage modulus. There was a statistical difference between the strain amplitudes at the 0.001 Hz and 0.01 Hz frequencies, but no significant difference was found at the 0.1 Hz and 1 Hz frequencies. Error bars represent the standard error.

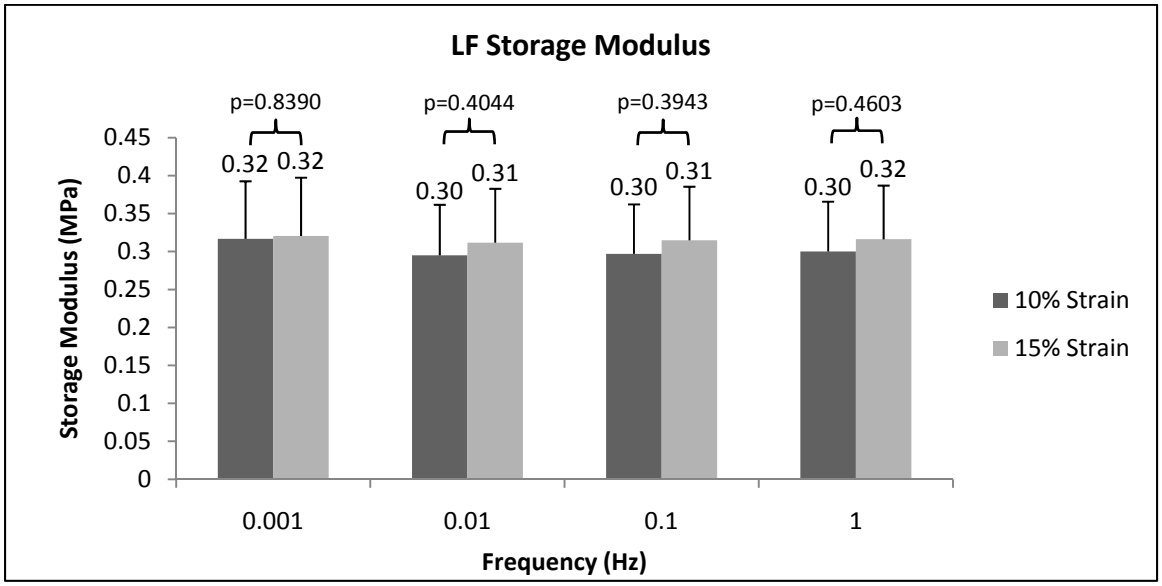

Figure 3.12: The LF storage modulus was found to be independent of the two strain amplitudes. Error bars represent the standard error.

As with the tan (δ) parameter, the data were analyzed by strain level in order to better observe the effect of frequency at each strain amplitude. For the ALL, the E' calculated at 0.001 Hz was statistically smaller than the E' calculated at all other frequencies for both amplitudes of strain ($p<0.05$), creating two statistically different groups (Figure 3.13). There was no statistical difference between the ALL E' calculated at the 0.01 Hz, 0.1 Hz and 1 Hz frequencies for both amplitudes of strain.

E' for the PLL had the same grouping as the E' for the ALL at the 10% strain amplitude, with the calculated E' at the 0.001 Hz frequency being significantly lower than each of the other frequencies ($p<0.05$) (Figure 3.14). However, a slightly different grouping was observed for the PLL E' at the 15% strain amplitude. At this amplitude, the PLL E' was different between the 0.001 Hz and the 0.1 Hz ($p=0.0099$) frequencies, and also the 0.001 Hz and the 1 Hz ($p=0.0015$) frequencies, but there was no difference between the 0.001 Hz and 0.01 Hz ($p=0.0774$) frequencies.

The LF E' behavior was different from that of both the ALL and the PLL, showing no statistical difference in the calculated E' across all frequencies for both strain amplitudes (Figure 3.15). This data suggest that the E' for the LF is independent of the tested range of frequencies.

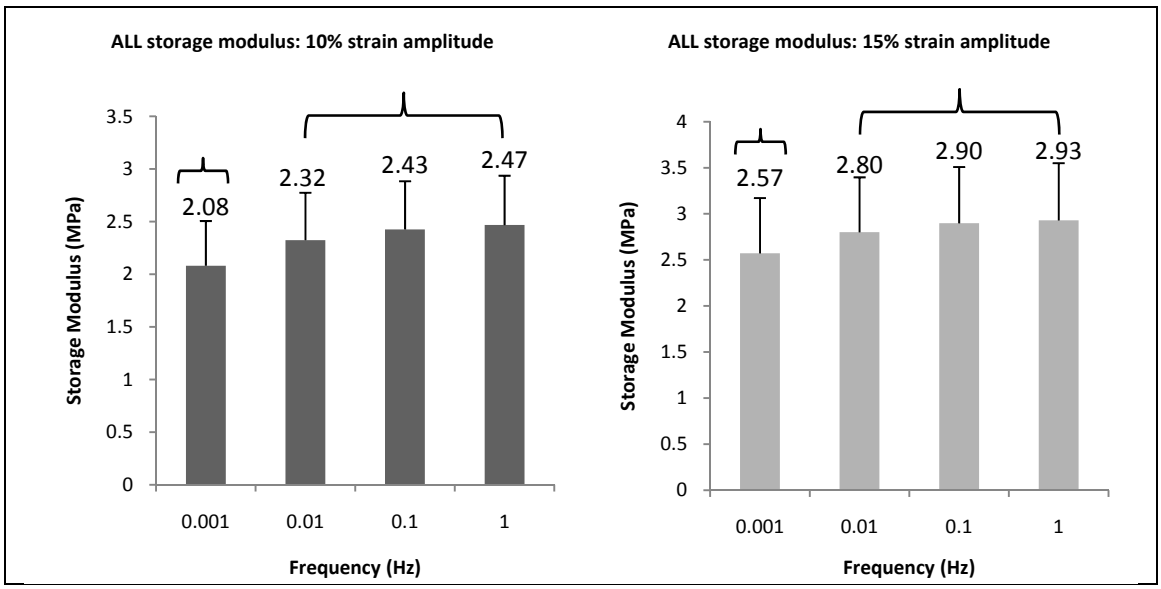

Figure 3.13: Frequency-dependent behavior of the ALL storage modulus. The storage modulus calculated at 0.001 Hz was different ($p<0.05$) than the storage modulus calculated at any other frequency for both strain amplitudes. Brackets indicate this grouping. Error bars represent the standard error.

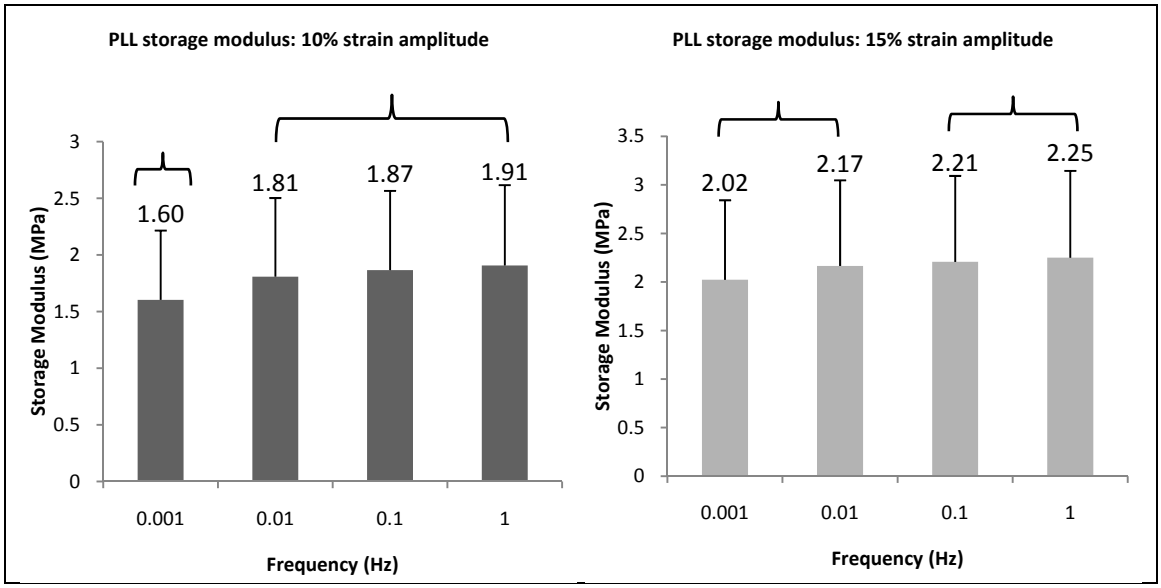

Figure 3.14: Frequency-dependent behavior of the PLL storage modulus. At the 10% strain amplitude, the storage modulus calculated at 0.001 Hz was different ($p<0.05$) than that calculated at any other frequency. For the 15% strain amplitude, only the 0.1 Hz and 1 Hz frequencies were different ($p=0.0099$ and $p=0.0015$, respectively) than the 0.001 Hz frequency. Brackets indicate comparisons with no statistical differences. Error bars represent the standard error.

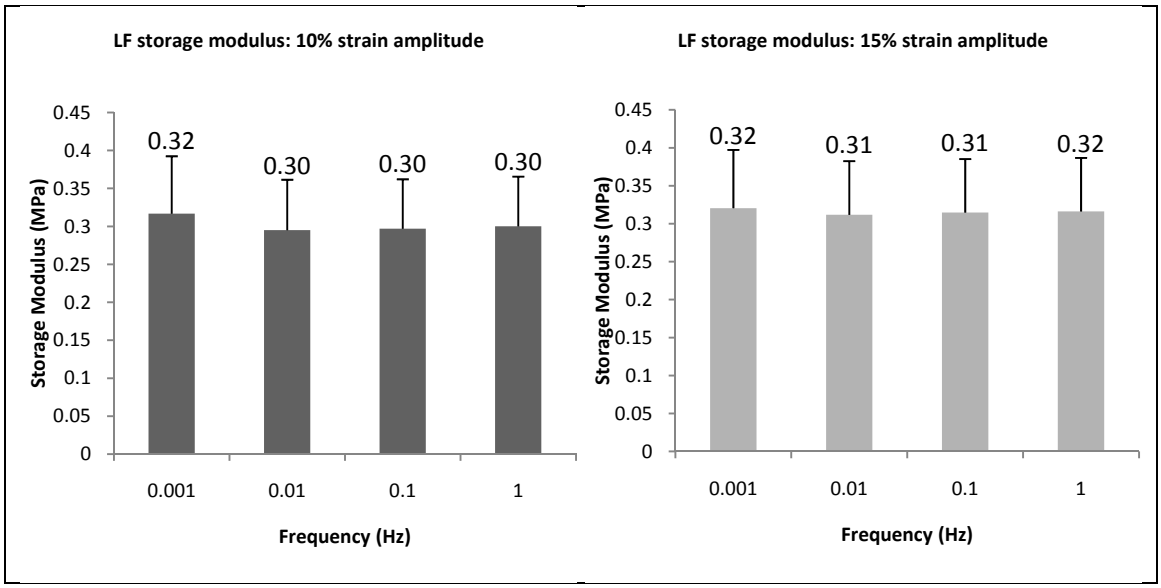

Figure 3.15: For each amplitude of strain, the LF storage modulus was not statistically different across all frequencies, indicating that it was independent of frequency. Error bars represent the standard error.

When comparing the E' across ligament types, no statistical difference existed between ALL E' and the PLL E' at each frequency in the 10% strain amplitude (Figure 3.16). Additionally, the E' calculated for the ALL and the PLL were both an order of magnitude larger than the E' calculated for the LF (ALL: $p<0.01$; PLL: $p<0.05$). Identical behavior was observed when comparing the E' across ligament types for the 15% strain amplitude; no statistical difference existed between the E' calculated for the ALL and the PLL, and the calculated E' for the ALL and PLL were both an order of magnitude larger than the LF (ALL: $p<0.01$; PLL: $p<0.05$) (Figure 3.17).

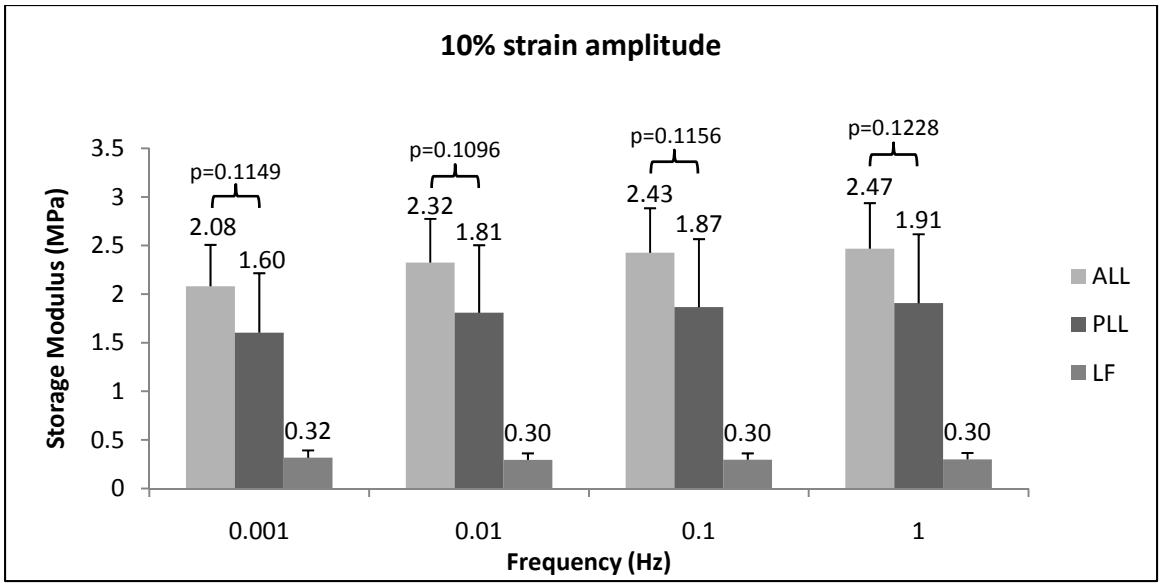

Figure 3.16: Comparing the storage modulus across ligament types at each frequency for the 10% strain amplitude. There was no statistical difference between the calculated storage moduli for the ALL and the PLL. However, the ALL and PLL storage moduli were both statistically different than the LF ($p<0.05$). Error bars represent the standard error.

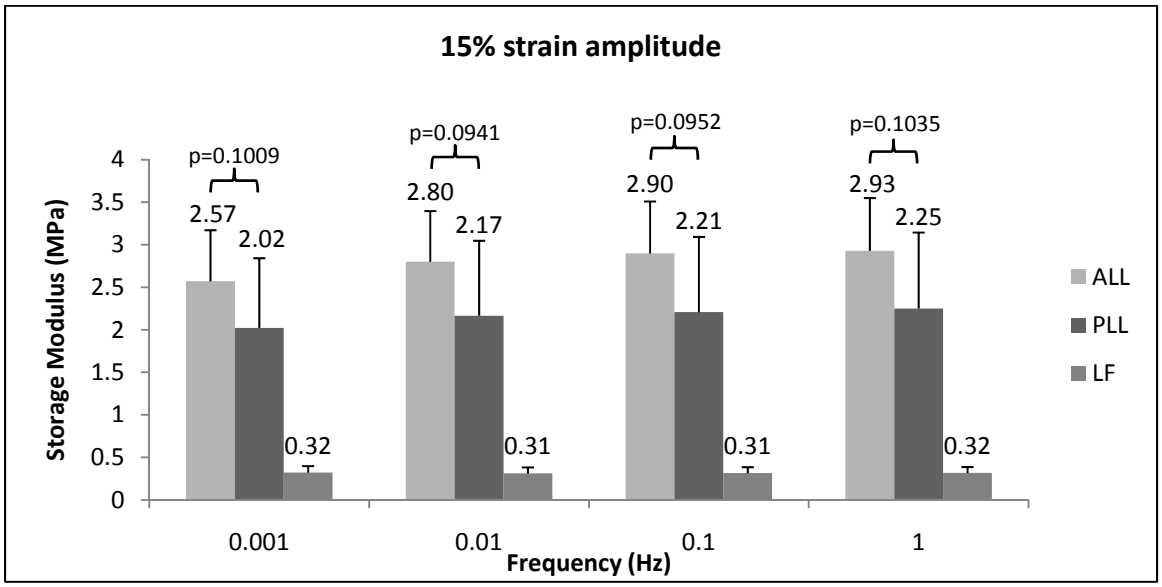

Figure 3.17: Comparing the storage modulus across ligament types at each frequency for the 15% strain amplitude. The storage modulus behavior was similar to the behavior at the 10% strain amplitude. Error bars represent the standard error.

Loss modulus

Statistical analyses indicated frequency ($p<0.0001$) and ligament type ($p=0.0002$) had significant effects on the loss modulus (E''). While strain amplitude was a significant effect for both the tan (δ) and E', it was not significant for E'' ($p=0.1578$). Therefore, no statistical comparisons are presented regarding strain level.

As before, to observe the effect of frequency on E'' (independent of strain amplitude), the E'' calculated for each strain amplitude was plotted separately. The E'' calculated for the ALL was observed to decrease with increasing frequency at both strain amplitudes (Figure 3.18). At the 10% strain amplitude, the E'' calculated for the ALL at each frequency was statistically different than that calculated at the other frequencies ($p<0.01$). At the 15% strain amplitude, no statistical difference was observed for the ALL E'' between the 0.001 Hz and 0.01 Hz frequencies ($p=0.0992$). However, the E'' calculated at all other frequencies were statistically different ($p<0.01$). The E'' calculated for the PLL also decreased as the frequency was increased for both strain amplitudes (Figure 3.19). The calculated PLL E'' at each frequency was statistically different from other frequencies ($p<0.01$), except for the comparison between the 0.01 Hz and 0.1 Hz frequencies at the 10% strain amplitude ($p=0.3969$), and between the 0.001 Hz and 0.01 Hz frequencies at the 15% strain amplitude ($p=0.0930$). For the LF, the calculated E'' also showed a decreasing trend as frequency was increased for both strain amplitudes (Figure 3.20). The calculated E'' were statistically different when compared across frequencies ($p<0.01$) for both strain amplitudes, except for comparisons between the 0.01 Hz and 0.1 Hz frequencies at the 10% ($p=0.5237$) and 15% ($p=0.8610$) strain amplitudes.

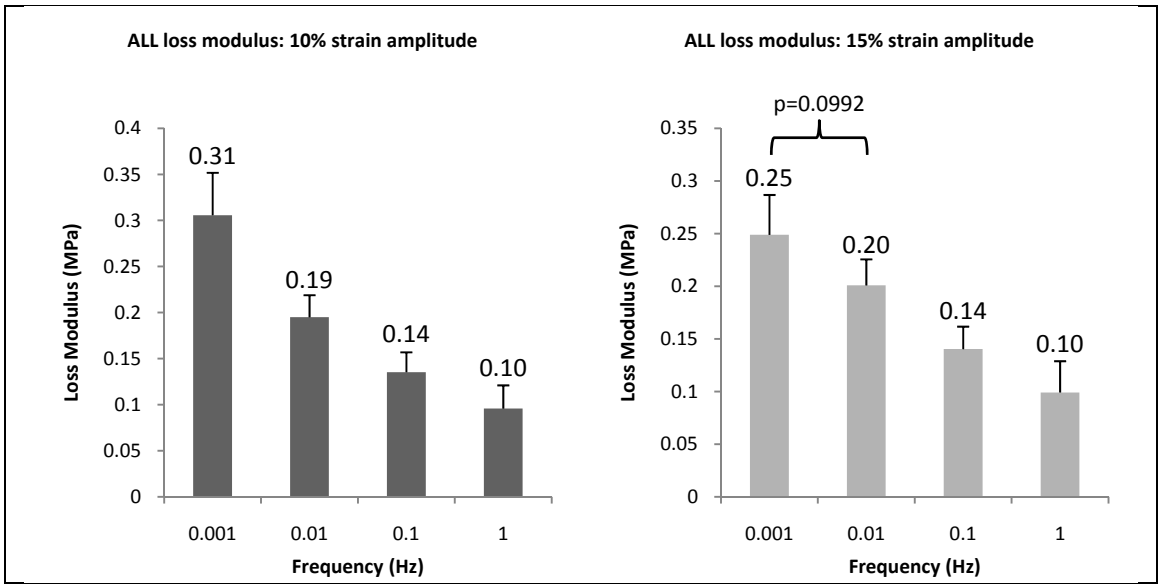

Figure 3.18: For each strain amplitude, the ALL loss modulus was observed to decrease as frequency was increased. The loss modulus was statistically different ($p<0.05$) at all frequencies, except between the 0.001 Hz and 0.01 Hz frequencies for the 15% strain amplitude. Error bars represent the standard error.

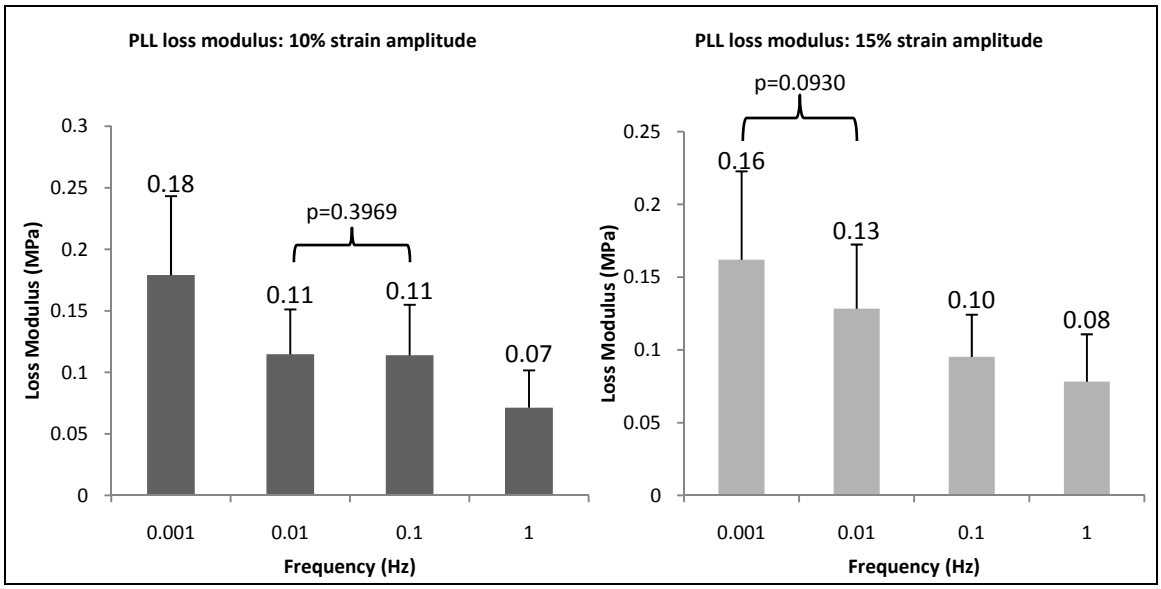

Figure 3.19: For each strain amplitude, the PLL loss modulus was observed to decrease as frequency was increased. Each loss modulus was statistically different ($p<0.05$) for all frequencies, except between 0.01 Hz and 0.1 Hz at the 10% strain amplitude and between 0.001 Hz and 0.01 Hz at the 15% strain amplitude. Error bars represent the standard error.

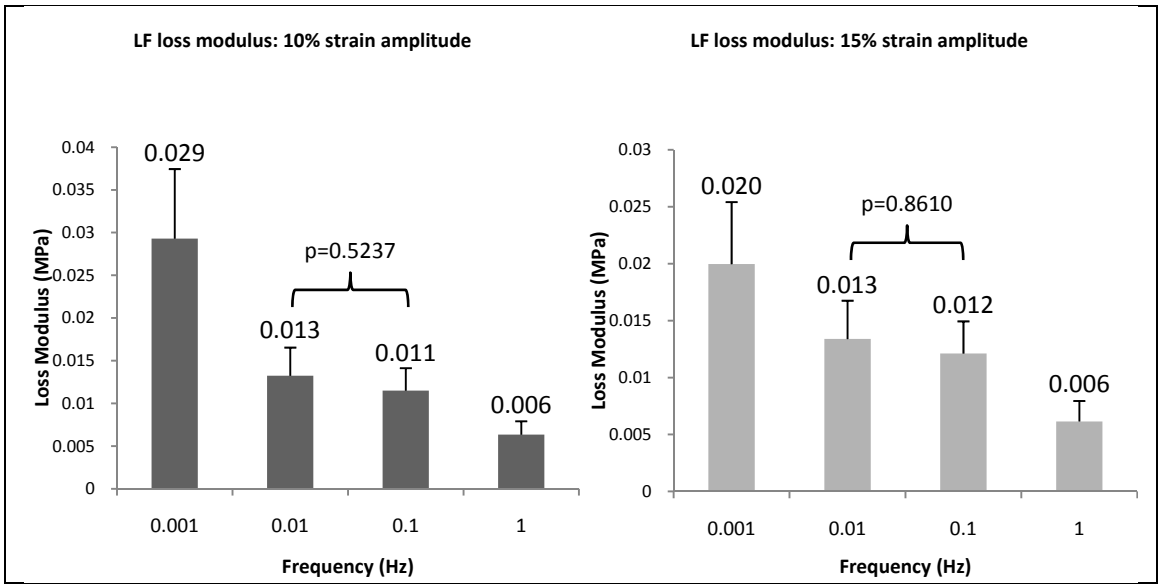

Figure 3.20: For each strain amplitude, the LF loss modulus was observed to decrease as frequency increased. Each calculated loss modulus was statistically different ($p<0.05$) for all frequencies, except between 0.01 Hz and 0.1 Hz at both the 10% and 15% strain amplitudes. Error bars represent the standard error.

When comparing the E'' across ligament types for the 10% and 15% strain amplitudes (Figure 3.21 and Figure 3.22, respectively), no statistical difference existed between the E'' calculated for the ALL and the PLL for all frequencies, except for the 0.001 Hz frequency at the 10% strain amplitude (p=0.0477). The E'' for the LF was an order of magnitude smaller than the E'' calculated for the ALL and the PLL at both strain amplitudes.

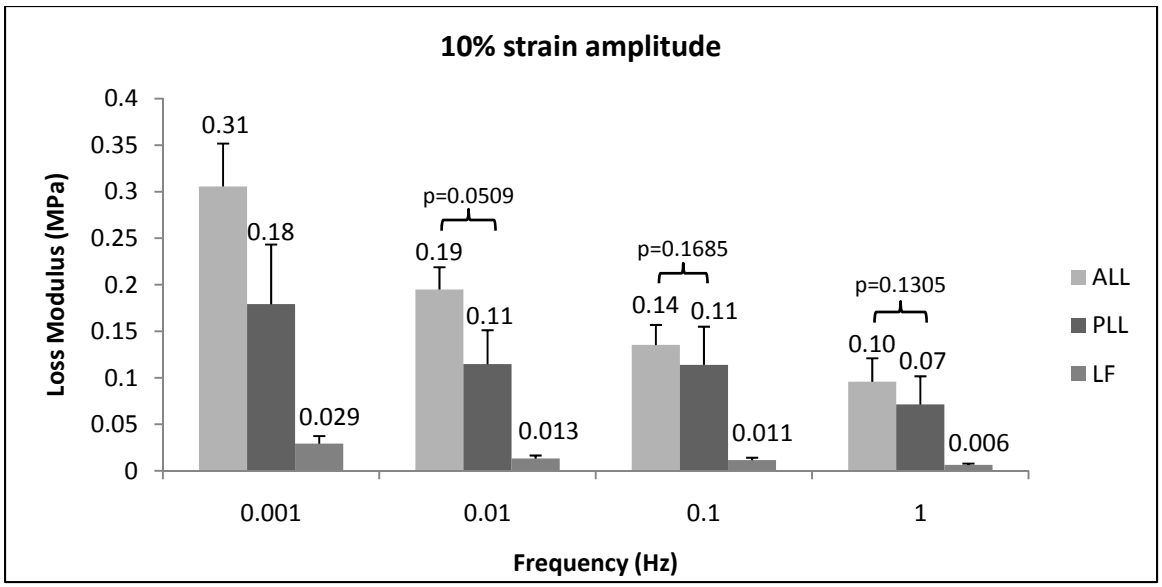

Figure 3.21: Comparing the loss modulus across ligament types at 10% strain amplitude. No statistical difference was observed between the loss moduli calculated for the ALL and the PLL, except for at the 0.001 Hz frequency (p=0.0477). The loss modulus for the LF was an order of magnitude smaller than the ALL and the PLL. Error bars represent the standard error.

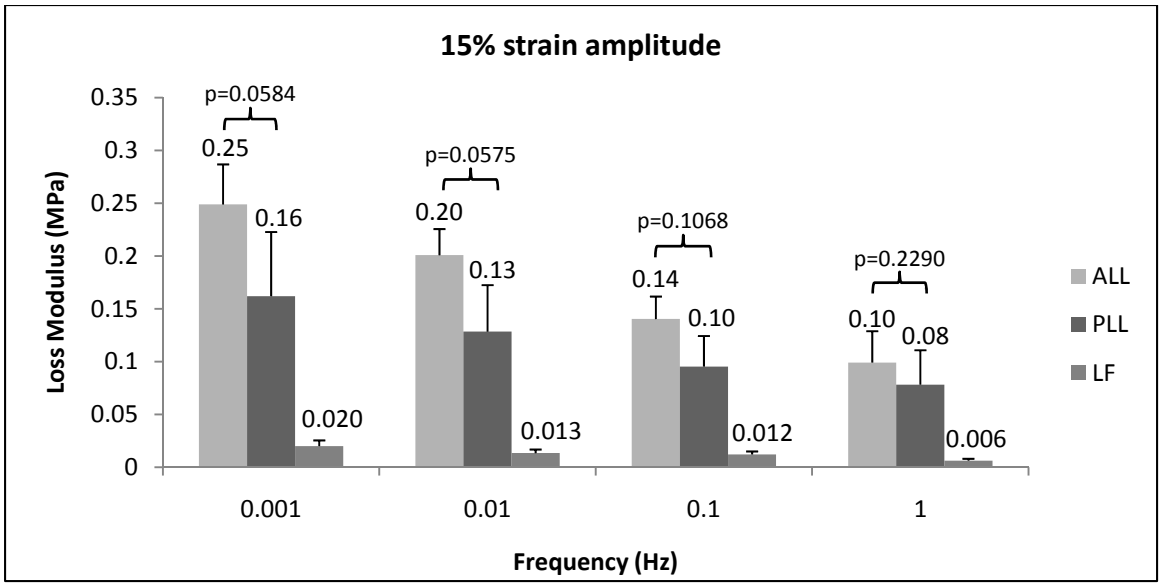

Figure 3.22: Comparing the loss modulus across ligament types at 15% strain amplitude. No statistical difference was observed between the loss moduli for the ALL and the PLL at all frequencies. The loss modulus calculated for the LF was an order of magnitude smaller than the ALL and the PLL. Error bars represent the standard error.

3.3. Stress Relaxation Results

3.3.1. QLV fitted parameters

Experimental stress relaxation versus time data at multiple strain magnitudes were fitted to QLV theory to determine the validity and applicability of this theory to model the viscoelastic behavior of the ALL, PLL, and LF over a range of applied strain magnitudes.

Sensitivity of Fitted Parameters to the Initial Guesses

Before determining the fitted parameter values, it was important to access the sensitivity of the fitting algorithm to the required initial guesses. Hence, for each preliminary fit, all initial guesses were fixed at a single value of 0.001, 0.01, 0.1, 1, 10, or 100 and the resulting fitted parameter values (at each strain magnitude) were compared using the statistical procedure outlined in Section 2.7.3.

For the set of initial guesses considered, the statistical analysis indicated that the fitted parameters for all ligaments were sensitive to the larger initial guesses of 100 and 10, and insensitive (i.e., no statistical difference in the fitted parameter values) to the smaller initial

guesses (1, 0.1, 0.01, and 0.001). Specifically, an initial guesses of 100 gave extremely large and erroneous values (on the order of 10^{50} for some fits) for the objective function, and often gave invalid fitted parameter values, (e.g., negative $G(t)$ coefficients and fitted values equal to the initial guess) for each ligament type. However, as the initial guesses were incrementally decreased from 100 to 0.001, the fitted parameter values appeared to converge to a unique solution since no statistical difference was observed between the fitted parameter values calculated with the smaller initial guesses.

For the ALL, statistical analysis indicated that parameters A, B, G_∞, and G_4 were dependent on the initial guesses over the entire (six decade) range (Table 3). However, when the range of initial guesses was decreased from 0.001-100 to 0.001-10, no statistical difference was observed between any of the parameter values. Therefore, the fitted parameter values for the ALL were determined to be insensitive to the initial guesses in the range from 0.001-10. Since there was no statistical difference between parameter values over the relatively large range of initial guesses from 0.001-10 (five decades), the fitted parameter values were assumed to be converged at a unique solution within this range.

Table 3: p-values for two-way interaction between the ALL fitted parameter values and the initial guess fixed at each decade value in the given range.

Parameter	Range: 0.001-100	Range: 0.001-10	Range: 0.001-1
A	<0.0001	0.9788	0.9311
B	<0.0001	0.9998	0.9994
G_∞	0.0058	1.0000	1.0000
G_1	0.7391	1.0000	1.0000
G_2	0.1401	1.0000	1.0000
G_3	0.1261	1.0000	1.0000
G_4	0.0056	1.0000	1.0000

For the PLL, the B, G_2, and G_3 parameter values were found to be sensitive to the initial guesses over the range of 0.001-100 (Table 4). However, similar to the ALL, no statistical difference was observed between the PLL fitted parameters for initial guesses in the range of 0.001-10. The fitted parameter values were less reliant (indicated by even larger p-values that

approximated unit) when an initial guess in the range of 0.001-1. Since such a small difference was observed between the fitted parameter values calculated from the initial guesses in the 0.001-1 range (four decades), the fitted parameter values were assumed to be converged within this range.

Table 4: p-values for two-way interaction between the PLL fitted parameter values and the initial guess fixed at each decade value in the given range.

Parameter	Range: 0.001-100	Range: 0.001-10	Range: 0.001-1
A	0.0741	0.6589	0.9259
B	<0.0001	0.3140	0.9995
G_∞	0.3565	1.0000	1.0000
G_1	0.9995	1.0000	1.0000
G_2	0.0002	1.0000	1.0000
G_3	<0.0001	1.0000	1.0000
G_4	0.1777	1.0000	1.0000

For the LF data, the fitted A, B, G_∞, and G_4 parameters were found to be significantly different over the entire range of initial guesses (0.001-100). As with the ALL and PLL, the fitted parameters for the LF were relatively insensitive to the smaller initial guesses, specifically over the 0.001-1 range (4 decades). Hence, the fitted parameter values were assumed to be converged within this initial guess range.

Table 5: p-values for two-way interaction between the LF fitted parameter values and the initial guess fixed at each decade value in the given range.

Parameter	Range: 0.001-100	Range: 0.001-10	Range: 0.001-1
A	<0.0001	0.0003	0.9857
B	<0.0001	0.3438	0.9998
G_∞	<0.0001	1.0000	1.0000
G_1	0.9675	0.9997	1.0000
G_2	0.9090	0.9985	1.0000
G_3	0.2119	1.0000	1.0000
G_4	<0.0001	1.0000	1.0000

It is interesting to note that the p-values in Table 3, Table 4, and Table 5 indicate that the fitted $G(t)$ parameters were less sensitive to the initial guesses than the A and B parameters for nearly all of the tested ranges. In fact, the fitted $G(t)$ parameters were observed to converge faster

than both the A and B parameters and in some cases the fitted $G(t)$ parameters were not statistically different over the entire range (six decades) of initial guesses.

For each ligament type, the fitted parameter values (determined from within the converged range of initial guesses described above) that gave the smallest average objective function ($f(\theta) + g(\theta)$) value were assumed to be the global minimum [44]. Hence, the parameter values for the fitted QLV model reported herein are those that gave the smallest average objective function value. The initial guesses that resulted in the smallest average objective function were: 10 for the ALL, 1 for the LF, and 0.01 for the PLL.

QLV Fitted Parameters

Table 6 gives the median coefficient of determination (r^2 value) between the fitted QLV model (equation (19)) and the experimental data. At each strain level, the fitted QLV model approximated the experimental data well with only three of the fits resulting in a poor median coefficient of determination ($r^2 < 0.5$). Additionally, the r^2 values in Table 6 increased with strain magnitude, indicating that the QLV model better approximated the experimental data as the strain magnitude increased. Representative experimental stress relaxation plots for the ALL, PLL, and LF, along with the fitted QLV model, are shown in Figure 3.23, Figure 3.24, and Figure 3.25, respectively.

Table 6: Median coefficients of determination (r^2 value) between the QLV model and the experimental data.

Strain magnitude (%)	ALL	PLL	LF
4	0.68	0.41	0.25
6	0.80	0.58	0.42
8	0.90	0.71	0.55
10	0.93	0.74	0.66
12	0.95	0.77	0.77
14	0.97	0.83	0.80
16	0.97	0.86	0.81
18	0.98	0.88	0.86
20	0.98	0.89	0.90
25	0.99	0.94	0.92

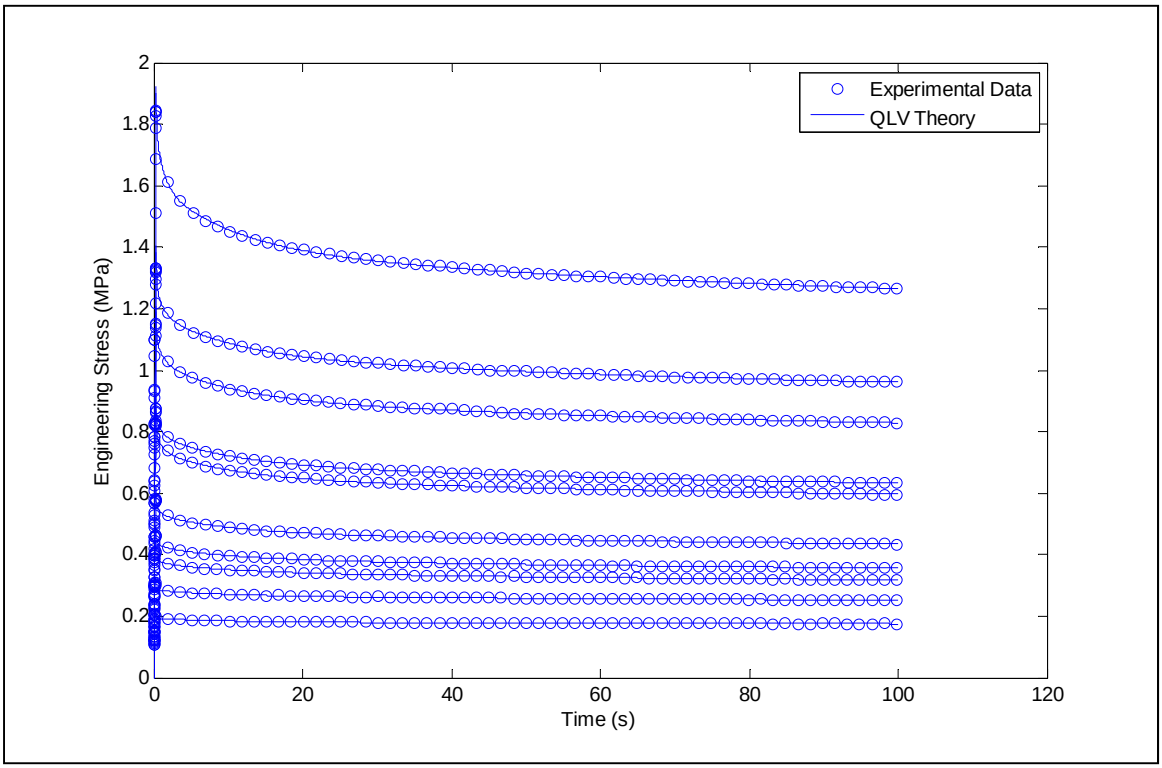

Figure 3.23: Representative stress relaxation curves for the ALL fitted using QLV theory.

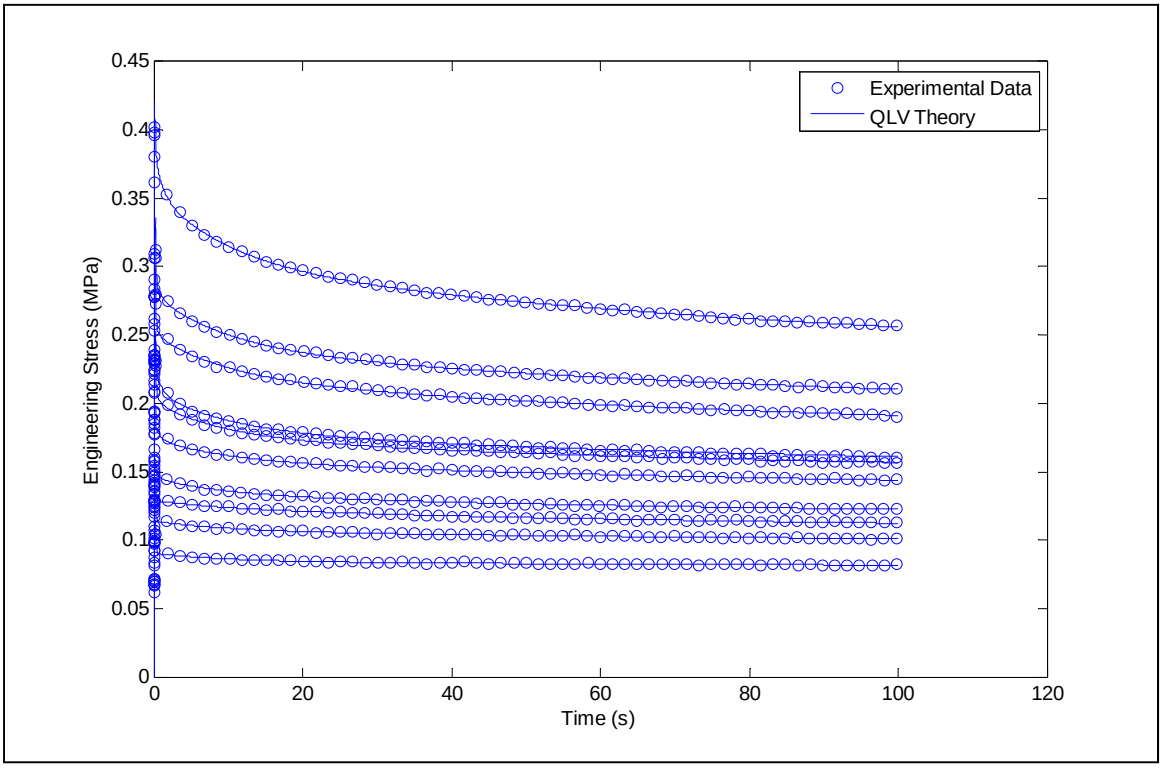

Figure 3.24: Representative stress relaxation curves for the PLL fitted using QLV theory.

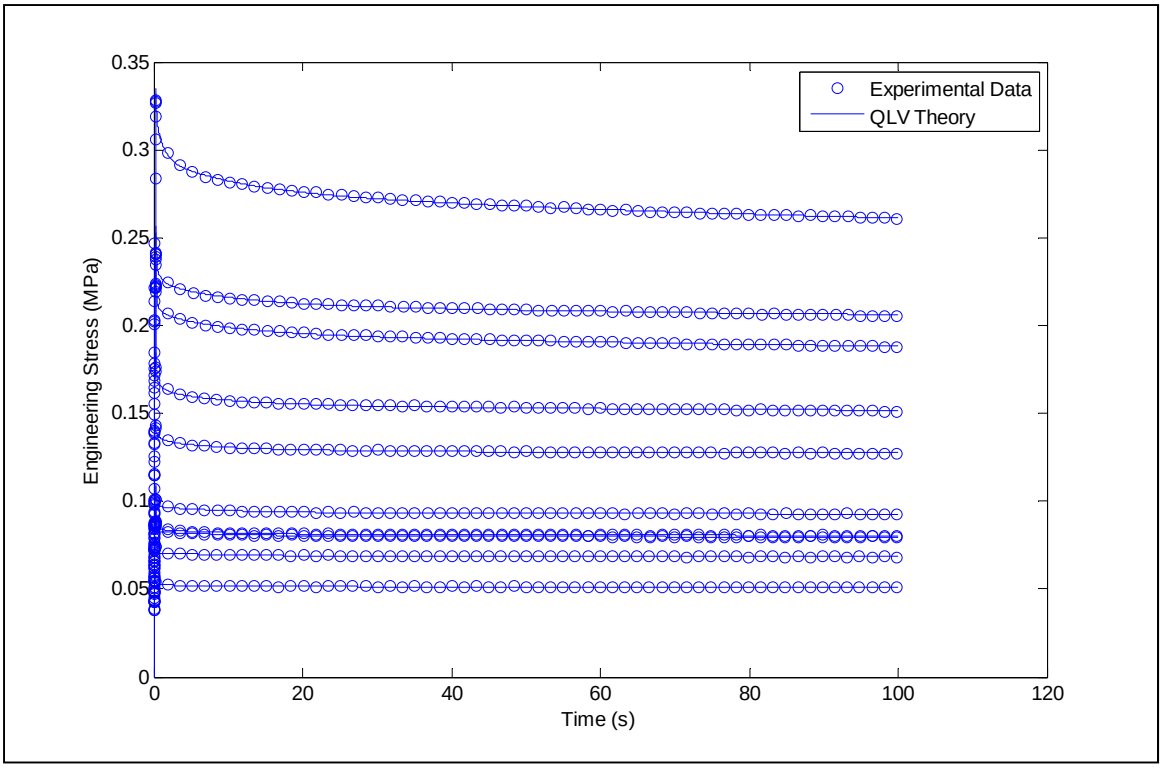

Figure 3.25: Representative stress relaxation curves for the LF fitted using QLV theory.

The average (± 1 SE) QLV fitted parameter values for the ALL, PLL, and LF are given in Table 7 to Table 9, respectively. For all ligament types, the stress relaxation behavior was dominated by the combination of the G_∞ and G_1 parameters, which accounted for approximately 80% of the relaxation behavior for the ALL, and approximately 90% of the PLL and LF relaxation behavior. The remaining portion of the relaxation behavior (approximately 20% for the ALL and approximately 10% for the PLL and LF) is described by the G_2, G_3, and G_4 relaxation parameters. Phenemelogically, each G_n parameter represents the strength of the relaxation at the τ_n time constant [47] and the G_∞ parameter is the *long-term* relaxation parameter, and is the proportion of the instantaneous stress that would remain in the ligament as time goes to infinity (equation (22)). For all ligament types, the fitted G_1 parameters were approximately an order of magnitude larger than G_2, G_3, and G_4 parameters, indicating that there was a large amount of stress relaxation within the first second of strain onset (recall: $\tau_1 = 0.1$ s, $\tau_2 = 1$ s, $\tau_3 = 10$ s, $\tau_4 = 100$ s). Further, the G_∞ parameter had the largest magnitude (> 0.5) of the $G(t)$ parameters

for all ligament types, indicating that each ligament type would maintain more than half of the induced instantaneous stress over an infinite time.

Table 7: Fitted QLV parameter vales for the ALL (mean ± 1 SE).

Strain (%)	A	B	G_∞	G_1	G_2	G_3	G_4
4	5.540 ± 0.730	0.619 ± 0.073	0.720 ± 0.017	0.177 ± 0.017	0.017 ± 0.005	0.044 ± 0.008	0.042 ± 0.008
6	5.733 ± 0.802	0.945 ± 0.493	0.685 ± 0.021	0.177 ± 0.020	0.029 ± 0.007	0.054 ± 0.005	0.055 ± 0.011
8	8.066 ± 0.992	0.429 ± 0.058	0.648 ± 0.024	0.183 ± 0.013	0.033 ± 0.003	0.059 ± 0.006	0.077 ± 0.014
10	6.614 ± 1.020	0.848 ± 0.375	0.635 ± 0.021	0.180 ± 0.011	0.039 ± 0.004	0.064 ± 0.006	0.082 ± 0.013
12	7.734 ± 1.295	1.383 ± 0.964	0.609 ± 0.023	0.184 ± 0.012	0.049 ± 0.006	0.076 ± 0.006	0.082 ± 0.012
14	7.108 ± 1.539	2.003 ± 1.148	0.585 ± 0.023	0.170 ± 0.009	0.066 ± 0.004	0.089 ± 0.005	0.089 ± 0.014
16	7.178 ± 1.682	1.424 ± 0.599	0.590 ± 0.021	0.186 ± 0.011	0.054 ± 0.004	0.084 ± 0.005	0.086 ± 0.014
18	5.857 ± 1.337	2.365 ± 1.111	0.586 ± 0.020	0.172 ± 0.007	0.067 ± 0.006	0.088 ± 0.006	0.087 ± 0.013
20	7.588 ± 1.604	2.365 ± 1.327	0.592 ± 0.023	0.179 ± 0.010	0.062 ± 0.006	0.082 ± 0.007	0.084 ± 0.013
25	4.655 ± 1.446	3.254 ± 1.189	0.582 ± 0.022	0.172 ± 0.008	0.074 ± 0.006	0.088 ± 0.006	0.084 ± 0.012

Table 8: Fitted QLV parameter values for the PLL (mean ± 1 SE).

Strain (%)	A	B	G_∞	G_1	G_2	G_3	G_4
4	3.621 ± 0.916	1.597 ± 0.439	0.665 ± 0.036	0.290 ± 0.039	0.006 ± 0.004	0.024 ± 0.006	0.015 ± 0.005
6	5.615 ± 1.707	0.485 ± 0.068	0.700 ± 0.023	0.235 ± 0.014	0.007 ± 0.003	0.032 ± 0.006	0.026 ± 0.008
8	5.823 ± 2.003	0.456 ± 0.074	0.691 ± 0.026	0.229 ± 0.017	0.008 ± 0.004	0.028 ± 0.008	0.043 ± 0.010
10	5.241 ± 1.255	0.407 ± 0.050	0.709 ± 0.023	0.187 ± 0.010	0.023 ± 0.007	0.042 ± 0.008	0.039 ± 0.009
12	5.703 ± 1.518	0.370 ± 0.049	0.693 ± 0.020	0.195 ± 0.014	0.024 ± 0.007	0.044 ± 0.007	0.044 ± 0.012
14	7.448 ± 2.243	0.358 ± 0.038	0.660 ± 0.036	0.209 ± 0.024	0.030 ± 0.005	0.060 ± 0.007	0.041 ± 0.008
16	7.640 ± 2.319	0.293 ± 0.034	0.677 ± 0.030	0.193 ± 0.012	0.030 ± 0.009	0.054 ± 0.009	0.047 ± 0.010
18	8.246 ± 2.658	0.332 ± 0.055	0.655 ± 0.027	0.204 ± 0.014	0.029 ± 0.009	0.057 ± 0.008	0.055 ± 0.012
20	7.845 ± 2.449	0.336 ± 0.053	0.661 ± 0.034	0.197 ± 0.017	0.032 ± 0.005	0.059 ± 0.007	0.051 ± 0.012
25	8.208 ± 2.978	0.439 ± 0.156	0.657 ± 0.028	0.173 ± 0.008	0.044 ± 0.006	0.065 ± 0.009	0.061 ± 0.015

Table 9: Fitted QLV parameter values for the LF (mean ± 1 SE).

Strain (%)	A	B	G_∞	G_1	G_2	G_3	G_4
4	0.884 ± 0.194	1.007 ± 0.212	0.845 ± 0.023	0.142 ± 0.022	0.000 ± 0.000	0.008 ± 0.002	0.004 ± 0.002
6	1.293 ± 0.208	0.472 ± 0.062	0.814 ± 0.018	0.170 ± 0.016	0.000 ± 0.000	0.012 ± 0.003	0.004 ± 0.001
8	1.702 ± 0.339	0.338 ± 0.042	0.787 ± 0.018	0.192 ± 0.016	0.000 ± 0.000	0.014 ± 0.004	0.007 ± 0.001
10	1.498 ± 0.284	0.390 ± 0.077	0.774 ± 0.025	0.202 ± 0.023	0.002 ± 0.001	0.014 ± 0.004	0.008 ± 0.001
12	1.719 ± 0.257	0.297 ± 0.031	0.725 ± 0.020	0.248 ± 0.024	0.003 ± 0.002	0.016 ± 0.004	0.008 ± 0.002
14	2.129 ± 0.398	0.356 ± 0.042	0.728 ± 0.024	0.212 ± 0.016	0.015 ± 0.008	0.028 ± 0.006	0.016 ± 0.004
16	1.480 ± 0.305	0.673 ± 0.367	0.723 ± 0.020	0.237 ± 0.027	0.008 ± 0.005	0.021 ± 0.005	0.011 ± 0.002
18	2.236 ± 0.440	0.394 ± 0.085	0.661 ± 0.033	0.261 ± 0.017	0.018 ± 0.010	0.028 ± 0.007	0.031 ± 0.011
20	1.712 ± 0.460	0.618 ± 0.213	0.690 ± 0.027	0.233 ± 0.008	0.020 ± 0.009	0.030 ± 0.006	0.027 ± 0.009
25	0.858 ± 0.327	2.717 ± 1.142	0.639 ± 0.025	0.242 ± 0.031	0.034 ± 0.013	0.048 ± 0.018	0.037 ± 0.011

To determine the effect of strain magnitude on the fitted parameters, a linear regression of the fitted (transformed) parameter values onto strain magnitude was performed (Section 2.7.3). The sign of the slope regression coefficients and its associated p-value (testing the null hypothesis that the slope is zero) are given in Table 10. The value of the slope regression coefficient is not reported since the slope was determined using the transformed parameter value, and thus has no physical significance. The sign of the slope, however, indicates if the transformed parameter is increasing or decreasing with strain magnitude, and therefore is reported. A significant slope ($p<0.05$) indicates strain dependence of the given parameter, while a non-significant slope indicates that the fitted parameter value did not change with strain magnitude.

Table 10: Slope and p-value determined by regressing the given parameter onto strain magnitude.

Parameter	ALL		PLL		LF	
	Slope sign	p-value	Slope sign	p-value	Slope sign	p-value
A	negative	0.2757	positive	**<0.0001**	negative	0.6091
B	positive	**<0.0001**	negative	**<0.0001**	positive	0.5202
G_∞	negative	**<0.0001**	negative	**0.0074**	negative	**<0.0001**
G_1	negative	0.4379	negative	**0.0025**	positive	**<0.0001**
G_2	positive	**<0.0001**	positive	**<0.0001**	positive	**<0.0001**
G_3	positive	**<0.0001**	positive	**<0.0001**	positive	**<0.0001**
G_4	positive	**<0.0001**	positive	**<0.0001**	positive	**<0.0001**

The instantaneous elastic stress parameter A was not dependent on strain magnitude for the ALL and the LF, but was observed to increase with increasing strain for the PLL. Parameter B showed an increasing trend with strain magnitude for the ALL, a decreasing trend for the PLL, and was not affected by strain magnitude for the LF. For all ligaments, each of the $G(t)$ relaxation parameters was dependent on strain level, except for parameter G_1 for the ALL. The long-term relaxation parameter G_∞ significantly decreased with increasing strain for all ligaments, indicating that a smaller proportion of the induced instantaneous elastic stress would remain in the ligament over long periods of time as greater strain magnitudes were applied. Additionally, the reduction of the G_∞ parameter with increasing strain magnitude indicates that more relaxation occurs at higher magnitudes of strain than at lower magnitudes. The G_1

relaxation parameter was not observed to depend on strain magnitude for the ALL, but was observed to decrease with increasing strain for the PLL and increase with strain for the LF. The remaining fitted G_2, G_3, and G_4 parameters were all observed to increase with increasing strain magnitude for all ligaments; indicating that the strength of the relaxation at the longer time constants (τ_2, τ_3, and τ_4) increased as the strain magnitude was increased in all ligaments.

The effect of strain magnitude on the reduced relaxation function $G(t)$, particularly the initial fast-rate relaxation region, is more clearly observed by plugging the constants from Table 7, Table 8, and Table 9 into equation (20), and plotting the reduced relaxation function on a logarithmic time scale [11]. For the ALL, the reduced relaxation function for all strain magnitudes overlap in the initial, fast-rate relaxation region (i.e. for $\tau_1 = 0.1$, Figure 3.26). This is consistent with the statistical findings that the fast-rate relaxation parameter G_1 is independent of strain magnitude for the ALL. Similar consistencies are observed for the fast-rate relaxation in the other ligaments (Figure 3.27); with the initial slope of the reduced relaxation function curve tending to decrease with increasing magnitudes of strain in the PLL, and tending to increase with increasing magnitudes of strain for the LF (Figure 3.28). Also, all ligaments show increasing long-term relaxation behavior (associated with τ_2, τ_3, and τ_4) with increasing magnitudes of strain. Interestingly, Figure 3.26 and Figure 3.27 indicate a possible converging behavior for the reduced relaxation function for the ALL and PLL, respectively, at higher magnitudes of strain. For the ALL, the difference in the reduced relaxation functions at different strain magnitudes appears to decrease with increasing strain, indicating a possible converging behavior for the ALL (Figure 3.26). The reduced relaxation function for the PLL displays a more varied relaxation behavior at the smaller strain magnitudes, but the difference in the reduced relaxation functions at the higher strain magnitudes decreases, indicating the $G(t)$ for the PLL may be converging as well. The $G(t)$ plot for the LF does not have any indication of possible convergence.

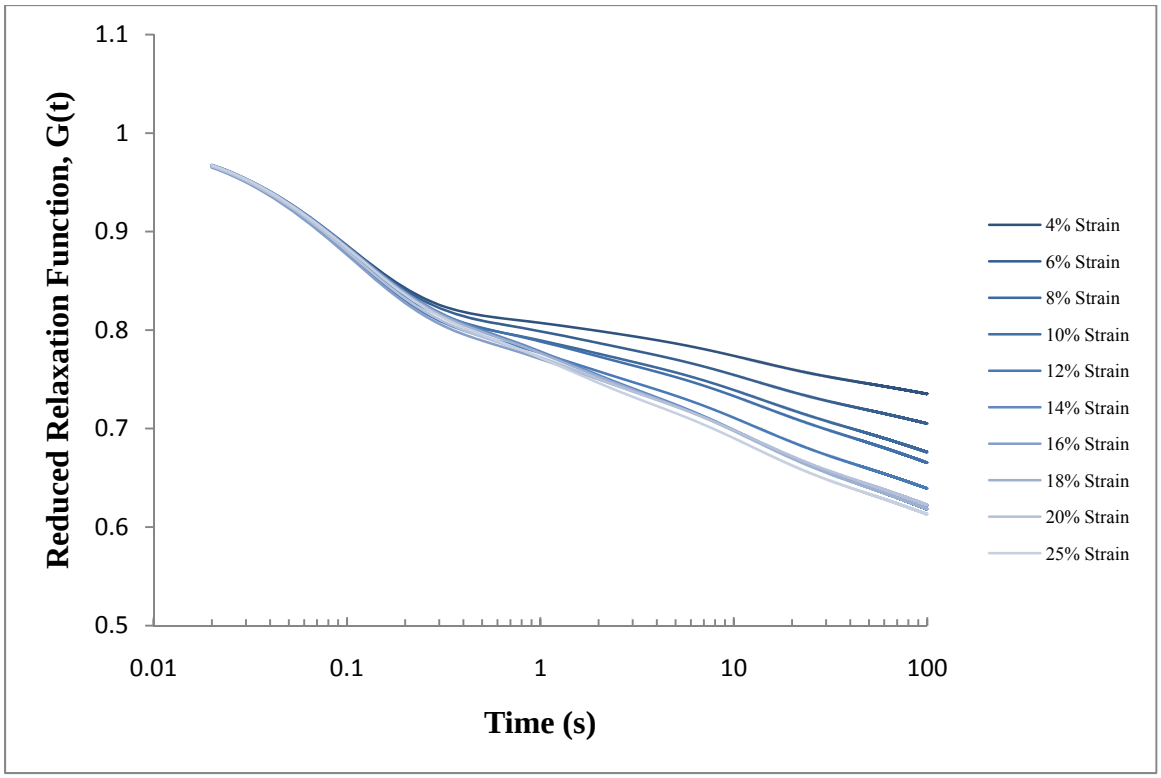

Figure 3.26: The reduced relaxation function at multiple magnitudes of strain for the ALL.

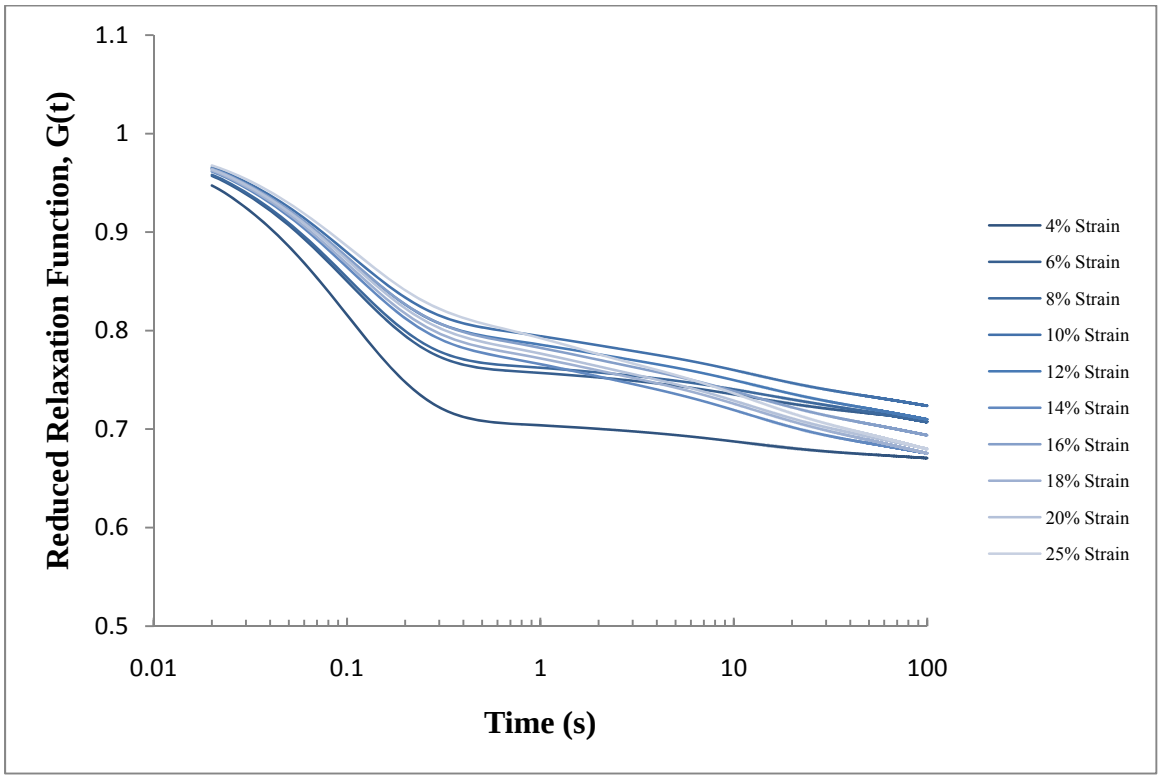

Figure 3.27: The reduced relaxation function at multiple magnitudes of strain for the PLL.

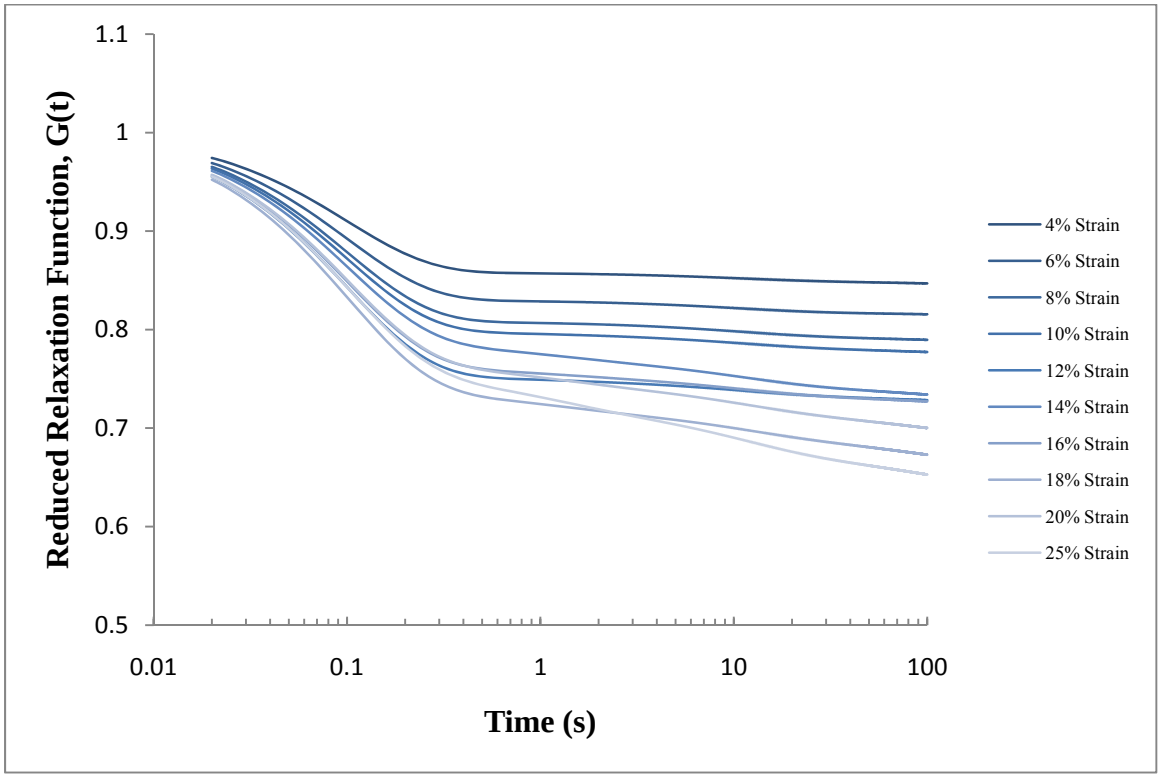

Figure 3.28: The reduced relaxation function at multiple magnitudes of strain for the LF.

The comparison of parameter values between the three ligament types indicated that the QLV fitted parameter values were unique to each ligament type (Table 11), suggesting that each ligament requires a unique relaxation function to describe its relaxation behavior. As described in more detail in Section 2.7.3, some of the parameter comparisons had slopes that were not significantly different. In this case, the slope term was removed from the regression model and a new regression analysis was performed. The intercepts determined from the new regression were subsequently compared (indicated by an asterisk in Table 11). Specifically, the presence of an asterisk indicates that the effect of strain on that parameter was the same for the compared ligaments (i.e., the slopes were parallel), and that these slopes were offset by a constant value (i.e., the intercept value).

Table 11: Comparison of parameters between ligament types. * indicates comparison of intercepts because the slopes were not significantly different.

Parameter	ALL-LF	ALL-PLL	PLL-LF
A	0.0053*	<0.0001	0.0018
B	0.0097	<0.0001	0.0003
G_∞	0.0245	<0.0001	<0.0001
G_1	<0.0001	0.0021	<0.0001
G_2	<0.0001*	0.0026*	0.0162*
G_3	0.0001*	0.0147*	0.0106*
G_4	0.0024	0.0128*	0.0122*

3.3.2. Power law fitted parameters

The power law fitted parameters along with the median r^2 values for the ALL, PLL, and LF are given in Table 12, Table 13, and Table 14, respectively. Equation (30) approximated the relaxation region of the data well, only observing a poor median r^2 value ($r^2 < 0.5$) at 4% strain for the LF (Table 14).

Table 12: Power law fitted parameters (± 1 SE) and the median r^2 for the ALL.

Strain (%)	σ_0 (MPa)			n			r^2
4	0.207	±	0.014	-0.022	±	0.004	0.92
6	0.293	±	0.019	-0.029	±	0.004	0.98
8	0.397	±	0.031	-0.037	±	0.005	0.98
10	0.471	±	0.041	-0.040	±	0.005	0.99
12	0.606	±	0.060	-0.046	±	0.005	0.99
14	0.861	±	0.088	-0.053	±	0.005	0.99
16	0.919	±	0.098	-0.050	±	0.005	0.99
18	1.217	±	0.135	-0.052	±	0.005	0.99
20	1.396	±	0.156	-0.050	±	0.005	0.99
25	1.981	±	0.235	-0.053	±	0.006	0.99

Table 13: Power law fitted parameters (± 1 SE) and the median r^2 for the PLL.

Strain (%)	σ_0 (MPa)			n			r^2
4	0.208	±	0.044	-0.012	±	0.003	0.76
6	0.262	±	0.062	-0.016	±	0.003	0.92
8	0.326	±	0.088	-0.019	±	0.004	0.94
10	0.390	±	0.117	-0.022	±	0.004	0.95
12	0.512	±	0.167	-0.025	±	0.005	0.97
14	0.615	±	0.213	-0.030	±	0.005	0.99
16	0.646	±	0.230	-0.029	±	0.006	0.99
18	0.823	±	0.310	-0.032	±	0.006	0.99
20	0.906	±	0.346	-0.032	±	0.006	0.99
25	1.203	±	0.480	-0.036	±	0.007	0.98

Table 14: Power law fitted parameters (± 1 SE) and the median r^2 for the LF.

Strain (%)	σ_0 (MPa)			n			r^2
4	0.057	±	0.006	-0.003	±	0.001	0.45
6	0.067	±	0.006	-0.004	±	0.001	0.60
8	0.074	±	0.008	-0.006	±	0.001	0.77
10	0.075	±	0.009	-0.006	±	0.001	0.84
12	0.083	±	0.010	-0.007	±	0.001	0.87
14	0.117	±	0.018	-0.013	±	0.003	0.96
16	0.102	±	0.014	-0.009	±	0.002	0.92
18	0.141	±	0.025	-0.018	±	0.006	0.98
20	0.148	±	0.027	-0.017	±	0.005	0.98
25	0.187	±	0.039	-0.026	±	0.009	0.98

From the statistical analysis outlined in Section 2.7.4, the mean initial stress σ_0 was observed to increase with the square of the strain magnitude for all ligaments ($p<0.0001$ for each ligament), indicating a quadratic relationship between σ_0 and strain magnitude. Additionally, the mean relaxation rate n was also found have a quadratic relationship with strain, becoming increasingly negative with increasing magnitudes of strain ($p<0.0001$ for each ligament). Hence, as the strain magnitude increased, all ligaments experienced a larger initial stress and a faster rate of relaxation (Figure 3.29 and Figure 3.30, respectively). The fitted equations shown in Figure 3.29 and Figure 3.30 were calculated via regression of the σ_0 and n, respectively, on strain. The regression equations representing $\sigma_0(\varepsilon)$ and $n(\varepsilon)$ and their corresponding r^2 values are provided in Table 15 and Table 16, respectively.

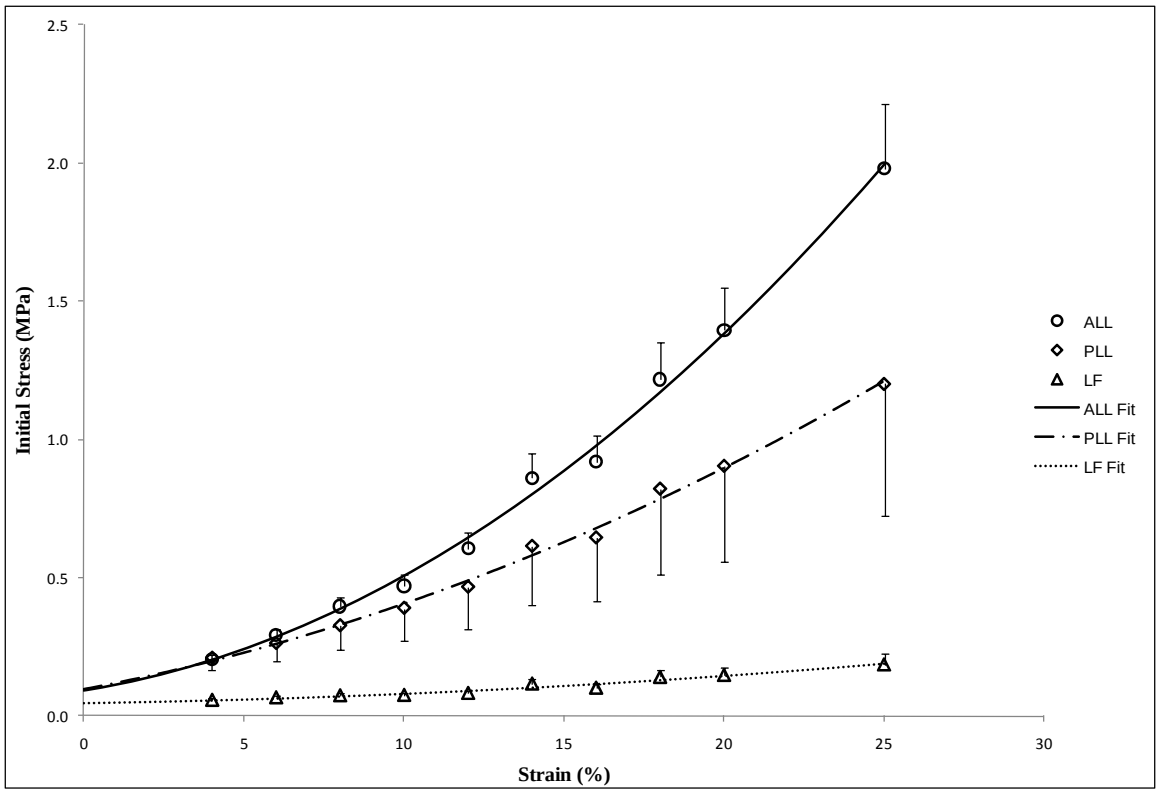

Figure 3.29: Initial stress increases with the square of the strain. Error bars indicate one standard error.

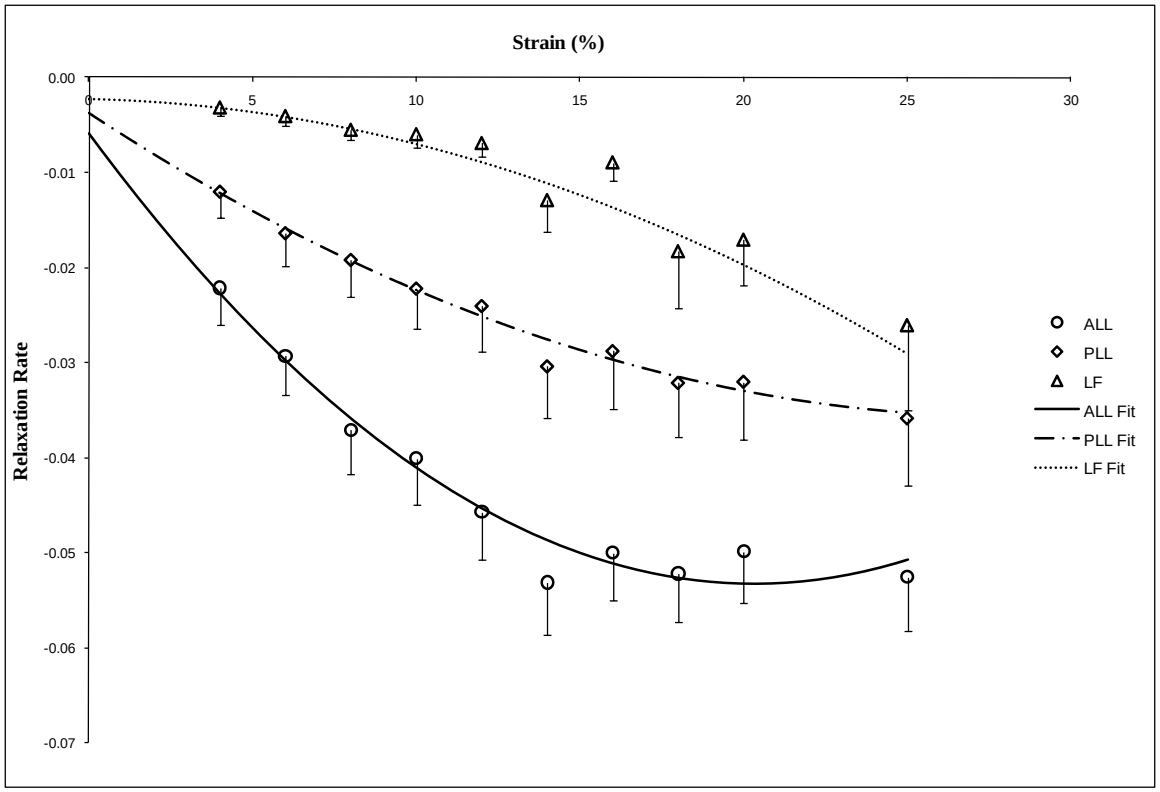

Figure 3.30: Relaxation rate becomes increasingly negative with the square of strain magnitude. Error bars indicate one standard error.

Table 15: Fitted equations for the initial stress.

Ligament	Equation	r^2
ALL	$\sigma_0(\varepsilon) = 0.09047 + 0.01837\varepsilon + 0.002313\varepsilon^2$	0.9957
PLL	$\sigma_0(\varepsilon) = 0.09573 + 0.02187\varepsilon + 0.000915\varepsilon^2$	0.9948
LF	$\sigma_0(\varepsilon) = 0.0476 + 0.00177\varepsilon + 0.000155\varepsilon^2$	0.9353

Table 16: Fitted equations for the relaxation rate.

Ligament	Equation	r^2
ALL	$n(\varepsilon) = -0.00588 - 0.00467\varepsilon + 0.000115\varepsilon^2$	0.9627
PLL	$n(\varepsilon) = -0.00382 - 0.00226\varepsilon + 0.00004\varepsilon^2$	0.9784
LF	$n(\varepsilon) = -0.00223 - 0.000075\varepsilon - 0.00004\varepsilon^2$	0.9343

As with the QLV fitted parameters, comparison of σ_0 and n across ligament types (using the statistical procedure described in Section 2.7.4) indicated that the relaxation behavior of each ligament was unique (Table 17). Within the range of experimental strain magnitudes, the initial stress of the ALL and the PLL increased faster than the LF, although the initial stress of the ALL increased faster than the PLL (Figure 3.29). Interestingly, although the relaxation rate increased with increasing strain magnitude for all ligaments, the shape of the relaxation rate curve (Figure 3.30) for the LF was opposite of that of both the ALL and PLL due to the negative quadratic regression coefficient of the LF regression equation (Table 16). As a result of the difference in regression equations, the rate of relaxation for the ALL and PLL appear to be slowing, and possibly converging to a constant n, at the higher strain magnitudes while the relaxation rate for the LF appears to be greatly increasing with increasing strain magnitude. The possible convergence behavior of the ALL and PLL relaxation curves, and the diverging behavior of the LF relaxation determined using the power law echoes the behavior observed for the reduced relaxation function $G(t)$ in Section 3.3.1 (see Figure 3.26 for the ALL, Figure 3.27 for the PLL, and Figure 3.28 for the LF).

Table 17: p-values comparing regression coefficients for different ligament types. * indicates a difference on the linear fit, but not the quadratic.

Regression coefficient	ALL-LF	PLL-LF	ALL-PLL
σ_0	0.0076	0.0137*	<0.0001*
n	<0.0001	0.0034	0.0016

In order to directly observe the effect of strain magnitude, and hence the validity of QLV theory to model the comprehensive viscoelastic behavior of these ligaments, a fitted power law

equation was calculated at the 4% strain level for a representative specimen from each ligament type and was superimposed onto the experimental relaxation data at all other strain magnitudes (ALL: Figure 3.31, PLL: Figure 3.32, LF: Figure 3.33) [21]. Since QLV assumes that the relaxation function is independent of strain magnitude, the fitted equation at 4% strain must approximate the experimental data at multiple magnitudes of strain. For all ligament types, the fit at 4% strain did not adequately approximate the experimental data at other strain magnitudes. Large deviations were observed between the multiple magnitudes of strain and the fit at 4% strain, especially at the larger strain magnitudes (Figure 3.31, Figure 3.32, and Figure 3.33). The experimental data indicate that the relaxation behavior of these ligaments is dependent on the magnitude of applied strain, and thus, QLV theory cannot adequately describe the comprehensive viscoelastic behavior of these ligaments.

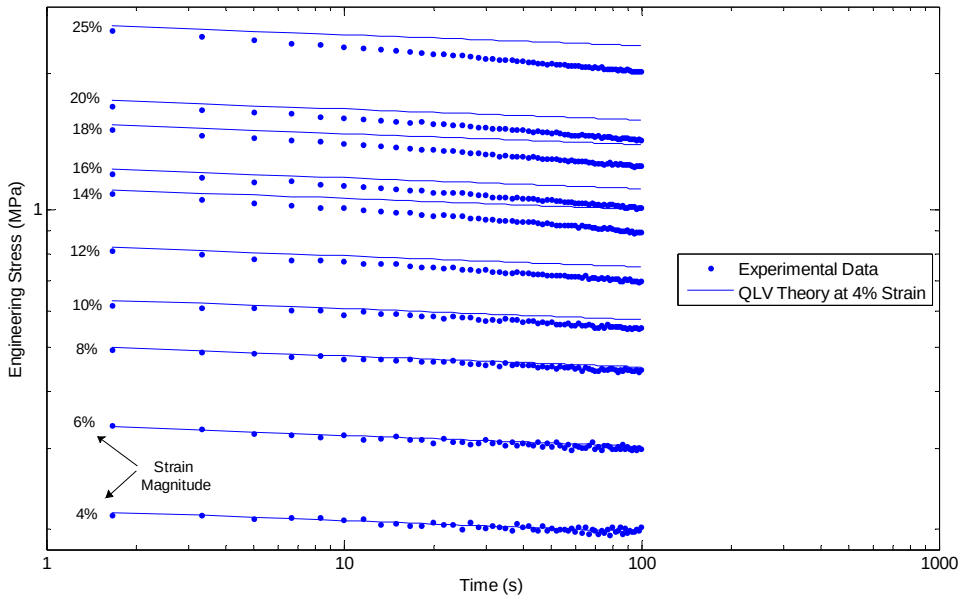

Figure 3.31: Fitted power law at 4% strain superimposed on all other strain magnitudes for the ALL.

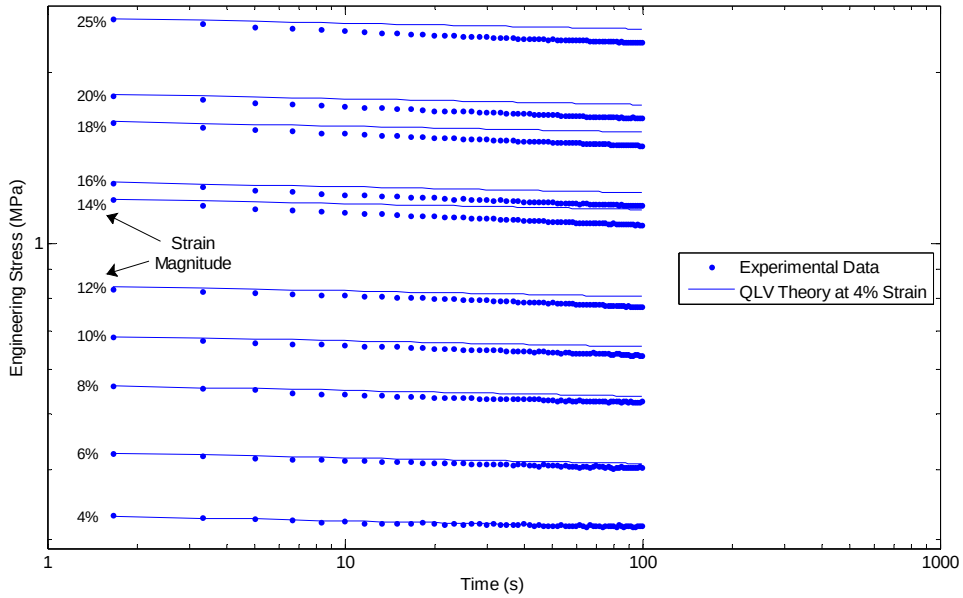

Figure 3.32: Fitted power law at 4% strain superimposed on all other strain magnitudes for the PLL.

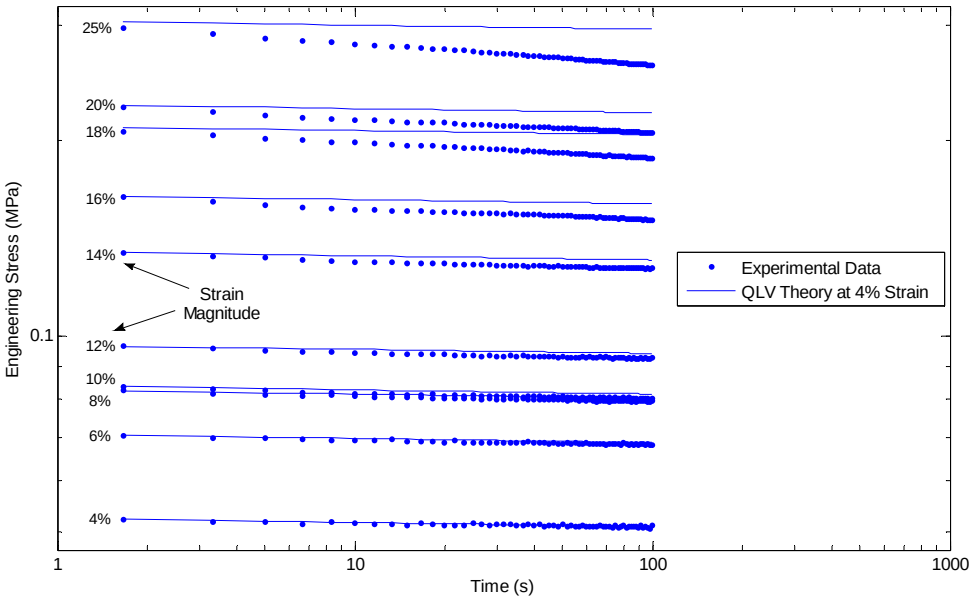

Figure 3.33: Fitted power law at 4% strain superimposed on all other strain magnitudes for the LF.

4. DISCUSSION

Cyclic and stress relaxation experiments were performed on three types of human cadaveric lower cervical spine ligaments (ALL, PLL, and LF) to characterize the viscoelastic behavior of these ligaments within their physiologic range. The cyclic testing protocol was performed to characterize the comprehensive cyclic viscoelastic properties of the ligaments when exposed to four physiologic frequencies (0.001 Hz, 0.01 Hz, 0.1 Hz, and 1 Hz) at two physiologic strain amplitudes (10% and 15%). Results indicated that the cyclic viscoelastic properties were dependent on both strain magnitude and frequency. Stress relaxation experiments were performed to characterize the comprehensive stress relaxation behavior of these ligaments when subjected to multiple magnitudes of strain. For all ligament types, the stress relaxation behavior was observed to depend on the applied strain magnitude.

4.1. Ligament Geometry

Measurement of the geometric properties of human cervical spine ligaments is challenging, owing to the small size of the ligaments and difficulties in distinguishing the ligament from surrounding tissues. Traditional medical imaging techniques, such as X-ray, MRI, and CT do not provide the resolution required to accurately define ligament geometry and/or cannot accurately delineate tissue boundaries [28]. Researchers have used many different measurement techniques to define the geometry of human cervical spine ligaments. These methods include: (1) stereophotogrammetry, to measure ligament length and width [12]; (2) laser micrometer, to measure the cross-sectional area [27]; (3) sequential axial and sagittal cryomicrotome images, to

measure ligament areas and lengths, respectively [33]; (4) and digital calipers, to define the ligament gage length while attached to a testing apparatus [11].

The current study used novel methods to measure the ligament initial gage length and the ligament cross-sectional area. Ligament gage length was defined as the distance between the cranial and caudal osseous insertion sites and was determined by recording the MTS crosshead displacement (measured via a built-in LVDT) after the segments were compressed together and the ligament was subsequently elongated at 5 N of pretension. Hence, the crosshead displacement output was the distance between the superior and inferior ligament-bone insertion points (i.e., the disc space) in the ALL and PLL, and the distance between the superior and inferior lamina for the LF. Previous studies have used the aforementioned dimensions to define the gage lengths of these ligaments [11, 27]. By defining the gage length in this manner, however, the resultant data holds an inherent assumption that all deformation of the ligament occurs in the in the section of the ligament spanning the disc space, and that the deformation in the section of the ligament attached to the bone is negligible.

The initial lengths measured for the ALL and LF from the present study are within one standard deviation of the ALL and LF initial lengths reported by Lucas et al. [11] (Table 18). However, the initial length of the PLL from the current study was considerably smaller than that reported by Lucas et al. The initial lengths reported by Lucas et al. are surprising in that they report nearly identical gage lengths for the ALL and PLL, which is unexpected since the human cervical spine displays lordosis, or convex curvature towards the anterior [1]. This spinal curvature gives the cervical intervertebral disc a wedge shape, with a reported posterior-to-anterior disc height ratio in the range of 41% – 49% at the C5-C6 level [28, 48]. Since the gage length definition for the longitudinal ligaments in this study is a measure of the disc space, it is natural to expect that the initial lengths for the ALL and PLL follow a ratio similar to that of the disc height. In fact, the ratio of the mean PLL initial length to the mean ALL initial length was

39% for the DMA experiments and 41% for the relaxation experiments (Table 18), approximating the reported posterior-to-anterior disc height range.

Table 18: Comparison of the initial gage lengths (mean ± 1 SD) from the current study to those reported by Lucas et al.

	ALL (mm)	PLL (mm)	LF (mm)
DMA	3.06 ± 1.29	1.19 ± 0.69	3.31 ± 0.45
Relaxation	3.17 ± 1.34	1.31 ± 0.67	3.44 ± 0.49
Lucas et al. [11]	3.47 ± 0.81	3.26 ± 0.85	3.87 ± 1.58

The ligament cross-sectional areas reported in this thesis were measured using *post hoc* digital image capture of a cross-sectional cut at the tissue's mid-substance. Few studies have reported the cross-sectional area of cervical spine ligaments [27, 33] (Table 19). The mean cross-sectional areas of the ALL and PLL determined from the present study were within one standard deviation of the cross-sectional areas reported by Przybylski et al., who measured ligament area using a laser micrometer while the ligament was under 1 N of tension [27]. However, the ligament cross-sectional areas in the present study were considerably larger than those reported by Yoganandan et al., who measured cross-sectional area using a cryomicrotome method [33]. The difference between the cross-sectional areas reported by Yoganandan et al. and those reported by both Przybylski et al. and in this thesis may be a result the different measurement techniques. Area measurements from the cryomicrotome were obtained from sections of intact, frozen cervical spines, while the measurements from both the present study and Przybylski et al. were taken from isolated, highly hydrated ligaments at room temperature. Thus, the discrepancy between the reported areas may be due to the combination of two factors: ligament pretension and ligament hydration. The cyromicrotome technique accounts for *in situ* ligament pretension, while the present study and the work of Przybylski et al. (with 1 N of ligament pretension and the intervertebral disc removed) did not. Pretensioned ligaments *in situ* may have a smaller cross-sectional area than unloaded ligaments because of the Poisson effect. It should be noted that the intrinsic ligament properties presented in the Results section of this thesis were calculated from the unloaded cross-sectional area, and should be interpreted as such. The cross-sectional area of

tendons, which also exhibit *in situ* pretension, are commonly measured without pretension using an "area micrometer" method described by Butler and collegues [49]. *In situ* ligament pretension has not been quantified, and thus warrants further investigation. Ligament hydration is also important in determining the cross-sectional area since ligaments are composed of nearly two-thirds water [50]. Yoganandan et al. do not comment on how ligament hydration was maintained during their cryomicrotome procedure, and it may be possible that the cryomicrotome frozen ligaments were not as hydrated as the ligaments used in this thesis and the study by Przybylski et al., where ligament hydration was closely monitored at room temperature. Because water is the dominant component of ligaments, it is expected that dehydrated ligaments will have a smaller cross-sectional area than well hydrated ligaments.

Table 19: Comparison of cross-sectional areas from the present study to previously reported data.

	ALL (mm^2)	PLL (mm^2)	LF (mm^2)
Present study	30.23 ± 6.33	31.92 ± 9.67	86.15 ± 15.26
Przybylski et al. [27]	33 ± 10	33 ± 18	N/A
Yoganandan et al. [33]	12.1 ± 2.68	14.7 ± 6.77	48.9 ± 7.9

As seen in the box-and-whisker plot (Figure 3.1) and in the standard deviations reported by previous the work (Table 19), there was a considerable amount of variability in the cross-sectional areas of these ligaments. While general cadaver specimen-to-specimen size differences likely contributed to the majority of the variation in the LF, previous studies have reported difficulties in delineating the lateral boundaries of the ALL and PLL during gross dissection because the deep ligament fibers are intertwined with the annulus fibrosis [12, 13, 37]. The PLL is even more difficult to distinguish because its fibers extend more broadly around the circumference of the intervertebral disc than the ALL, and due to its direct attachment to the dura matter [37, 38]. These difficulties were observed during the gross dissection of the longitudinal ligaments in this thesis, and possibly explain the variability in the cross-sectional area of the ALL and PLL. As stated in the Methods (Section 2.2.1), the ligaments were carefully separated from

the surrounding tissue, and dissection was ceased once the tissue was no longer readily removed to avoid damaging the ligament.

4.2. Dynamic Mechanical Analysis

Under the linear viscoelastic material assumption (standard linear solid), for which the relaxation behavior, $E(t)$, can be described as:

$$E(t) = E_2 + E_1 e^{-t/\tau_r} \tag{32}$$

where τ_r is the relaxation time, the storage (E') and loss (E'') modulus can be written as [19]:

$$E'(\omega) = E_2 + E_1 \frac{\omega^2 \tau_r^2}{1 + \omega^2 \tau_r^2} \tag{33}$$

$$E''(\omega) = E_1 \frac{\omega \tau_r}{1 + \omega^2 \tau_r^2} \tag{34}$$

where ω is frequency. As presented in this thesis, the reduced relaxation function for quasi-linear viscoelastic theory is often written as a generalized form of equation (32) by adding more exponential terms [17]. Using equations (33) and (34), the complex modulus (E^*) is written as:

$$E^* = E'(\omega) + iE''(\omega) \tag{35}$$

where the magnitude of E^* is given by: $|E^*| = \sqrt{[E'(\omega)]^2 + [E''(\omega)]^2}$. Additionally, the $\tan(\delta)$ can be written as [19]:

$$\tan(\delta) = \frac{E_1/E_2}{\sqrt{1 + E_1/E_2}} \left[\frac{\omega t_r \sqrt{1 + E_1/E_2}}{1 + \omega^2 \left(t_r \sqrt{1 + E_1/E_2} \right)^2} \right] \tag{36}$$

Note that under the assumption of a linear (and quasi-linear) viscoelastic material, the storage modulus, the loss modulus, the complex modulus, and the $\tan(\delta)$ are independent of the applied strain amplitude. Therefore, for a material subjected to a cyclic disturbance to satisfy the assumptions of linear and quasi-linear viscoelastic theory, the dynamic moduli and the $\tan(\delta)$ must be independent of strain.

From the DMA analysis, all ligament types exhibited a nonlinear viscoelastic (i.e., strain amplitude-dependent) response, especially at slower frequencies. The $\tan(\delta)$ was dependent on strain amplitude at the 0.001 Hz frequencies for all ligament types. The storage moduli were dependent upon strain amplitude at all frequencies for the ALL and at the 0.001 Hz and 0.01 Hz frequencies for the PLL. Strain amplitude-dependent nonlinear viscoelastic behavior has been observed in human lumbar facet joint capsule (FJC) [20] and human medial collateral ligament (MCL) [51]. Little and Khalsa reported that the storage and loss moduli, and hence the complex modulus, for human lumbar FJC increased with cyclic amplitude, but were unaffected by changes in frequency. However, the FJC phase lag (δ) was independent of cyclic amplitude [20]. Bonifasi-Lista et al. observed the magnitude of the complex modulus for human MCL to increase with increasing strain amplitude when the ligaments were loaded parallel and transverse to the collagen fiber direction, as well as when loaded in shear [51]. Additionally, the MCL phase lag was strain amplitude-dependent when loaded parallel to the collagen fibers, but not when loaded transverse to the fibers or in shear [51].

The nonlinear strain amplitude-dependent viscoelastic behavior of the ligaments in this thesis was found to be dependent on frequency. For example, the $\tan(\delta)$ for all ligaments was strain amplitude-dependent at the (slow) 0.001 Hz frequency, but was not dependent on strain amplitude at the faster frequencies. Further, the storage modulus for the PLL was dependent on strain amplitude at the 0.001 Hz and 0.01 Hz frequency, and exhibited weak evidence ($p \approx 0.09$) of strain amplitude-dependent behavior at the 0.1 Hz and 1 Hz frequencies. Yoganandan et al. previously reported strain-rate dependent tensile mechanical properties (failure force, stiffness, and energy-absorbing capacity) for cervical spine ALL and LF [29]. Strain amplitude-dependent viscoelastic behavior at different frequencies may indicate that different viscoelastic behavior is observed when the ligament structure has sufficient time to react to the applied load [28]. Though there is not currently an agreement on the specific underlying microstructural mechanism that causes the viscoelastic behavior of ligaments, the time-dependent behavior of ligaments and

tendons has been attributed to the inherent viscoelasticity of collagen fibrils, along with their interactions with other microstructural components such as elastin fibers, ground substance, and water [52]. Thus, the complicated nonlinear viscoelastic behavior of the ALL, PLL and LF at slow loading rates may be a result of the viscous aspect of the tissue structure having time to significantly contribute to the mechanical behavior as the ligament elongates. The results of this thesis suggest that these viscous contributions vary depending on the amount of ligament elongation.

The results of the DMA procedure also indicate that the cyclic material properties of the ALL, PLL and LF (storage modulus, loss modulus, and $\tan(\delta)$) are dependent upon frequency, especially over multiple frequency decades. These findings are consistent with previous reports of strain-rate dependent behavior of the tensile mechanical properties of human lower cervical ALL and LF [29] and upper cervical alar and transverse ligaments [53], and the frequency dependent cyclic properties of the human lumbar FJC $\tan(\delta)$ [20].

The present study found that the lower cervical spine ALL, PLL, and LF became more elastic (storing more energy than they were dissipating) as frequency was increased. Examples of more elastic behavior include: the $\tan(\delta)$ decreased with increasing frequency for all ligament types, the ALL and PLL storage moduli at the 0.001 Hz frequency were smaller than the storage moduli calculated for the faster frequencies, and the loss modulus decreased with increasing frequency for all ligament types. These results are consistent with the observed increase in tensile stiffness, failure load, and energy absorbing capacity with increasing strain-rate reported for the lower cervical ALL and LF [29]. However, the decreasing $\tan(\delta)$ observed in the lower cervical ALL, PLL, and LF is in opposition to the phase lag trend found by Little and Khalsa for the lumbar FJC, which was reported to increase with increasing frequency [20]. Furthermore, the storage and loss moduli of the human FJC were found to be insensitive to frequency. The discrepancy of the dynamic mechanical properties of the cervical ALL, PLL and LF, and the lumbar FJC may be due to the different anatomical locations and functions of these ligaments. In

addition, these differences are most likely also the product of variations in the range of frequencies that were investigated. Rumian et al. reported that the structures of individual ovine knee ligaments are unique to their anatomical location [54]. Since the mechanical behavior of ligaments is determined by their structural organization [17], it is possible that the mechanical behavior of ovine knee ligaments is also dependent on their anatomical locations. Individual spinal ligaments, like ovine knee ligaments, have unique structures that are conductive to their intended function [14]. Thus, differences in the cyclic mechanical behavior of the lower cervical ALL, PLL, and LF, and the lumbar FJCs may be due to unique microstructural differences between these ligaments. Furthermore, Little and Khalsa only tested the FJC at two frequency decades (0.2 Hz – 2 Hz), while the present study measured the ligament response over four decades (0.001 Hz – 1 Hz) [20]. In fact, many of the cyclic material properties of the ligaments in this thesis (e.g. the storage modulus for the PLL) were not statistically different over the range of two decades, but were statistically different over the four decade range. Hence, human lumbar FJC may exhibit frequency dependent behavior that is outside of the range tested by Little and Khalsa.

Nearly no statistical differences were observed between the ALL and PLL cyclic material properties at any strain amplitude or frequency. However, the longitudinal ligaments had a markedly different, more viscoelastic, cyclic material behavior than the LF. While the LF $\tan(\delta)$ was statistically smaller than both the ALL $\tan(\delta)$ and the PLL $\tan(\delta)$, the most notable differences between the longitudinal ligaments and the LF were in the storage and loss moduli, which were both an order of magnitude smaller for the LF than the longitudinal ligaments at each frequency and strain amplitude. The different material properties may be a result of the different morphologies of the longitudinal ligaments compared to the LF. As stated earlier in Section 1.1.3, the longitudinal ligaments have similar microstructures that contain a large proportion of highly aligned (parallel) collagen fibers and relatively little elastin content [13-15]. In contrast, the LF has been shown to have an elastin-to-collagen ratio of 2:1 with the collagen fibers loosely

dispersed in the elastic tissue [14, 16]. Elastin fibers are highly extensible, offering little resistance to deformation [13]. Thus, the high elastin content of the LF allows it to be stretched considerably more than the longitudinal ligaments before the inherently viscoelastic collagen fibrils become aligned and recruited [13, 52]. Previous work has shown that the highly aligned collagen fibers in the longitudinal ligaments become recruited at smaller strains than those of the LF [14], and therefore the longitudinal ligaments would be expected to exhibit a more viscoelastic response than the LF at the same strain amplitude.

The results of the DMA procedure are consistent with the functional role of ligaments [1]. At slower frequencies, all ligaments were observed to dissipate more energy than at the higher frequencies. Dissipating energy at slow loading rates would allow the spinal column to move in its physiologic regime at without injury. However, as the ligaments, specifically the longitudinal ligaments, were subjected to higher loading rates (frequencies) the ligaments began storing (absorbing) more energy. This observed behavior of these lower cervical longitudinal ligaments may be important to maintain stability of the spine and/or absorb energy during trauma, such as whiplash.

4.3. QLV Fitted Parameters

Quasi-linear viscoelastic theory is widely applied to model the viscoelastic behavior of ligaments and tendons [52]. The coefficients of determination in this study suggested that QLV theory adequately explained the experimental relaxation data of these ligaments at individual strain magnitudes; however, statistical analysis indicated strong dependence of the fitted reduced relaxation function $G(t)$ coefficients on the applied strain magnitude for all ligament types. For a material to be modeled as quasi-linear viscoelastic, it is necessary that the relaxation function be independent of strain [19]. However, the reduced relaxation function $G(t)$ determined by fitting the experimental stress relaxation data of the ALL, PLL and LF to QLV theory at each strain magnitude were found to be strongly dependent upon strain level. Therefore, a more general,

fully nonlinear viscoelastic theory is required to adequately characterize the comprehensive relaxation behavior of these ligaments when subjected to multiple magnitudes of strain. Furthermore, because of the good agreement between QLV theory and the experimental data at specific strain magnitudes, these results reiterate that stress relaxation experiments at a single strain magnitude is not sufficient to determine if the ligament exhibits linear, quasi-linear, or nonlinear viscoelastic behavior [19].

In contrast to the results presented in this thesis, Lucas at al. recently reported on the adequacy of QLV theory to describe the viscoelastic behavior of human lower cervical ALL, PLL, and LF [11]. They validated their claim by performing stress relaxation experiments on these ligaments at two different strain magnitudes (25% and 50%) and predicted the experimental response from a relaxation test at one strain magnitude (25%) from a QLV model determined by fitting the stress relaxation test at the other strain magnitude (50%). The ability of the QLV model to predict the experimental relaxation data was quantified by computing the square of the correlation coefficient (i.e., the coefficient of determination or R^2 value) between the QLV model and the predicted force response. The reported mean squared correlation coefficients were greater than 0.78 (see [11], Table 1). In addition to the correlation coefficient, Lucas et al. state that the normalized force response from the two strain magnitudes were "…comparable, although not identical" [11]. Although the coefficients of determination appear to suggest good agreement between the two strain magnitudes, the high correlation between the QLV model at 50% strain and the experimental data at 25% strain may be due to the long-term relaxation behavior of these ligaments and not necessarily because the relaxation curves demonstrated correspondence. The large magnitude of the G_1 coefficient in relation to the G_2, G_3, and G_4 coefficients observed in this thesis indicate that the short-term relaxation behavior is highly important in determining the shape of the relaxation curve. To illustrate the possible inadequacy of using the R^2 value to test if the shape of two curves are different, and thus to examine the validity of this method to validate the adequacy of QLV theory to model cervical spine ligament behavior, a representative stress

relaxation curve (an ALL specimen) from the present work was fitted to QLV theory at 25% strain and the resulting model was used to predict the 4% stress relaxation behavior (Figure 4.1). The coefficient of determination between the QLV model at 25% strain and the experimental data at 4% strain was calculated to be 0.78, even though there are notable differences between these curves (Figure 4.1). Interestingly, Lucas et al. report a mean R^2 value of 0.78 for the female LF at the C3-C4 level (see [11], Table 1). The inadequacy of this method is more clearly seen when the normalized QLV model at 25% strain is plotted against the normalized experimental data at 4% strain (Figure 4.2). The important short-term relaxation behavior is poorly correlated while the long-term behavior is highly correlated. Since there are many more datum points in the long-term relaxation region, the long-term behavior dominates the calculation of the R^2 value, resulting in a moderate R^2 value. Furthermore, if the QLV model at 25% strain was indeed a good predictor of the experimental data at 4% strain, the slope of a best-fit line in Figure 4.2 should converge to unity. Hence, the preceding example illustrates that a high R^2 value does not provide assurance that the shape of the relaxation curves are equal. Therefore, the current study utilized a more rigorous statistical method to make inferences about the shape of the relaxation curve, and thus the validity of QLV theory.

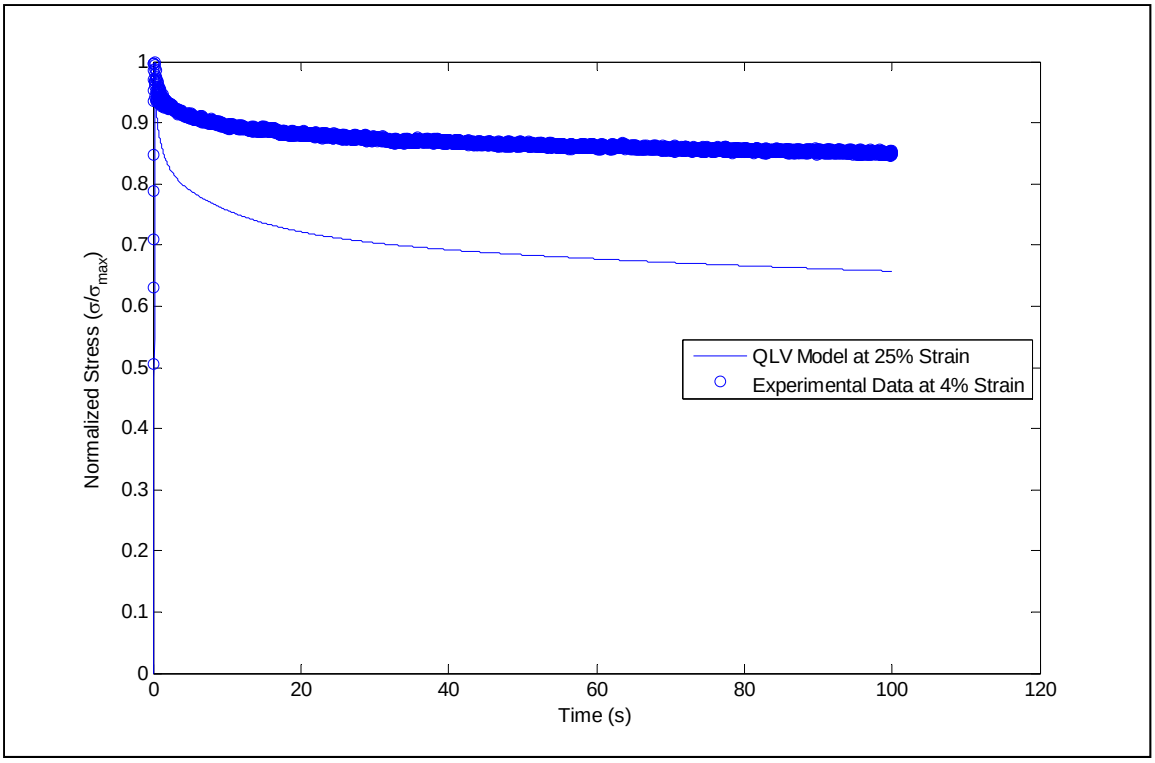

Figure 4.1: Normalized experimental relaxation data at 4% strain and QLV model fitted to 25% strain.

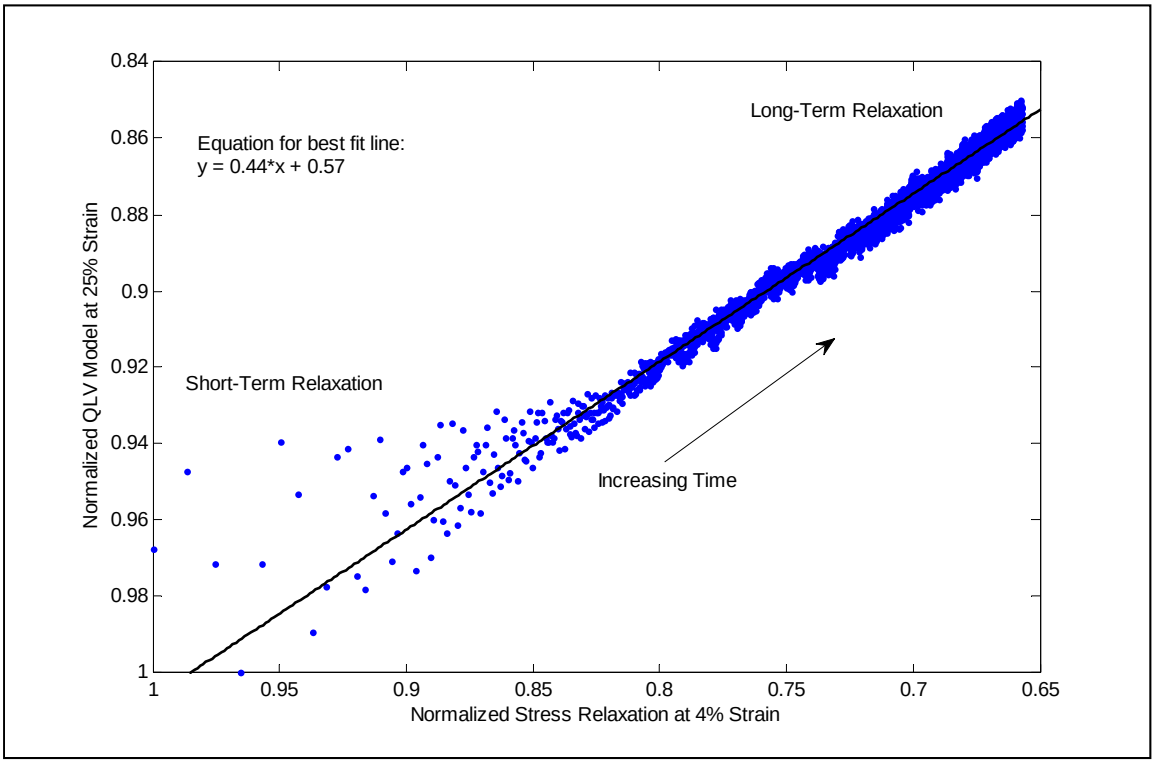

Figure 4.2: A moderate R^2 value (0.78) between the QLV model at 25% strain and the experimental data at 4% strain may be a result of the data being highly weighted by the long-term relaxation behavior and, thus, does not guarantee that the shapes of the relaxation curves are equal. Note that the scales of the x- and y-axes have been reversed for better interpretation.

The coefficients of determination at each strain magnitude, which correlated the fitted QLV theory to the experimental data at each strain level, were observed to increase with increasing strain magnitude indicating a more viscoelastic response, and thus a better fit, at higher strains. There is much speculation in the literature as to the underlying microstructural mechanism of ligament viscoelasticity. The viscoelastic behavior of ligaments has been attributed to fluid flow [21, 55-57], interactions between the collagen fibers and the proteoglycan ground substance [58], and progressive collagen fiber recruitment [59]. A recent study on porcine lumbar PLL collagen fiber fascicles suggested that the stress relaxation behavior of spinal ligaments is related to the intrinsic viscoelastic properties of individual collagen fiber fascicles because these fascicles were found to posses similar relaxation characteristics to full ligaments [46]. However, it is possible that each microstructure constituent contributes to the viscoelastic behavior of these ligaments, and further investigations are required to determine the specific contributions of each microstructural component.

Ligament microstructure may be responsible for the apparent asymptotic converging behavior observed in the reduced relaxation function $G(t)$ for the ALL and PLL, and the apparent diverging behavior of the LF $G(t)$. Converging behavior of the reduced relaxation function with increasing strain magnitude has been reported for human medial collateral ligament [51]. Microstructural collagen fibers are initially crimped in the unloaded state, and become progressively recruited [52] and aligned [14] as the ligament is elongated. Thorton et al. related the viscoelastic creep of ligaments to progressive collagen fiber recruitment, and hypothesized that under stress relaxation a discrete group of fibers are recruited at a prescribed elongation [21, 59]. Under this hypothesis, less collagen fibers will be available for recruitment at higher strains, and there would be less difference in the viscoelastic response at higher strains. Collagen fibers of human lumbar ALL have been shown to become highly aligned during gross ligament elongation (with little difference in collagen fiber alignment observed at higher strains) at much lower strains than the collagen fibers of the lumbar LF [14]. The data presented herein appear to support the

hypothesis of Thorton et al. because the viscoelastic relaxation behavior of the ALL and PLL (which have similar microstructures with a high proportion of collagen fibers [15]) appears to converge as strain magnitude is increased and more collagen fibers are recruited. Highly extensible elastic fibers, however, dominate the LF microstructure [13, 16] and prevent the collagen fibers from aligning as quickly as those in the ALL and PLL [14]. Thus, the relaxation behavior of the LF continued to show signs of increasing viscoelastic behavior as the ligament was continuously strained possibly because the collagen fibers were still being recruited. However, further microstructural analysis is required to confirm these hypotheses.

The fitted QLV reduced relaxation function coefficients indicate that the relaxation behavior of the human cervical ALL, PLL, and LF are dominated by the short-term G_1 and the long-term G_∞ relaxation parameters, with the long-term coefficient governing the behavior. The dominating behavior of both the short-term and long-term relaxation coefficients has been reported previously by Lucas et al. [11]. However, Lucas et al. report that the relaxation behavior was dominated by the short-term coefficient (see Table 2, coefficient G_4 in [11]) and not the long-term coefficient observed in this study. The reason for the discrepancy possibly lies in the different time scales used in each study. In the present study, each ligament was held for 100 s after strain application and the entire relaxation (100 s) curve was fitted. Lucas et al. held each strain for 60 s and fitted only the first second (1000 ms) of the relaxation curve. Fung reported that when the reduced relaxation function is represented as a sum of exponentials, as in the present study and that of Lucas et al., one may mistakenly arrive at an erroneous long-term coefficient if the experiment is prematurely ceased [17]. The reduced relaxation coefficients presented in this thesis were obtained from stress relaxation experiments that were two orders of magnitude longer than those carried out by Lucas et al. Hence, the difference may indicate that the experiments of Lucas et al. were temporally inadequate and do not represent the full relaxation spectrum of these ligaments.

The long-term relaxation parameter G_∞ was observed to decrease with increasing strain for all ligament types, signifying that the ligaments dissipated more energy, and therefore underwent a greater amount of relaxation, at higher strains. However, the magnitude of the long-term parameter indicated that all ligaments maintained more than half of the applied instantaneous elastic stress. The ability of the ligaments to retain more than half of the induced initial stress may aid in maintaining stability of the cervical spine under dynamic loading events. Further, the large fast-rate G_1 in relation to the other G_n coefficients indicated that the majority of the relaxation occurs around the $\tau_1 = 0.1$ s time constant. One possible phenomenological explanation for this behavior is that when the ligaments are relaxing the musculature may be working to stabilize the spine. In this case, fast relaxation times would minimize the muscle expenditure required to maintain spinal stability.

The increasing and decreasing behavior observed for the LF and PLL G_1 parameters, respectively, appears to further support the microstructural collagen fiber recruitment hypothesis proposed Thorton et al. [59]. Under this hypothesis, the decrease in the fast-rate G_1 parameter observed in the PLL as strain was increased could be attributed to a smaller amount of collagen fibers being recruited at higher strains than in the preceding strain magnitude. Also, if collagen fibers were still actively being recruited the hypothesis made by Thorton and colleagues would predict that a more viscoelastic response would be observed with increasing strain, as was observed in the LF, which has fewer collagen fibers that are more randomly oriented than the PLL [13, 14].

Each ligament type had a unique instantaneous elastic response, which may be linked to the microstructure and function of the ligament. For the LF, the instantaneous elastic parameters A and B were not affected by strain magnitude. This may be a result of the aforementioned high elastin content of the LF, which possibly dominates the instantaneous elastic behavior of this ligament at the tested strain magnitudes [13, 16]. For the ALL, the instantaneous elastic

parameter B was observed to increase with increasing strain, indicating a more nonlinear instantaneous elastic response as strain increased [44]. The instantaneous elastic behavior of the PLL was more complex; parameter A increased with increasing strain while parameter B decreased. The strain-dependent instantaneous elastic behavior of the ALL and PLL may be due to the collagen fibers in the ligament. If individual collagen fibers of the ALL and PLL are represented as discrete elastic components (springs) of different lengths that become progressively recruited as the ligament is elongated [45], then an increasingly nonlinear elastic response (parameter B) with increasing strain magnitude, as observed in the ALL, would indicate that collagen fibers were actively being recruited. Conversely, the reduction in the nonlinear elastic response of the PLL may indicate a large amount of collagen fiber recruitment, and thus further strain would be resisted by the combined effort of nearly all collagen fibers, resulting in an increase in parameter A. Anatomically, the PLL lies close to the center of rotation of the spinal motion segment, and thus a large stiffness is required to maintain spinal stability [27]. The ALL is located farther away from the center of rotation, and is required to be more compliant (i.e., allow more collagen fiber recruitment) than the PLL to permit spinal extension. Previous studies have shown the PLL to be grossly stiffer than the ALL [11, 27, 33].

4.4. Power Law

Quasi-linear viscoelastic theory assumes that the shape of the stress relaxation curve is independent of the applied strain magnitude. To directly study the shape of a stress relaxation curve, previous investigations have fit relaxation data using a power law [21, 22]. Plotting relaxation data on a log-log scale produces a line; where different relaxation curve shapes are represented by different slopes. Data from the experimental relaxation region of the human cervical ALL, PLL, and LF from the current study were fitted to a power law at each strain magnitude, and statistical analyses indicated that the slope of the relaxation curves (and thus the shape of the curve) were strongly dependent on the applied strain magnitude. Therefore, the

results from fitting the model using a power law formulation indicate that QLV theory cannot adequately model the comprehensive viscoelastic behavior of these ligaments within the tested strain range. Furthermore, the power law described the viscoelastic behavior at an individual strain magnitude well, but the data from one strain magnitude was not able to predict the behavior at another strain magnitude. These results are in agreement with the aforementioned strain-dependent reduced relaxation function observed in the QLV fits. Thus, a more general, fully nonlinear viscoelastic formulation is required to model the comprehensive viscoelastic behavior of these ligaments.

The relaxation rate n was observed to increase with increasing strain for each ligament type, indicating that the ligaments displayed a more viscoelastic response at higher strains than at lower strains. Previous studies report similar viscoelastic behavior for mouse tail tendons [60], porcine digital flexor tendon [23], and ovine digital tendons [61]. However, a contrary viscoelastic behavior (decreasing viscoelastic response with increasing strain) was previously observed for rat [21], rabbit [22] and human [51] MCLs, and for human lumbar FJC [20]. While differences in testing methodologies, such as temperature control (warmed bath [51, 60, 61] versus room temperature bath [20-23]), and tissue type (tendon [23, 60, 61] versus ligament [20-22, 51]) may account for some of the observed discrepancies, the anatomical location and the specific functional microstructure of individual ligaments and tendons may be more important in determining the biomechanical behavior of the tissue. Rumian et al. found differences in the overall morphological and molecular compositions in the extracellular matrix of various ovine ligaments and tendons, and also found specific differences within ligament and tendon groups [54]. Rumian et al. speculated that the differences were dependent on anatomical location and intended function of each ligament or tendon [23, 54]. The observations of Rumian et al. are further justified by reports of the similar viscoelastic behavior observed between porcine and ovine digital flexor tendons [23, 61] and rat, rabbit, and human MCLs [21, 22, 51] since the intended function of these tendons and ligaments are similar among species.

Although the increasing relaxation rate with increasing strain trend observed for the ALL, PLL, and LF of the present study were contrary to the decreasing relaxation rate trends reported by Provenzano et al. [21] and Hingorani et al. [22] for rat and rabbit MCLs, both of these previous works also reported a similar relaxation rate convergence which was observed for the ALL and the PLL in the present study. Provenzano et al. and Hingorani et al. related the decreasing viscoelastic response with increasing strain to ligament water loss (termed the *wringing out effect*), speculating that higher strains caused a greater amount of water loss making the tissue less viscous at higher strains [21, 22]. However, as strain magnitude increased, these investigators reported that there was less of a difference between the relaxation rates, possibly indicating asymptotic converging behavior of the rat and rabbit MCLs. This behavior was similar to the asymptotic converging behavior observed herein for the ALL and PLL. While the effect of strain magnitude on the relaxation rate was observed to be different between the MCLs and the spine ligaments of this study (possibly because of the aforementioned differences in anatomical location and functional requirements of knee ligaments versus spinal ligaments), the mechanism of the converging behavior may be the same. As stated in the QLV discussion, the asymptotic behavior of the ALL, PLL, and the MCLs may be due to collagen fiber recruitment hypothesis of Thorton et al. [59], where a discrete amount of collagen fibers are recruited at each prescribed strain magnitude. Under this hypothesis, the difference between relaxation rates at higher strain magnitudes would be smaller because less additional collagen fibers will become recruited as strain increases [21, 22].

Plots of the relaxation rate (n) versus strain magnitude indicated that the LF had a notably different relaxation response than the longitudinal ligaments. While the ALL and PLL exhibited possible asymptotic converging behavior as strain magnitude increased, the LF displayed a diverging behavior with increasing strain, consistent with the results observed for the QLV reduced relaxation function. As stated previously, the difference in the relaxation behaviors of the LF and the longitudinal ligaments could be a result of the distinctly different

microstructures of the LF compared to the longitudinal ligaments. The highly aligned, dense collagen fibers in the ALL and PLL exhibit a greater amount of recruitment at smaller strain magnitudes than the randomly oriented, loosely dispersed LF collagen fibers [14]. The longitudinal ligament morphology may result in a greater initial increase in relaxation rate compared to the LF. Since the LF collagen fibers are loosely dispersed in elastin, the ligament has to be elongated more than the ALL and PLL to activate the collagen fibers. In the present study, it is hypothesized that the highly extensible elastin fibers dominate the deformation at the small strain magnitudes resulting the relatively small viscoelastic response. As strain is increased, however, the collagen fibers become progressively recruited, yielding a more viscoelastic response for the LF. In accordance with the hypothesis of Thorton et al. [59], it is suggested that the LF did not display converging behavior because there was still a substantial amount of collagen fibers to be recruited beyond the highest strain magnitude (25%) investigated in this study. It has been shown that unrecruited collagen fibers of the lumbar LF remain at 50% strain, while the collagen fibers of the lumbar ALL were highly recruited at strains of 15% [14].

4.5. Limitations

There are a number of limitations that should be addressed for proper interpretation of the results presented herein. The first is that the viscoelastic properties were obtained from ligaments dissected from highly variable cadaveric specimens, and potential confounding factors, such as donor age and gender, were not rigorously accounted for. Previous work has shown that the rate-dependent mechanical properties of the lumbar ALL are also dependent on bone mineral content, which can change with age [62]. While bone mineral content was not directly measured in this thesis, care was taken to select cervical spines from donors with no reported pre-existing bone or ligament pathology. In addition, Lucas et al. observed that the instantaneous elastic parameter used in their QLV fit was dependent on gender [11]. However, in this previous study a gender-dependent parameter was derived from a simplified (linear) instantaneous elastic equation, while

the present work used a nonlinear (exponential) instantaneous elastic relationship. While it is possible that the nonlinear instantaneous relationship may also be dependent on gender, to the best of the author's knowledge, there is no literature that supports this assertion. Lucas et al. report that their fitted reduced relaxation function coefficients were not found to be dependent on gender [11].

The ligament cross-sectional area was measured using a *post hoc* digital image capture of the ligaments cross-section. Thus, the ligaments were assumed to have a constant cross-sectional area that was the same dimension as the cut surface. Furthermore, the ligament cross-sectional area was measured in its unloaded state. Previous studies have used laser microscopy [27] and cryomicrotome [33] techniques to measure the cross-sectional area of cervical spine ligaments while under tension. However, the laser microscopy technique could not be used because the device could not be used inside the environmental chamber. Further, the cryomicrotome technique requires the ligaments to be cut from an intact spine, preventing the measurement of the cross-sectional area of the same ligaments that were subjected to mechanical testing. Therefore, the cross-sectional area of the ligaments was measured in the unloaded state after the ligaments were tested. Previous ligament studies have reported the use of the unloaded cross-sectional area [49, 63].

The viscoelastic parameters determined herein are presented under the assumption that the ligaments were completely isolated from the surrounding tissue. While the LF was easily identifiable, the deep fibers of the ALL and PLL are interdigitated with the outer annulus layer [13, 37], making the lateral boundaries of the ligament difficult to distinguish from the surrounding annulus tissue of some specimens. Furthermore, the dura matter was strongly attached to the PLL in some specimens. Previous work has reported the difficulties in distinguishing the ALL and PLL from the surrounding tissues [13, 37, 38]. It is possible that extraneous tissue remained attached to the ligament.

The viscoelastic formulations used in this thesis, such as QLV theory, assumes a step increase in strain, which is theoretical and impossible to produce experimentally. The moderate elongation rate (5 mm/s) used herein was selected in an attempt to minimize the experimental errors associated with high elongation rates, but still have a ramp time fast enough to compare to previously reported data. Previous studies have attempted to experimentally produce an approximate step increase in strain [64], but they reported experimental errors, such as overshoot and vibrations, that are a result of these fast strain rates [44]. The elongation rate used herein is two orders of magnitude slower than that used to experimentally approximate a step increase in strain. Abramowitch and Woo developed a method (used herein) of fitting experimental data obtained from experiments with finite ramp times to QLV theory by simultaneously fitting the ramping and relaxation regions of the experimental data, accounting for relaxation that occurs in the ramping region [44]. Furthermore, the selected elongation rate produced a maximum ramp time of less than 0.3 s (a maximum ramp time of 0.28 s was observed for an ALL specimen at the 25% strain magnitude), fast enough to fit the experimental relaxation portion of the data could be fit to a power relation and compared to previously reported data [21, 22]. This ramp time is on the same order of magnitude as a previous stress relaxation experiments using cervical spine ligaments [11].

Although the elongation rate was two orders of magnitude smaller than experiments that attempted to produce a step increase in strain, errors were observed with the testing apparatus. Specifically, the MTS crosshead displacement did not reflect a perfect linear ramp (Figure 4.3), which is assumed in the QLV fitting procedure (Section 2.5). The MTS crosshead has to overcome inertial effects when ramping at sufficiently high strain rates, resulting in a slightly sigmoidal-shaped ramping region (from approximately $0 < t < 0.1$ in Figure 4.3) [29]. Therefore, the strain rate used in the fitting procedure was taken from the slope of the approximately linear portion of the ramping region. The MTS actuator inertial effects at larger

strain magnitudes were reduced from that shown in Figure 4.3 because of the increased ramp time.

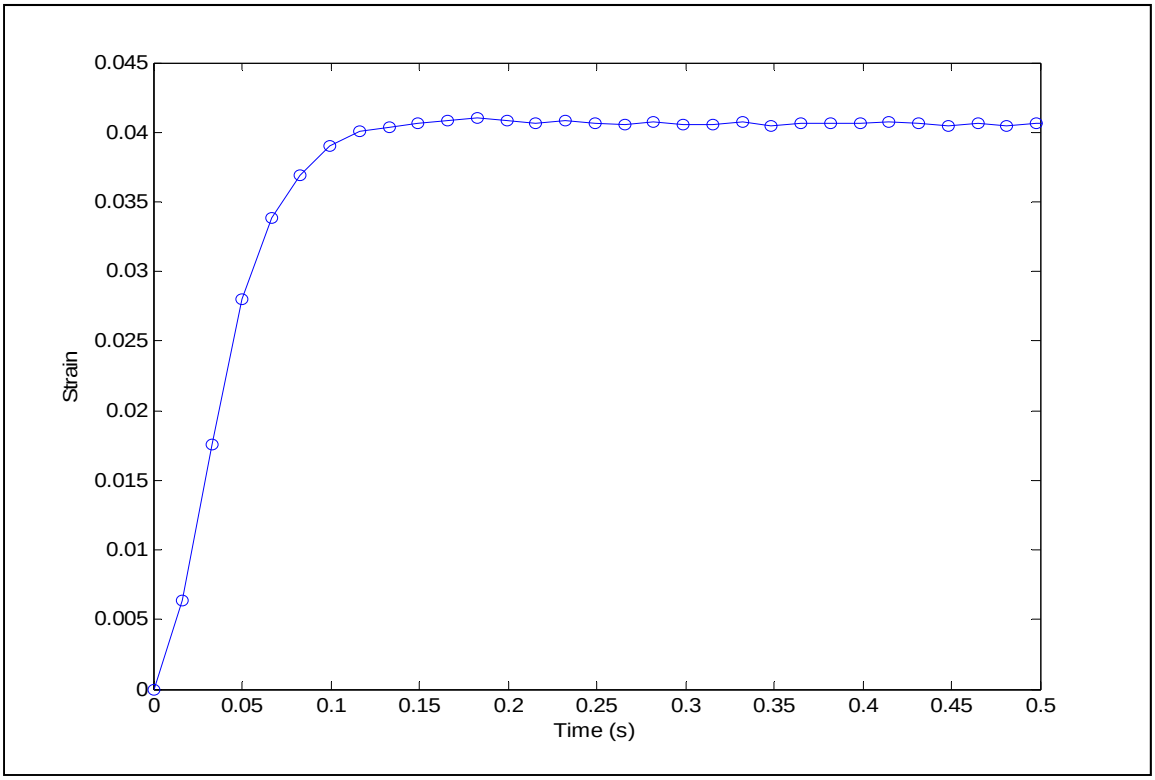

Figure 4.3: MTS crosshead displacement for a ligament subjected to 4% strain.

All displacement and strain measurements were recorded using the built-in MTS LVDT. As a result, the stress relaxation data is presented under the assumption that all of the deformation takes place in the ligament, and any localized ligament deformation is neglected. This method has been used previously to define the mechanical properties of cervical spine ligaments [11, 29, 33, 42]. Przybylski et al. previously used Verhoeff stain to mark the ligaments, and tracked these marks using a video analysis system [27]. However, this marking method was not used because the size of the environmental chamber could not accommodate a video camera and optical refraction caused by the different media (saline bath, curved plastic environmental chamber) would prevent accurate marker tracking if the video camera was placed outside the environmental chamber.

4.6. Future Work

The work in this thesis presents the comprehensive viscoelastic material properties of human lower cervical ALL, PLL, and LF. Future experimentation, however, could lead to a more in-depth understanding of the mechanical properties of these ligaments. For example, this thesis presents the phenomenological mechanical behavior of these ligaments and implicitly relates the observed behavior to the ligament microstructure based on the results of previous studies. Microstructural studies, such as those that examine the mechanical behavior of individual collagen fascicles [46], are required to determine the underlying cause of the global viscoelastic behavior.

Also, calculation of the ligament area in real-time would have provided a more accurate approximation of the true stress within the specimen. Bass et al. suggest the use of a three-dimensional video analysis setup to measure the dynamic cross-sectional area [42]. Such a video analysis setup could also be used to study the localized ligament deformation and strain. However, video analyses are complicated by the use of an environmental chamber, requiring waterproof systems or adjustments for optical refraction if placed outside the chamber. The development of such a detailed imaging technique was beyond the scope of this thesis, and is a topic that warrants further investigation.

Ligaments are mechanically anisotropic due to their composite fiber structure [65]. Previous studies have characterized the biaxial viscoelastic behavior of human lumbar FJC [20]. However, this thesis characterized the uniaxial viscoelastic properties of the ligaments along the axis of the spine. Though ligaments are strongest along the main fiber direction, and the spinal anatomy effectively loads the ligaments along this direction [1], complete mechanical characterization of these ligaments would include mechanical experiments that are not along the main axis of the fibers (e.g. perpendicular to the main fiber direction). Additionally, multiaxial experiments could provide insight to the mechanical behavior of other microstructural

constituents, such as the ground substance, and therefore may reveal underlying microstructural viscoelastic mechanisms that are unattainable through uniaxial experiments.

4.7. Conclusions

DMA conclusions

- All ligament types exhibited nonlinear (strain amplitude-dependent) viscoelastic cyclic behavior.
- The storage modulus, loss modulus, and $\tan(\delta)$ for all ligament types were dependent on frequency.
- All ligament types exhibited an increased cyclic viscoelastic response at slower frequencies, with diminished viscoelasticity as frequency increased.
- The ALL and PLL exhibited similar cyclic viscoelastic material properties.
- Overall, the LF exhibited a more elastic response than the ALL and PLL.

QLV fitted parameter conclusions

- Since the reduced relaxation function $G(t)$ was observed to be dependent on strain magnitude, the comprehensive viscoelastic behavior of these ligaments cannot be accurately described with QLV theory.
- The fitted QLV coefficients were found to be unique to each ligament type, indicating a unique relaxation response for each ligament type.
- The reduced relaxation function $G(t)$ for the ALL and PLL appeared to converge at higher strain magnitudes, while the LF $G(t)$ exhibited diverging behavior with increasing strain.

Power law conclusions

- The relaxation rates (n) were strongly dependent on strain level for all ligament types, indicating that these ligaments are nonlinear viscoelastic.

- The initial stress (σ_0) increased positively with the square of the strain magnitude, and the relaxation rate (n) increased negatively with the square of the strain.
- The ALL and PLL relaxation rate (n) behavior indicated possible convergence behavior at high strain magnitudes, while the LF relaxation rate (n) diverges with increasing strain.

REFERENCES

1. Augustus A. White, M.M.P., *Clinical Biomechanics of the Spine*. 2nd ed. 1990: Lippincott, Williams, and Wilkins.

2. Gray, H., W.H. Lewis, and Bartleby.com Inc., *Anatomy of the human body*. 2000, Bartleby.com: New York.

3. Penning, L. and J.T. Wilmink, *Rotation of the cervical spine. A CT study in normal subjects.* Spine, 1987. **12**(8): p. 732-8.

4. Bogduk, N. and S. Mercer, *Biomechanics of the cervical spine. I: Normal kinematics.* Clin Biomech (Bristol, Avon), 2000. **15**(9): p. 633-48.

5. Adams, M.A. and P.J. Roughley, *What is intervertebral disc degeneration, and what causes it?* Spine (Phila Pa 1976), 2006. **31**(18): p. 2151-61.

6. Urban, J.P.G., S. Roberts, and J.R. Ralphs, *The nucleus of the intervertebral disc from development to degeneration.* American Zoologist, 2000. **40**(1): p. 53-61.

7. Wu, H.C. and R.F. Yao, *Mechanical-Behavior of Human Annulus Fibrosis.* Journal of Biomechanics, 1976. **9**(1): p. 1-&.

8. Moore, R.J., *The vertebral end-plate: what do we know?* Eur Spine J, 2000. **9**(2): p. 92-6.

9. Urban, J.P., S. Smith, and J.C. Fairbank, *Nutrition of the intervertebral disc.* Spine, 2004. **29**(23): p. 2700-9.

10. Walsh, W.R., *Repair and regeneration of ligaments, tendons, and joint capsule*. Orthopedic biology and medicine. 2006, Totowa, N.J.: Humana Press. x, 324 p.

11. Lucas, S.R., et al., *Viscoelastic properties of the cervical spinal ligaments under fast strain-rate deformations.* Acta Biomater, 2008. **4**(1): p. 117-25.

12. Panjabi, M.M., T.R. Oxland, and E.H. Parks, *Quantitative anatomy of cervical spine ligaments. Part II. Middle and lower cervical spine.* J Spinal Disord, 1991. **4**(3): p. 277-85.

13. Hukins, D.W.L. and J.R. Meakin. *Relationship between structure and mechanical function of the tissues of the intervertebral joint*. 2000.

14. Hukins, D.W., et al., *Comparison of structure, mechanical properties, and functions of lumbar spinal ligaments.* Spine (Phila Pa 1976), 1990. **15**(8): p. 787-95.

15. Nakagawa, H., Y. Mikawa, and R. Watanabe, *Elastin in the human posterior longitudinal ligament and spinal dura. A histologic and biochemical study.* Spine (Phila Pa 1976), 1994. **19**(19): p. 2164-9.

16. Nachemson, A.L. and J.H. Evans, *Some mechanical properties of the third human lumbar interlaminar ligament (ligamentum flavum).* Journal of Biomechanics, 1968. **1**(3): p. 211-20.

17. Fung, Y.C., *Biomechanics : mechanical properties of living tissues*. 2nd ed. 1993, New York: Springer-Verlag. xviii, 568 p.

18. Findley, W.N., J.S. Lai, and K. Onaran, *Creep and relaxation of nonlinear viscoelastic materials with an introduction to linear viscoelasticity*. 1976, New York: American Elsevier Pub. Co. xiii, 367 p.

19. Lakes, R.S., *Viscoelastic solids*. CRC mechanical engineering series. 1999, Boca Raton: CRC Press. 476 p.

20. Little, J.S. and P.S. Khalsa, *Material properties of the human lumbar facet joint capsule.* J Biomech Eng, 2005. **127**(1): p. 15-24.

21. Provenzano, P., et al., *Nonlinear ligament viscoelasticity.* Ann Biomed Eng, 2001. **29**(10): p. 908-14.

22. Hingorani, R.V., et al., *Nonlinear viscoelasticity in rabbit medial collateral ligament.* Ann Biomed Eng, 2004. **32**(2): p. 306-12.

23. Duenwald, S.E., R. Vanderby, Jr., and R.S. Lakes, *Viscoelastic relaxation and recovery of tendon.* Ann Biomed Eng, 2009. **37**(6): p. 1131-40.

24. Waters, R.L. and J.M. Morris, *An in vitro study of normal and scoliotic interspinous ligaments.* J Biomech, 1973. **6**(4): p. 343-8.

25. Tkaczuk, H., *Tensile properties of human lumbar longitudinal ligaments.* Acta Orthop Scand, 1968: p. Suppl 115:1+.

26. Panjabi, M.M., V.K. Goel, and K. Takata, *Physiologic strains in the lumbar spinal ligaments. An in vitro biomechanical study 1981 Volvo Award in Biomechanics.* Spine (Phila Pa 1976), 1982. **7**(3): p. 192-203.

27. Przybylski, G.J., et al., *Human anterior and posterior cervical longitudinal ligaments possess similar tensile properties.* Journal of Orthopaedic Research, 1996. **14**(6): p. 1005-1008.

28. Yoganandan, N., S. Kumaresan, and F.A. Pintar, *Biomechanics of the cervical spine Part 2. Cervical spine soft tissue responses and biomechanical modeling.* Clin Biomech (Bristol, Avon), 2001. **16**(1): p. 1-27.

29. Yoganandan, N., et al., *Dynamic response of human cervical spine ligaments.* Spine (Phila Pa 1976), 1989. **14**(10): p. 1102-10.

30. Thornton, G.M., C.B. Frank, and N.G. Shrive, *Ligament creep behavior can be predicted from stress relaxation by incorporating fiber recruitment.* Journal of Rheology, 2001. **45**(2): p. 493-507.

31. Viidik, A., *Simultaneous mechanical and light microscopic studies of collagen fibers.* Z Anat Entwicklungsgesch, 1972. **136**(2): p. 204-12.

32. Kirby, M.C., et al., *Structure and mechanical properties of the longitudinal ligaments and ligamentum flavum of the spine.* J Biomed Eng, 1989. **11**(3): p. 192-6.

33. Yoganandan, N., S. Kumaresan, and F.A. Pintar, *Geometric and mechanical properties of human cervical spine ligaments.* J Biomech Eng, 2000. **122**(6): p. 623-9.

34. Chazal, J., et al., *Biomechanical properties of spinal ligaments and a histological study of the supraspinal ligament in traction.* J Biomech, 1985. **18**(3): p. 167-76.

35. Yahia, L.H., J. Audet, and G. Drouin, *Rheological properties of the human lumbar spine ligaments.* J Biomed Eng, 1991. **13**(5): p. 399-406.

36. Womack, W.J., *Computational Modeling of the Lower Cervical Spine: Facet Cartilage Distribution and Disc Replacement*, in *Mechanical Engineering*. 2009, Colorado State University: Fort Collins.

37. Putz, R., *The detailed functional anatomy of the ligaments of the vertebral column.* Ann Anat, 1992. **174**(1): p. 40-7.

38. Loughenbury, P.R., S. Wadhwani, and R.W. Soames, *The posterior longitudinal ligament and peridural (epidural) membrane.* Clin Anat, 2006. **19**(6): p. 487-92.

39. Bass, C.R., et al., *The temperature-dependent viscoelasticity of porcine lumbar spine ligaments.* Spine (Phila Pa 1976), 2007. **32**(16): p. E436-42.

40. Hoffman, A.H., et al., *Determining the effect of hydration upon the properties of ligaments using pseudo Gaussian stress stimuli.* Journal of Biomechanics, 2005. **38**(8): p. 1636-1642.

41. Ivancic, P.C., et al., *Dynamic mechanical properties of intact human cervical spine ligaments.* Spine J, 2007. **7**(6): p. 659-65.

42. Bass, C.R., et al., *Failure properties of cervical spinal ligaments under fast strain rate deformations.* Spine (Phila Pa 1976), 2007. **32**(1): p. E7-13.

43. Goel, V.K. and J.D. Clausen, *Prediction of load sharing among spinal components of a C5-C6 motion segment using the finite element approach.* Spine, 1998. **23**(6): p. 684-691.

44. Abramowitch, S.D. and S.L. Woo, *An improved method to analyze the stress relaxation of ligaments following a finite ramp time based on the quasi-linear viscoelastic theory.* J Biomech Eng, 2004. **126**(1): p. 92-7.

45. Woo, S.L., *Mechanical properties of tendons and ligaments. I. Quasi-static and nonlinear viscoelastic properties.* Biorheology, 1982. **19**(3): p. 385-96.

46. Lucas, S.R., et al., *Viscoelastic and failure properties of spine ligament collagen fascicles.* Biomech Model Mechanobiol, 2009.

47. Park, S.W. and R.A. Schapery, *Methods of interconversion between linear viscoelastic material functions. Part I - a numerical method based on Prony series.* International Journal of Solids and Structures, 1999. **36**(11): p. 1653-1675.

48. Pooni, J.S., et al., *Comparison of the Structure of Human Intervertebral Disks in the Cervical, Thoracic and Lumbar Regions of the Spine.* Surgical and Radiologic Anatomy, 1986. **8**(3): p. 175-182.

49. Butler, D.L., et al., *Effects of Structure and Strain-Measurement Technique on the Material Properties of Young Human Tendons and Fascia.* Journal of Biomechanics, 1984. **17**(8): p. 579-596.

50. Frank, C.B., *Ligament structure, physiology and function.* J Musculoskelet Neuronal Interact, 2004. **4**(2): p. 199-201.

51. Bonifasi-Lista, C., et al., *Viscoelastic properties of the human medial collateral ligament under longitudinal, transverse and shear loading.* Journal of Orthopaedic Research, 2005. **23**(1): p. 67-76.

52. Woo, S.L.Y., G.A. Johnson, and B.A. Smith, *Mathematical-Modeling of Ligaments and Tendons.* Journal of Biomechanical Engineering-Transactions of the Asme, 1993. **115**(4): p. 468-473.

53. Panjabi, M.M., et al., *The mechanical properties of human alar and transverse ligaments at slow and fast extension rates.* Clin Biomech (Bristol, Avon), 1998. **13**(2): p. 112-120.

54. Rumian, A.P., A.L. Wallace, and H.L. Birch, *Tendons and ligaments are anatomically distinct but overlap in molecular and morphological features--a comparative study in an ovine model.* J Orthop Res, 2007. **25**(4): p. 458-64.

55. Chimich, D., et al., *Water content alters viscoelastic behaviour of the normal adolescent rabbit medial collateral ligament.* J Biomech, 1992. **25**(8): p. 831-7.

56. Atkinson, T.S., R.C. Haut, and N.J. Altiero, *A poroelastic model that predicts some phenomenological responses of ligaments and tendons.* Journal of Biomechanical Engineering-Transactions of the Asme, 1997. **119**(4): p. 400-405.

57. Butler, S.L., et al., *Interstitial fluid flow in tendons or ligaments: a porous medium finite element simulation.* Medical & Biological Engineering & Computing, 1997. **35**(6): p. 742-746.

58. Weiss, J.A., J.C. Gardiner, and C. Bonifasi-Lista, *Ligament material behavior is nonlinear, viscoelastic and rate-independent under shear loading.* Journal of Biomechanics, 2002. **35**(7): p. 943-950.

59. Thornton, G.M., et al., *Ligament creep cannot be predicted horn stress relaxation at low stress: A biomechanical study of the rabbit medial collateral ligament.* Journal of Orthopaedic Research, 1997. **15**(5): p. 652-656.

60. Elliott, D.M., et al., *Effect of altered matrix proteins on quasilinear viscoelastic properties in transgenic mouse tail tendons.* Ann Biomed Eng, 2003. **31**(5): p. 599-605.

61. Sverdlik, A. and Y. Lanir, *Time-dependent mechanical behavior of sheep digital tendons, including the effects of preconditioning.* Journal of Biomechanical Engineering-Transactions of the Asme, 2002. **124**(1): p. 78-84.

62. Neumann, P., et al., *Effect of Strain-Rate and Bone-Mineral on the Structural-Properties of the Human Anterior Longitudinal Ligament.* Spine, 1994. **19**(2): p. 205-211.

63. Shetye, S.S., et al., *Determination of mechanical properties of canine carpal ligaments.* Am J Vet Res, 2009. **70**(8): p. 1026-30.

64. Funk, J.R., et al., *Linear and quasi-linear viscoelastic characterization of ankle ligaments.* Journal of Biomechanical Engineering-Transactions of the Asme, 2000. **122**(1): p. 15-22.

65. Pena, E., et al., *An anisotropic visco-hyperelastic model for ligaments at finite strains. Formulation and computational aspects.* International Journal of Solids and Structures, 2007. **44**(3-4): p. 760-778.